# SEISMIC BEARING CAPACITY APPROACH FOR VEHICLE MOBILITY PROBLEMS

by

Çağlar Çağbayır

B.S. in Civil Engineering, Middle East Technical University, 2004

Submitted to the Institute for Graduate Studies in
Science and Engineering in partial fulfillment of
the requirements for the degree of
Master of Science

Graduate Program in Civil Engineering

Boğaziçi University

2008

SEISMIC BEARING CAPACITY APPROACH FOR VEHICLE MOBILITY PROBLEMS

APPROVED BY:

| | |
|---|---|
| Assist. Prof. Özer ÇİNİCİOĞLU (Thesis Supervisor) | ..... |
| Prof. Dr. Gökhan BAYKAL | ..... |
| Assist. Prof. İlknur BOZBEY | ..... |

DATE OF APPROVAL: 11.06.2008

# ACKNOWLEDGEMENTS

First of all, I would like to thank my supervisor, Assist. Prof. Özer Çinicioğlu, for his assistance, advices and motivative approach in all stages of my thesis studies. Working with him has been a very special experience.

Further and especially, I would like to thank my dear brother Çağlayan Çağbayır for his ineffable supports during my whole graduate education. He is the one with whom I have been able to discuss the progress and the concept of the thesis. I should also emphasize that I would not have been able to finish or even begin this thesis without his support.

# ABSTRACT

## SEISMIC BEARING CAPACITY APPROACH FOR VEHICLE MOBILITY PROBLEMS

This thesis introduces a new approach in soil-vehicle interaction analysis for quick determination of vehicle mobility in off-road conditions. Geotechnical analysis for the problems of vehicle-soil interaction is an almost unmentioned subject in literature because of the extraordinariness and the complexity of the situation. Here, the aim is to transform the problem into well-known and more comprehensible geotechnical issue which is bearing capacity of soils. The main argument is that there is a strong mechanical analogy between two distinct problems, namely, the behavior of the soil under seismic activity and the behavior of the soil beneath a mobile vehicle. According to this approach, the tracks or the wheels of an off-road vehicle correspond to the footings of a structure, the traction loads corresponds to horizontal loads of the structure during an earthquake and the seismic degradation of the soil strength under seismic loads corresponds to the difference between bearing capacities of soil of a sloped and soil of a horizontal ground. The decrease in the bearing capacity of the soil on a slope and beneath a mobile vehicle is defined by introducing a mobility reduction factor. This reduction factor covers strength loss of soil due to both tractive force and inclination of the ground. The mobility reduction factors for each component of the bearing capacity equation are derived on the basis of seismic fluidization concept. The whole theoretical works are assembled on a computer program and results for various types of terrains and vehicles are presented.

# ÖZET

## ARAÇ HAREKET YETENEĞİ PROBLEMLERİ İÇİN SİSMİK TAŞIMA GÜCÜ YAKLAŞIMI

Bu tez, ham zeminlerde araç hareketliliğinin ivedi belirlenmesi için araç - zemin etkileşimi incelemelerine yeni bir yaklaşım ortaya koymaktadır. Durumun yaygın olmayışı ve karmaşıklığı nedeniyle araç-zemin etkileşimi problemleri için geoteknik inceleme litaratürde nerdeyse hiç değinilmemiş bir konudur. Burada amaç, bu problemi daha anlaşılır ve bilinen bir geoteknik konu olan zemin taşıma gücü problemine dönüştürmektir. Temel iddia ise, zeminin depremsel etkinlik sırasındaki davranışı ve araç altında kalan zeminin davranışı gibi iki ayrı problem arasında mekanik benzerlik olmasıdır. Bu yaklaşıma göre, bir arazi aracının paletleri ya da tekerlekleri bir yapının temellerine, aracın çekiş yükleri yapının deprem sırasında oluşan yatay yüklerine ve zemindeki dayanımın sismik etkinlik sırasında azalması da şevli zemin ile yatay durumdaki zemin arasındaki taşıma gücü farkına denk gelmektedir. Eğimli bir yüzeyde ve hareket halinde olan bir aracın altında olan zeminin taşıma kapasitesindeki azalış, hareketlilik düşüş katsayısı ortaya konularak tanımlanmaktadır. Bu düşüş katsayısı zeminin dayanımının hem çekiş yüklerinden hem de yüzeyin eğiminden kaynaklanan azalmayı kapsamaktadır. Zemin taşıma gücü eşitliğindeki her bileşene ait hareketlilik düşüş katsayısı sismik akışkanlaşma kavramı temel alınarak elde edilmektedir. Yapılan tüm kuramsal çalışmalar bir bilgisayar programında toparlanıp, çeşitli zemin ve araç tipleri için hesaplanan sonuçlar sunulmaktadır.

# TABLE OF CONTENTS

ACKNOWLEDGEMENTS . . . . . iii
ABSTRACT . . . . . iv
ÖZET . . . . . v
LIST OF FIGURES . . . . . ix
LIST OF TABLES . . . . . xii
LIST OF SYMBOLS/ABBREVIATIONS . . . . . xiv
1. INTRODUCTION . . . . . 1
1.1. Structure of the Thesis . . . . . 1
2. LITERATURE REVIEW . . . . . 3
2.1. Bearing Capacity of Soils . . . . . 3
2.1.1. Introduction . . . . . 3
2.1.2. Failure Mechanisms . . . . . 4
2.1.3. Bearing Capacity Theories . . . . . 5
2.1.3.1. Prandtl's Bearing Capacity Theory . . . . . 5
2.1.3.2. Terzaghi's Bearing Capacity Theory . . . . . 6
2.1.3.3. Meyerhof's Bearing Capacity Theory . . . . . 7
2.1.3.4. Brinch Hansen's Bearing Capacity Theory . . . . . 8
2.1.3.5. Veśic's Bearing Capacity Theory . . . . . 8
2.1.4. Summary . . . . . 8
2.2. Dynamic Fluidization of Soils . . . . . 8
2.2.1. Seismic Fluidization Concept . . . . . 8
2.2.2. Mechanics of Fluidization . . . . . 11
2.2.2.1. Initial Fluidization: . . . . . 12
2.2.2.2. Intermediate Fluidization: . . . . . 16
2.2.2.3. General Fluidization: . . . . . 17
2.2.3. Fluidization of $c - \phi$ Soils . . . . . 18
2.3. Seismic Bearing Capacity . . . . . 22
2.3.1. Static Bearing Capacity Calculations by Coulomb Mechanism . 22
2.3.2. Seismic Bearing Capacity Calculations by Coulomb Mechanism 25

2.3.3. Inclination Factors For Seismic Bearing Capacity Calculations . 29
2.3.4. Seismic Bearing Capacity Calculations for Cohesive Soils . . . . 34
2.4. Mechanics of Vehicle-Soil Interaction (Terramechanics) . . . . . 37
2.4.1. Introduction . . . . . 37
2.4.2. Empirical Models . . . . . 38
2.4.2.1. Tracked Vehicle Performance: . . . . . 38
2.4.2.2. Wheeled Vehicle Performance: . . . . . 41
2.4.3. Semi-Empirical Models . . . . . 43
2.4.3.1. Bevameter Tests: . . . . . 44
2.4.4. Analytical Methods . . . . . 48
2.4.4.1. Theory of Elasticity . . . . . 48
2.4.4.2. Theory of Plasticity . . . . . 52
2.4.5. Numerical Methods . . . . . 55
2.4.6. Shearing Resistance Between Solids and Soil . . . . . 56
3. INTRODUCTION TO THE METHOD OF SOLUTION . . . . . 59
4. VEHICLE LOADS EXERTED TO THE GROUND . . . . . 62
4.1. Introduction . . . . . 62
4.2. Wheeled Vehicles . . . . . 63
4.3. Tracked Vehicles . . . . . 65
4.4. Summary . . . . . 68
5. SLIPPING OF THE VEHICLES . . . . . 70
6. MOBILITY ANALYSIS BY MODIFIED SEISMIC BEARING CAPACITY APPROACH . . . . . 73
6.1. Introduction . . . . . 73
6.2. Determination of $N_{qm}$ and $N_{\gamma m}$ . . . . . 74
6.3. Determination of $N_{cm}$ . . . . . 79
6.3.1. Determination of $N_{cm}$ for Frictional Soils . . . . . 80
6.3.2. Determination of $N_{cm}$ for Frictionless Soils . . . . . 82
6.4. Reduction Factors for Bearing Capacity Analysis of Mobile Vehicles . . 85
6.5. Modified Bearing Capacity Equation for Off-Road Mobility . . . . . 86
7. COMPUTATION SCHEME FOR MOBILITY DECISION . . . . . 87
7.1. Computation Scheme for Allowable Vehicle Weight . . . . . 88

7.2. Computation Scheme for Allowable Slope Angle . . . . . 89
7.3. Computation Scheme for Allowable Acceleration . . . . . 89
8. DISCUSSION OF RESULTS . . . . . 93
8.1. Seismic Reduction in $N_c$ . . . . . 93
8.2. Example Cases to Illustrate the Proposed Mobility Model . . . . . 98
8.2.1. Allowable Weight Determination of a Wheeled Vehicle . . . . . 98
8.2.2. Allowable Slope Angle Determination of a Wheeled Vehicle . . . 100
8.2.3. Allowable Acceleration Determination of a Wheeled Vehicle . . 101
8.2.4. Allowable Weight Determination of a Tracked Vehicle . . . . . 103
8.2.5. Allowable Slope Angle Determination of a Tracked Vehicle . . . 104
8.2.6. Allowable Acceleration Determination of a Tracked Vehicle . . . 106
9. CONCLUSION . . . . . 108
APPENDIX A: MATLAB CODE FOR MOBILITY DECISION . . . . . 110
A.1. Main Body . . . . . 110
A.2. Calculation of $N_{qm}$ and $N_{\gamma m}$ . . . . . 122
A.3. Calculation of $N_{cm}$ . . . . . 122
A.4. Calculation of $N_{qm=0}$ and $N_{\gamma m=0}$ . . . . . 124
A.5. Calculation of $N_{cm=0}$ . . . . . 125
A.6. Iteration of $k$ for Unknown Weight . . . . . 125
A.7. Iteration of $N_{qm}$ and $N_{\gamma m}$ for Unknown Weight . . . . . 126
A.8. Iteration of $N_{cm}$ for Unknown Weight . . . . . 126
A.9. Iteration of $N_{qm=0}$ and $N_{\gamma m=0}$ for Unknown Weight . . . . . 128
A.10.Iteration of $N_{cm=0}$ for Unknown Acceleration . . . . . 129
A.11.Iteration of $k$ for Unknown Acceleration . . . . . 129
A.12.Iteration of $N_{qm}$ and $N_{\gamma m}$ for Unknown Acceleration . . . . . 130
A.13.Iteration of $N_{cm}$ for Unknown Acceleration . . . . . 130
REFERENCES . . . . . 133
REFERENCES NOT CITED . . . . . 136

# LIST OF FIGURES

Figure 2.1. Modes of failure: (a)general shear, (b)local shear, (c)punching shear 4

Figure 2.2. Prandtl's failure mechanism . . . . . 5

Figure 2.3. Terzaghi's failure mechanism . . . . . 7

Figure 2.4. Meyerhof's failure mechanism . . . . . 7

Figure 2.5. Dynamic free field . . . . . 12

Figure 2.6. Mohr circle representation of initial fluidization . . . . . 14

Figure 2.7. Orientation of slip surfaces and principle planes . . . . . 16

Figure 2.8. Initial slip field . . . . . 17

Figure 2.9. Intermediate fluidization . . . . . 18

Figure 2.10. General fluidization . . . . . 19

Figure 2.11. Mohr circle of $c - \phi$ soils under seismic loading . . . . . 20

Figure 2.12. Comparison of Prandtl and Coulomb types failure mechanisms . . 22

Figure 2.13. Static forces acting on Coulomb wedges . . . . . 23

Figure 2.14. Seismic forces acting on Coulomb wedges . . . . . 27

Figure 2.15. Coulomb analysis for $\phi = 30$ (a) failure surface inclination (b) seismic pressure coefficients (c) failure mechanism for $\tan\theta = 0.3$ 28

Figure 2.16. Seismic to static bearing capacity ratios . . . . . 30

Figure 2.17. Forces acting on Coulomb weges . . . . . 31

Figure 2.18. Bearing capacity reduction (a)$N_{\gamma E}/N_{\gamma S}$ (b)$N_{qE}/N_{qS}$ . . . . . 33

Figure 2.19. Static and seismic failure surfaces . . . . . 34

Figure 2.20. Forces acting on seismic failure surfaces . . . . . 35

Figure 2.21. ERDC trafficability equipments . . . . . 41

Figure 2.22. Schematic representation of bevameter tests (after Bekker 1969): (a)plate-penetration test, (b) shear test . . . . . 44

Figure 2.23. Method for determining sinkage moduli and exponent . . . . . 46

Figure 2.24. Stresses due to point load . . . . . 50

Figure 2.25. Stresses due to line load . . . . . 51

Figure 2.26. Stresses due to strip load . . . . . 52

Figure 2.27. Equal vertical stress curves under tracked vehicles . . . . . 53

Figure 2.28. Rigid-perfectly plastic and elastic-plastic behavior of soils . . . . . 53

Figure 2.29. Principle stresses on mohr circle and failure planes . . . . . 54

Figure 2.30. Shearing stress -strain relationship of frictional soils in loose and dense state . . . . . 57

Figure 3.1. Footing and body forces exerted on (a) sloped soil (b) soil under seismic loads . . . . . 60

Figure 4.1. Forces acting on a wheeled vehicle on slope . . . . . 63

Figure 4.2. Forces acting on a tracked vehicle on slope . . . . . 66

Figure 5.1. Shear forces between track and soil . . . . . 70

Figure 6.1. Loads and Coulomb wedges on a slope . . . . . 75

Figure 6.2. Coulomb's type failure mechanism for $c = 0$ . . . . . 76

Figure 6.3. Modified Vesic's surface for mobility analysis . . . . . 80

Figure 6.4. Forces acting on failure surfaces . . . . . 82

Figure 6.5. Coulomb's failure mechanism for $\phi = 0$ $q_s = 0$ . . . . . 83

Figure 8.1. Comparison of the results of Coulomb wedge method with Budhu and Al-Karni (1993) method for $\kappa = 0.1$ . . . . . 95

Figure 8.2. Comparison of the results of Coulomb wedge method with Budhu and Al-Karni (1993) method for $\kappa = 0.5$ . . . . . 96

Figure 8.3. Comparison of the results of Coulomb wedge method with Budhu and Al-Karni (1993) method for $\kappa = 1.0$ . . . . . 97

# LIST OF TABLES

Table 2.1. Bearing capacity factors of various theories . . . . . 9

Table 2.2. Shape factors of various theories for rectangular footings . . . . . 9

Table 2.3. Depth factors of various theories . . . . . 10

Table 2.4. Inclination factors of various theories . . . . . 10

Table 2.5. Comparison of Prandtl and Coulomb types mechanisms for $N_c$ and $N_q$ . . . . . 26

Table 2.6. Comparison of seismic and static bearing capacity factors for $\phi = 30°$ . . . . . 29

Table 2.7. $n$, $k_c$ and $k_\phi$ values for various soil types . . . . . 47

Table 6.1. Analysis methods for bearing capacity factors . . . . . 73

Table 7.1. Computer program scheme for determination of allowable vehicle weight . . . . . 90

Table 7.2. Computer program scheme for determination of allowable slope angle . . . . . 91

Table 7.3. Computer program scheme for determination of allowable acceleration . . . . . 92

Table 8.1. Comparison of the results of Coulomb wedge method with Budhu and Al-Karni (1993) method . . . . . 94

Table 8.2. Allowable weight determination of a wheeled vehicle . . . . . 99

Table 8.3. Allowable slope angle determination of a wheeled vehicle . . . . . 101

Table 8.4. Allowable acceleration determination of a wheeled vehicle . . . . . 102

Table 8.5. Allowable weight determination of a tracked vehicle . . . . . 104

Table 8.6. Allowable slope angle determination of a tracked vehicle . . . . . 105

Table 8.7. Allowable acceleration determination of a tracked vehicle . . . . . 107

# LIST OF SYMBOLS/ABBREVIATIONS

| | |
|---|---|
| $a$ | Acceleration |
| $a_{ws}$ | Adhesion between tyre and soil |
| $a_{rs}$ | Adhesion between rubber and soil |
| $a_{ss}$ | Adhesion |
| $A_e$ | Effective contact area at the base of the foundation |
| $A_l$ | Area of lugs in tyre-soil interaction |
| $A_t$ | Area of tyre-soil interaction |
| $A_v$ | Area of voids in tyre-soil interaction |
| $B$ | Width of footing |
| $B'$ | Effective width of footing |
| $c$ | Cohesive strength |
| $c_a$ | Adhesion of the foundation soil to the footing base |
| $d_c, d_q, d_{gamma}$ | Depth factors in bearing capacity equation |
| $D$ | Depth of footing base with respect to ground |
| $e$ | Eccentricity distance |
| $E$ | Wheel or track width |
| $E_y$ | YOUNG's modulus |
| $F$ | Force |
| $F_n$ | Normal component of reaction force on front wheel |
| $F_t$ | Tangential component of reaction force on front wheel |
| $g$ | Gravitational acceleration |
| $G$ | Shear modulus |
| $h$ | Vertical distance between the bottom and center of the gravity of the vehicle |
| $H$ | Depth of failure surface |
| $i$ | Inclination |
| $i_c, i_q, i_{gamma}$ | Inclination factors in bearing capacity equation |
| $k$ | Vehicle load distribution constant |
| $k_h$ | Horizontal seismic acceleration factor |

| | |
|---|---|
| $k_c$ | Empirical cohesion parameter in Bekker's equation |
| $k_v$ | Vertical seismic acceleration factor |
| $k_\phi$ | Empirical friction parameter in Bekker's equation |
| $K$ | Coefficient of of lateral earth pressure |
| $K_{PE}$,$K_{AE}$ | Coefficient of of lateral earth pressure under seismic activity |
| $l_F$ | Horizontal distance between the front axis and the center of the gravity of vehicle |
| $l_R$ | Horizontal distance between the rear axis and the center of the gravity of vehicle |
| $L$ | Length of footing |
| $m$ | Strength mobilization factor |
| $M$ | Moment |
| $n$ | Seismic shear factor |
| $N_\gamma$, $N_c$, $N_q$ | Bearing capacity factors for weight, cohesion and surcharge respectively |
| $N_{\gamma E}$, $N_{cE}$, $N_{qE}$ | Seismic bearing capacity factors for weight, cohesion and surcharge respectively |
| $N_{\gamma S}$, $N_{cS}$, $N_{qS}$ | Static bearing capacity factors for weight, cohesion and surcharge respectively |
| $N_{\gamma m}$, $N_{cm}$, $N_{qm}$ | Mobility bearing capacity factors for weight, cohesion and surcharge respectively |
| $p$ | Pressure |
| $P_A$ | Active force on coulomb wedge |
| $P_h$ | Horizontal component of the inclined foundation load |
| $P_P$ | Passive force on coulomb wedge |
| $P_v$ | Vertical component of the inclined foundation load |
| $q_0$ | Surcharge pressure |
| $q_{all}$ | Allowable bearing capacity |
| $q_t$ | Distributed track load |
| $q_u$,$q_f$ | Ultimate bearing capacity |
| $q_w$ | Distributed wheel load |
| $q_{w/t}$ | Distributed wheel or track load |
| $w_v$ | Vehicle weight in plane strain condition |

| | |
|---|---|
| $Q$ | Point load |
| $r_0$ | Radius of radial failure surface |
| $R_1$, $R_2$ | Coulomb wedge analysis factors |
| $R_A$ | Reaction force on active wedge |
| $R_P$ | Reaction force on passive wedge |
| $R_n$ | Normal component of reaction force on rear wheel |
| $R_t$ | Tangential component of reaction force on rear wheel |
| $s$ | Shear strength |
| $s_c, s_q, s_d$ | Shape factors in bearing capacity equation |
| $s_{rs}$ | Shear strength between rubber and soil |
| $s_{ws}$ | Shear strength between wheel and soil |
| $t_g$ | Horizontal distance between center of gravity and rear bottom of track |
| $W$ | Weight |
| $W_v$ | Vehicle weight |
| $z$ | Soil depth |
| $\alpha$ | Rotation angle of principle planes |
| $\beta_{c,q,\gamma}$ | Seismic degradation factors for cohesion, surcharge and soil weight components |
| $\delta$ | Wall friction angle |
| $\epsilon$ | Strain |
| $\gamma$ | Unit weight |
| $\kappa$ | Soil cohesion and weight ratio factor |
| $\nu$ | POISSON's ratio |
| $\rho$ | Orientation angle of slip surfaces |
| $\phi$ | Internal friction angle |
| $\phi_{ws}$ | Friction angle between soil and tyre |
| $\phi_{rs}$ | Friction angle between soil and rubber |
| $\sigma$ | Normal stress |
| $\sigma_x$,$\sigma_y$,$\sigma_z$ | Normal stresses in x,y,z direction - cartesian coordinates |
| $\tau$ | Shear stress |
| $\theta$ | Inclination angle |

| | |
|---|---|
| CI | Cone index |
| ERDC | US Armys Engineer Research and Development Center |
| FEM | Finite element method |
| MI | Mobility index |
| RCI | Rating cone index |
| WES | US Army Waterways Experiment Station |
| VCI | Vehicle cone index |

# 1. INTRODUCTION

The main propose of this thesis is to construct a simplistic approach to soil-vehicle interaction problem and to suggest a new method for determining soil strength capacity for vehicle mobility. In off-road vehicle mobility analysis, the main difficulty is the complexity of the real situation to construct a satisfactory analytical model. Therefore researchers and designers often resort to emprical solutions. Moreover the majority of the work conducted on the subject focus on vehicle performance rather the soil response.

Mobility of off-road vehicles have become an important subject since World War II. Although the starting point of the issue has a militaristic aim, it is not the only area of application. From agriculture to construction works where there is no possibility of reinforcement of the soil, the mobility of the vehicles is a subject of investigation.

The scope of this study is limited by geotechnical point of view, that means, the proposed method considers only the situation of shear failure of soil resulting in the total loss of mobility.

## 1.1. Structure of the Thesis

Chapter 2 provides a comprehensive review of literature about previous studies related to the presented method. In order to utilize seismic bearing capacity approach in vehicle mobility analysis, the mechanisms of bearing failure and common static bearing capacity equations are presented in Section 2.1, the seismic fluidization concept is presented in Section 2.2 and seismic bearing capacity theories are presented in Section 2.3. In Section 2.4 the previous methods to determine off-road vehicle mobility are classified according to their solution methods and discussed under the topic of Terramechanics.

Chapter 3 introduces the approach to the off-road vehicle mobility problems and basic assumptions of the analytical model in the proposed method.

In Chapter 4, equations of the vehicle loads are developed to be able to construct a full method for the mobility determination according to the some basic vehicle parameters as well.

Chapter 5 discusses the shear strength between the soil and the tracks or the wheels of vehicles and provides a condition equation in the method for mobility loss because of vehicle slip but not failure of soil.

Chapter 6 describes a whole analytical model in details and comes up with the mobility reduction factors. The derivation of each reduction factor for the components of the bearing capacity equation are explained in details. Afterwards, the mobility bearing capacity equation is derived by introducing these factors in the classical bearing capacity equation.

Chapter 7 summarizes the whole method of analysis and presents a computation scheme for computer programs.

In Chapter 8, the results of proposed methods for some example cases are provided. The results of proposed method for calculation of seismic bearing capacity of frictionless soils is compared with present methods. Then several numerical illustrations of the new mobility model is presented by providing the results of analysis for different type of vehicles and various terrain parameters.

# 2. LITERATURE REVIEW

## 2.1. Bearing Capacity of Soils

### 2.1.1. Introduction

The stability of foundations depends on the bearing capacity and the settlement of the soil beneath the foundation. Bearing capacity is defined as the maximum average contact pressure between the structure and the soil which should not produce shear failure in soil. In simpler terms, bearing capacity is the capacity of soil to support the loads applied to the ground. So, the shearing resistance of the soil provides the bearing capacity and the consolidation properties determine the settlement and these two conditions together determine the stability of the foundation.

There are various bearing capacity definitions that relate to different design considerations. For example, for the sake of practicality, the two independent criteria of shear failure and settlement problem have been molded into a single parameter called the allowable bearing capacity ($q_{all}$). It is the maximum permissible pressure that can be applied to the soil without creating neither shear failure nor excessive settlements. On the other hand, the ultimate bearing capacity ($q_u$ or $q_f$) is the theoretical maximum pressure which can be supported without shear failure of the soil.

Clearly, allowable bearing capacity inherently includes a factor of safety whereas ultimate bearing capacity does not. Therefore, this research focuses on the ultimate bearing capacity and accordingly the underlying mechanisms of bearing capacity problem will be discussed. Here, some of the well-known ultimate bearing capacity determination methods will be introduced.

The ultimate bearing capacity of a foundation may be determined by analytical methods, fields tests or building codes which are based on experience. Here, a summary of analytical methods (bearing capacity theories) will be introduced.

### 2.1.2. Failure Mechanisms

Bearing capacity failure modes can be basically divided into three broad classes. These are general shear failure, local shear failure, and punching shear failure as shown in Fig. 2.1.

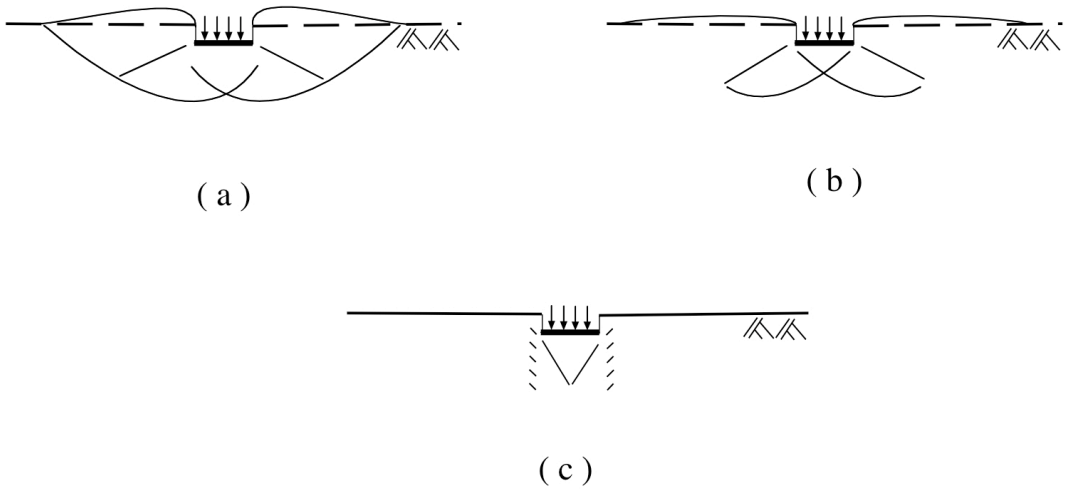



Figure 2.1. Modes of failure: (a)general shear, (b)local shear, (c)punching shear

General shear failure is generally observed in soils of low compressibility. Continuous failure surfaces develop between the edges of footing and ground surface. Plastic equilibrium is initially reached in the soil around the footing edges and spreads throughout the failure surface. Final slip movement would occur on one side. However, heaving is observed on both sides (Fig. 2.1.a).

In case of local shear failure, the state of plastic equilibrium is partially developed with significant compression of the soil. Failure surfaces do not reach the ground surface, large settlements occur with slight heaving of ground however tilting of the footing is not expected (Fig. 2.1.b).

Punching shear failure occurs in highly compressible soils. There is no tilting of footing or heaving of ground (Fig. 2.1.c)

Large settlements accompanying local shear and punching shear failure modes are not acceptable. Unfortunately, there is no clear definition of bearing capacity in these types of failure modes. However, in case of general shear failure, the state of plastic equilibrium is fully developed therefore, the ultimate bearing capacity is well defined. [1]

### 2.1.3. Bearing Capacity Theories

There are a number of theories for calculating the ultimate bearing capacity of soils analytically. The most commonly used ones are:

#### 2.1.3.1. Prandtl's Bearing Capacity Theory

Prandtl (1921) [2] combined Mohr's stress theory with Airy's stress function and derived a second order differential equation which he solved to obtain an analytical expression for ultimate bearing stress at failure. The underlying assumptions used in this solution are:

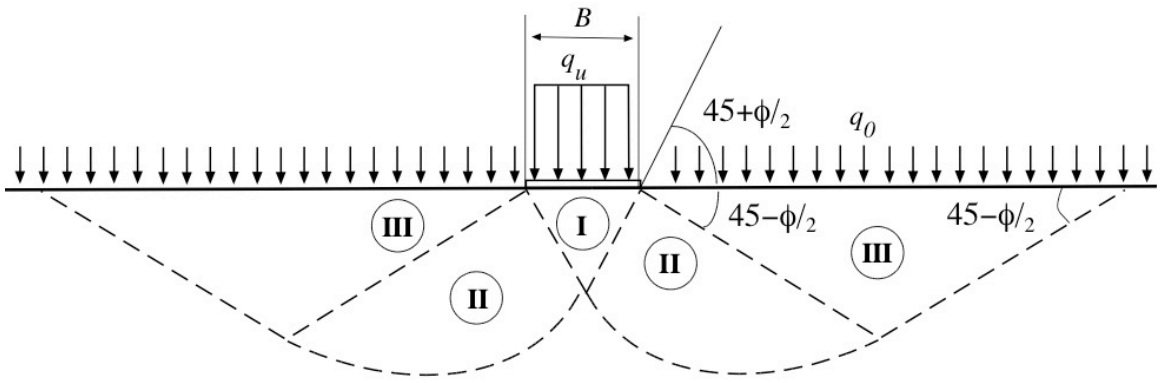



Figure 2.2. Prandtl's failure mechanism

1. Continuous footing is applying uniform pressure to the soil.
2. Homogenous and isotropic soil has a perfectly plastic stress-strain relationship.
3. Soil is weightless, purely cohesive or $c$-$\phi$ soil.
4. The shear resistance of the soil above the base of the footing is neglecting.
5. The failure line is composed of two straight lines (Zone I and Zone III) and a log-spiral line (Zone II) as shown in Fig.2.2.
6. Zone I beneath the base of the footing behaves as a rigid body..
7. The base of the footing is smooth.
8. The principle of superposition is valid.

The Prandtl solution for the bearing capacity of soils according to these assumptions is:

$$q_u = c\cot\phi[\exp(\pi\tan\phi)\tan^2(45^o+\phi/2)-1]+[q_0[\exp(\pi\tan\phi)\tan^2(45^o+\phi/2)] \quad (2.1)$$

where $q_0$ is surcharge pressure, $\phi$ internal friction angle of the soil and $c$ is the cohesive strength of the soil.

2.1.3.2. Terzaghi's Bearing Capacity Theory

In 1943 Terzaghi presented a solution to the bearing capacity problem that was based on the Prandtl solution. However Terzaghi modified the solution to account for the deficiencies inherent in the Prandtl's assumptions as applied to the soils. Prandtl equation is improved by adding an additional term to take into account the component of the bearing capacity due to self weight of the soil. Terzaghi, also assumed that the friction acts along the interface between the soil and the footing. As a result the base angles of Zone I are $\phi$, not $45+\phi/2$ (Fig.2.3). Furthermore Zone I is in elastic state and moves with footing. Considering the equilibrium of the Zone I, Terzaghi presented the following bearing capacity expression for general bearing capacity failure [3]:

$$q_u = \frac{1}{2}\gamma B N_\gamma s_\gamma + cN_c s_c + q_0 N_q s_q \quad (2.2)$$

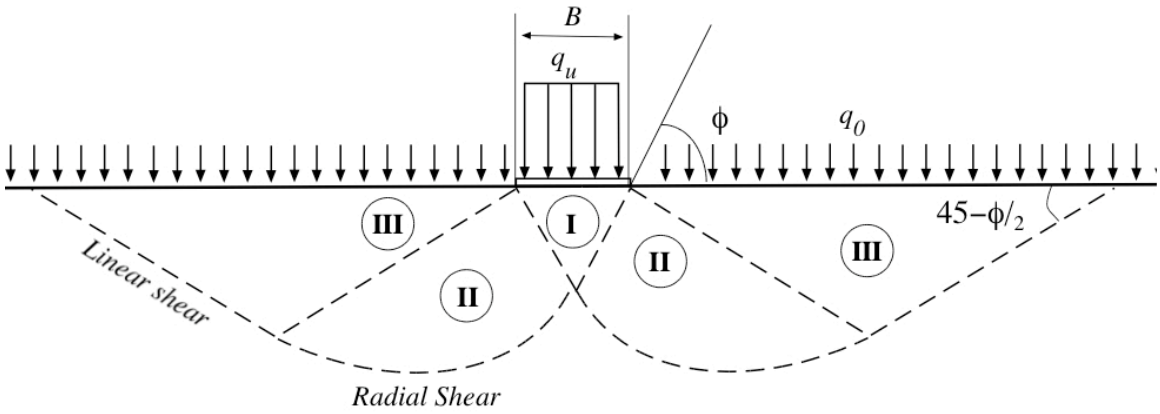



Figure 2.3. Terzaghi's failure mechanism

where $N_\gamma$, $N_c$ and $N_q$ are bearing capacity factors for weight of the soil, cohesion and surcharge, respectively. Table 2.1 shows the equations for the bearing capacity factors. As shown, these equations are dependent only on the value of $\phi$. Moreover, $B$ is the width of the footing and $s_\gamma$, $s_c$ and $s_q$ are the semi-empirical shape factors which are used in extending the problem to three dimensions. Terzaghi proposed shape factors for only circular and square areas.

2.1.3.3. Meyerhof's Bearing Capacity Theory

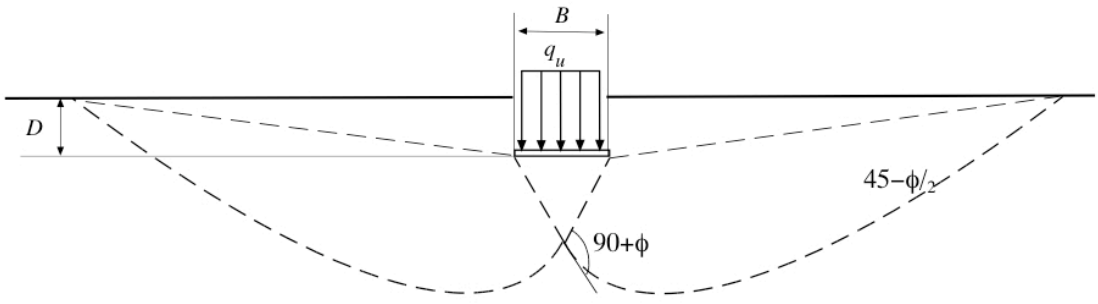



Figure 2.4. Meyerhof's failure mechanism

Meyerhof (1953, 1963) improved Terzaghi's bearing capacity equation by taking into account the shear strength of the soil above the base of the footing. He assumed a

failure mechanism similar to Terzaghi's but extended it up to ground surface as shown in Fig.2.4.[4],[5]

2.1.3.4. Brinch Hansen's Bearing Capacity Theory

Brinch Hansen (1970) proposed a revised and extended formula for bearing capacity. The strength of the soil above the base of the foundation and also the decrease in the bearing capacity because of the inclination of the load are taken into account. [6]:

$$q_u = \frac{1}{2}\gamma B N_\gamma s_\gamma d_\gamma i_\gamma + c N_c s_c d_c i_c + q_0 N_q s_q d_q i_q \tag{2.3}$$

where $d_\gamma$, $d_c$ and $d_q$ are depth factors; $i_\gamma$, $i_c$ and $i_q$ are inclination factors (Table 2.3 and Table 2.4).

2.1.3.5. Veśic's Bearing Capacity Theory

Veśic (1975) proposed essentially same method as Hansen's with a slightly different $N_\gamma$ equation (see Table 2.1) and also different inclination factors (see Table 2.4).

### 2.1.4. Summary

The bearing capacity factors used in various bearing capacity theories are summarized in Tables 2.1, 2.2, 2.3 and 2.4:

## 2.2. Dynamic Fluidization of Soils

### 2.2.1. Seismic Fluidization Concept

Richards *et al.* (1990) [8] proposed a different approach to behavior of soils under seismic activity. According to this approach, imposed accelerations at some critical

Table 2.1. Bearing capacity factors of various theories

| | |
|---|---|
| Terzaghi (1943) | $N_q = \frac{a^2}{2\cos^2(45+\phi/2)}$ $\quad a = e^{0.75\pi-0.5\phi}\tan$<br>$N_c = (N_q - 1)\cot\phi \quad (N_c = 1.5\pi + 1 \text{ for } \phi = 0)$<br>$N_\gamma = \frac{\tan\phi}{2}(\frac{K_{p\gamma}}{\cos^2\phi} - 1)$ |
| Meyerhof (1953, 1963) | $N_q = e^{\pi\tan\phi}\tan^2(45 + \frac{\phi}{2})$<br>$N_c = (N_q - 1)\cot\phi \quad (N_c = \pi + 2 \text{ for } \phi = 0)$<br>$N_\gamma = (N_q - 1)\tan(1.4\phi)$ |
| Brinch Hansen (1970) | $N_q = e^{\pi\tan\phi}\tan^2(45 + \frac{\phi}{2})$<br>$N_c = (N_q - 1)\cot\phi \quad (N_c = \pi + 2 \text{ for } \phi = 0)$<br>$N_\gamma = 1.8(N_q - 1)\tan\phi$ |
| Veśic (1975) | $N_q = e^{\pi\tan\phi}\tan^2(45 + \frac{\phi}{2})$<br>$N_c = (N_q - 1)\cot\phi \quad (N_c = \pi + 2 \text{ for } \phi = 0)$<br>$N_\gamma = 2(N_q + 1)\tan\phi$ |

Table 2.2. Shape factors of various theories for rectangular footings

| | $s_c$ | $s_q$ | $s_\gamma$ |
|---|---|---|---|
| Meyerhof (1953, 1963) | $1 + 0.2K_p\left(\frac{B}{L}\right)$ | $1 + 0.1K_p\left(\frac{B}{L}\right)$ | $1 + 0.1K_p\left(\frac{B}{L}\right)$ |
| Brinch Hansen (1970) | $1 + \left(\frac{N_q}{N_c}\right)\left(\frac{B}{L}\right)$ | $1 + \left(\frac{B}{L}\right)\tan\phi$ | $1 - 0.4\left(\frac{B}{L}\right)\sin\phi \geqslant 0.6$ |
| Veśic (1975) | $1 + \left(\frac{N_q}{N_c}\right)\left(\frac{B}{L}\right)$ | $1 + \left(\frac{B}{L}\right)\sin\phi$ | $1 - 0.4\left(\frac{B}{L}\right)\sin\phi \geqslant 0.6$ |

$L$: Length of the footing

Table 2.3. Depth factors of various theories

| | $d_c$ | $d_q$ | $d_\gamma$ |
|---|---|---|---|
| Meyerhof (1953, 1963) | $1+0.2\sqrt{K_p}\,(\frac{D}{B})$ | $1+0.1\sqrt{K_p}\,(\frac{D}{B})$ | $1+0.1\sqrt{K_p}\,(\frac{D}{B})$ |
| Brinch Hansen (1970) | $1+0.4k$ | $1+2\tan\phi(1-\sin\phi)^2k$ | 1 |
| Veśic (1975) | $1+0.4k$ | $1+2\tan\phi(1-\sin\phi)^2k$ | 1 |
| | $k=\frac{D}{B}$ for $\frac{D}{B}\leqslant 1$ $\quad k=\tan^{-1}\frac{D}{B}$ for $\frac{D}{B}>1$ | | |
| | $D$: Depth of the soil above the base of the footing | | |

Table 2.4. Inclination factors of various theories

| | $i_c$ | $i_q$ | $i_\gamma$ |
|---|---|---|---|
| Meyerhof (1953, 1963) | $1-\left(\frac{\theta^o}{90^o}\right)^2$ | $1-\left(\frac{\theta^o}{90^o}\right)^2$ | $1-\left(\frac{\theta^o}{\phi^o}\right)^2$ |
| Brinch Hansen (1970) | $i_q-\frac{1-i_q}{N_q-1}$ | $\left(1-\frac{0.5P_h}{P_v+A_ec_a\cot\phi}\right)^5$ | $\left(1-\frac{0.7P_h}{P_v+A_ec_a\cot\phi}\right)^5$ |
| Veśic (1975) | $i_q-\frac{1-i_q}{N_q-1}$ | $\left(1-\frac{P_h}{P_v+A_ec_a\cot\phi}\right)^m$ | $\left(1-\frac{P_h}{P_v+A_ec_a\cot\phi}\right)^{m+1}$ |
| $\theta^o=\tan^{-1}\frac{P_h}{P_v}$ $P_h$ horizontal, $P_v$ vertical components of the load | | | |
| $A_e$: Effective contact area at the base of the foundation | | | |
| $c_a$: Adhesion of the foundation soil to the footing base | | | |
| $m=(2+B/L)/(1+B/L)$ | | | |

level changes the state of soil as a whole and general plastification takes place. Consequently flow can be possible within a bounded range of directions. This phenomenon is different from a local plastic flow because it takes place over a broad region. In order to distinguish this difference, authors prefer to call it "seismic shear fluidization" or more concisely "fluidization".

Another phenomenon related to strength of soils under seismic acceleration is liquefaction. Initial fluidization can lead to an increase in pore water pressure, which can lead to liquefaction. So liquefaction can be tought as a limiting case of fluidization. However, in most cases two situations are quite different. In shear fluidization, flow take place at finite levels of effective stress, whereas when liquefaction occurs, the pore water pressure increase reduces the effective stress to zero. Shear fluidization can take place in dry soil in which no pore water is present and loose and dense soils will dynamically fluidize even if they do not liquefy. Also liquefaction can be catastrophic with characteristic boiling, local flooding and sudden failures of foundations. Fluidization on the other hand is more insidious. Displacements are only periodic and therefore appear slow in comparison even if, eventually, they cause major damage.[8]

### 2.2.2. Mechanics of Fluidization

Richards *et al.* (1990) derived a free field stress solution for granular soils under moderate seismic loading where the soil is idealized as an elastic-perfectly plastic material with a Mohr-Coulomb yield criterion. According to this stress solution shear stress varies linearly with the acceleration[8].

Using the same solution but without considering vertical acceleration , a homogeneous horizontal layer of granular soil with unit weight, $\gamma$,subjected to horizontal acceleration $k_h g$ will be as shown in Figure 2.5.

At rest condition, the static stress field in the principle x-y plane is:

$$\sigma_z = \gamma z; \qquad \sigma_x = K\gamma z; \qquad \tau_{zx} = 0 \tag{2.4}$$

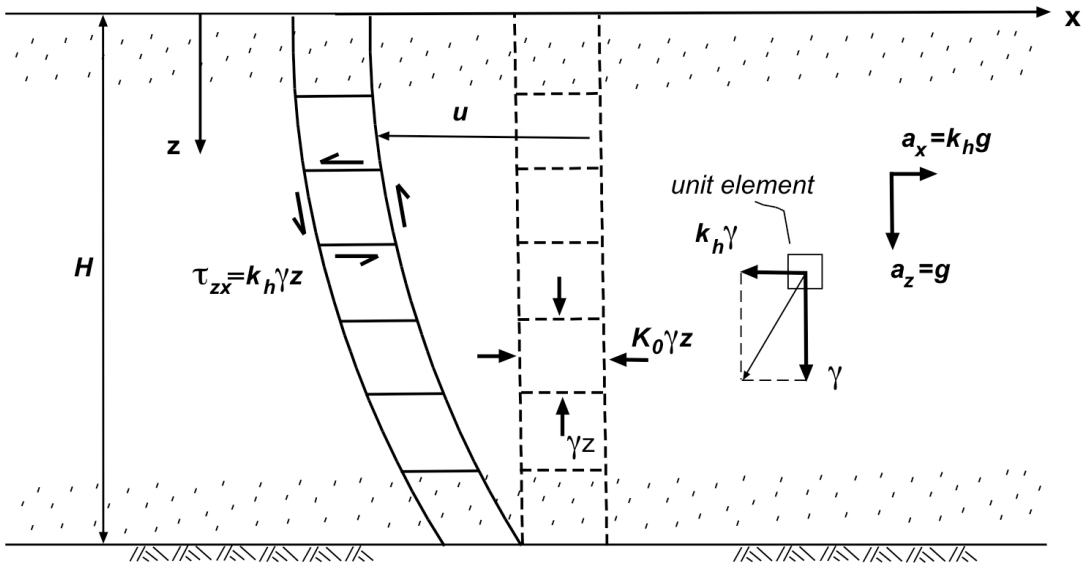



Figure 2.5. Dynamic free field

where $K$ is the coefficient of lateral earth pressure, z is the depth of the element. At rest or in the elastic range, the coefficient of lateral earth pressure $K$ can be related approximately to the internal friction angle $\phi$ by the following formula proposed by Jacky [9]:

$$K = K_0 = 1 - \sin\phi \tag{2.5}$$

2.2.2.1. Initial Fluidization: If uniform horizontal acceleration is now applied to the soil as in Figure 2.3, two- dimensional differential equations of equilibrium will become:

$$\frac{\partial \sigma_x}{\partial x} + \frac{\partial \tau_{xz}}{\partial z} = k_h\gamma \tag{2.6}$$

$$\frac{\partial \tau_{xz}}{\partial x} + \frac{\partial \sigma_z}{\partial z} = \gamma \tag{2.7}$$

with the solution:

$$\sigma_x = K\gamma z; \qquad \sigma_z = \gamma z; \qquad \tau_{xz} = -k_h \gamma z \tag{2.8}$$

Essentially this dynamic solution for the free field is the static free-field solution with pure shear introduced by the horizontal acceleration. The stress-strain relationship is assumed to be linear where longitudinal strain in x direction is zero ($\epsilon_x = 0$). and the deformation $u$ due to shear is:

$$u = -k_h \frac{\gamma(H^2 - z^2)}{2G} \tag{2.9}$$

in terms of the shear modulus $G$, is parabolic as shown Figure 2.3 [8]

Richards *et al.* (1990) [8] explained the stress path that the free field must follow under seismic load with assumptions of the granular soil is an elastic, perfectly plastic material and suitable for Mohr - Coulomb failure criterion. The effect of increasing the horizontal acceleration is best illustrated by the use of Mohr's circle. (Figure 2.6).

As the horizontal acceleration increases, the shear stress in the soil increases with a constant lateral pressure coefficient $K = K_0$ until the Mohr Circle of stress reaches the Mohr-Coulomb failure line. This state is called initial fluidization.

Initial stress state on a unit element before the application of horizontal acceleration is shown in the figure with dashed circle and the stress at the horizontal surface of the unit element is at point A with a value of $\sigma_z = \gamma z$. Addition of horizontal acceleration will produce a shear stress component, $\tau = k_h \gamma z$, which will move the stress point along a stress path vertically upward (or downward depending on the sign) and the diameter of the mohr circle will increase about a fixed axis (with the assumption of lateral earth pressure remains constant). This increase in the diameter of the Mohr circle is limited by the point that the circle touches the failure line and stress path

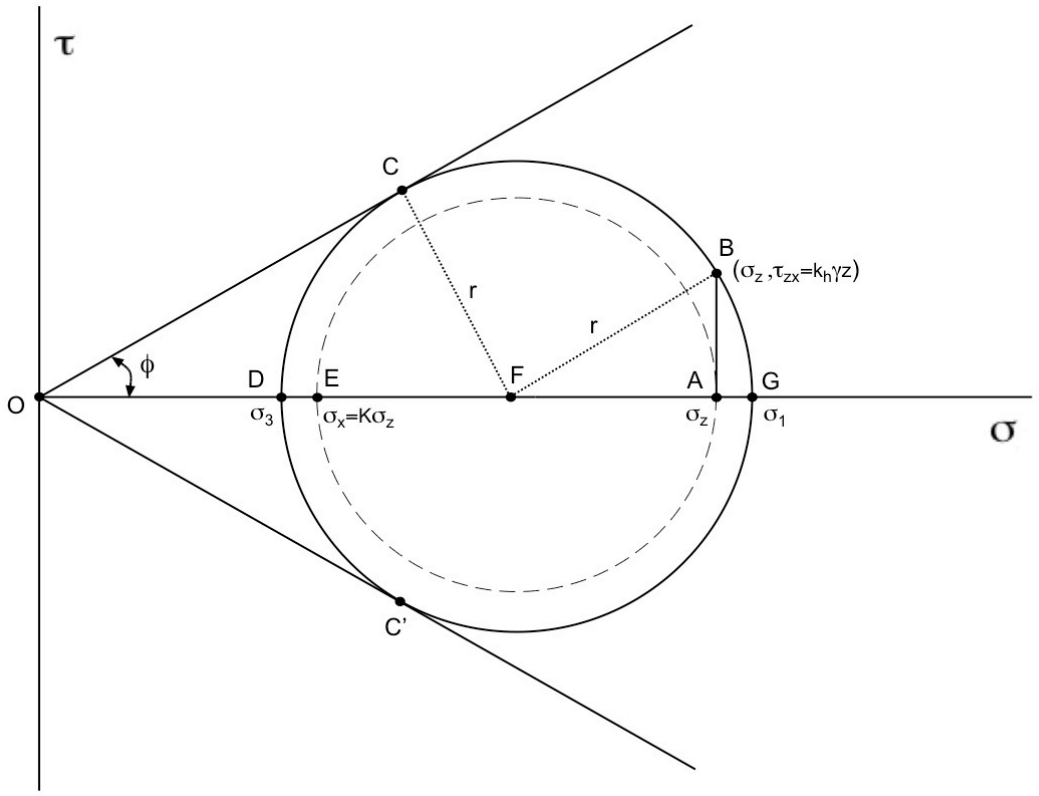



Figure 2.6. Mohr circle representation of initial fluidization

reaches to point B. [8] At this stage, soil has fluidized. From the geometry of Fig. 2.6:

$$|OF| \sin\phi = \sqrt{|FA|^2 + |AB|^2} = r \tag{2.10}$$

in terms of $K$, $\gamma$, $z$, $k_h$ and $\phi$:

$$\left[\frac{1+K}{2}\gamma z\right] \sin\phi = \left\{ \left[\frac{1-K}{2}\gamma z\right]^2 + (k_h \gamma z)^2 \right\}^{1/2} \tag{2.11}$$

If Eq. 2.11 is solved for $k_h$, resulting equation will be:

$$k_h = \frac{1}{2}\sqrt{(K+1)^2 \sin^2\phi - (K-1)^2} \tag{2.12}$$

As mentioned previously up to failure condition, in other words in elastic range, lateral

earth pressure $K$ can be defined by Jacky's formula:

$$K = K_0 = 1 - \sin\phi \tag{2.5}$$

Using Eq. 2.12 and Eq.2.5, horizontal acceleration, $k_h$, that causes initial fluidization of the soil can be expressed in terms of internal friction angle, $\phi$:

$$k_h = \frac{\sin\phi}{2}\left[(\sin\phi - 3)(\sin\phi - 1)\right]^{1/2} \tag{2.13}$$

The orientation of the major and minor planes and slip surface can be found on Mohr circle (Figure 2.7). At point B, stresses act on horizontal surface so a horizontal line from that point meets the circle at the origin of the planes P. The orientation of the major and minor principle planes are found by drawing lines from point P through the principle stresses at points D and G. Similarly, the slip surface orientations may be found by drawing lines from the origin of planes through the failure points C and C'. [8]

The counterclockwise orientations of the slip surfaces $\rho_z$ and $\rho_x$ with respect to coordinate axis will be:

$$\rho_z = 45 + \frac{\phi}{2} - \alpha \tag{2.14}$$

$$\rho_x = 45 - \frac{\phi}{2} - \alpha = \rho_z - \phi \tag{2.15}$$

where $\alpha$ is the clockwise rotation angle of principle planes. An illustration of slip planes during initial fluidization is shown in Fig. 2.8.

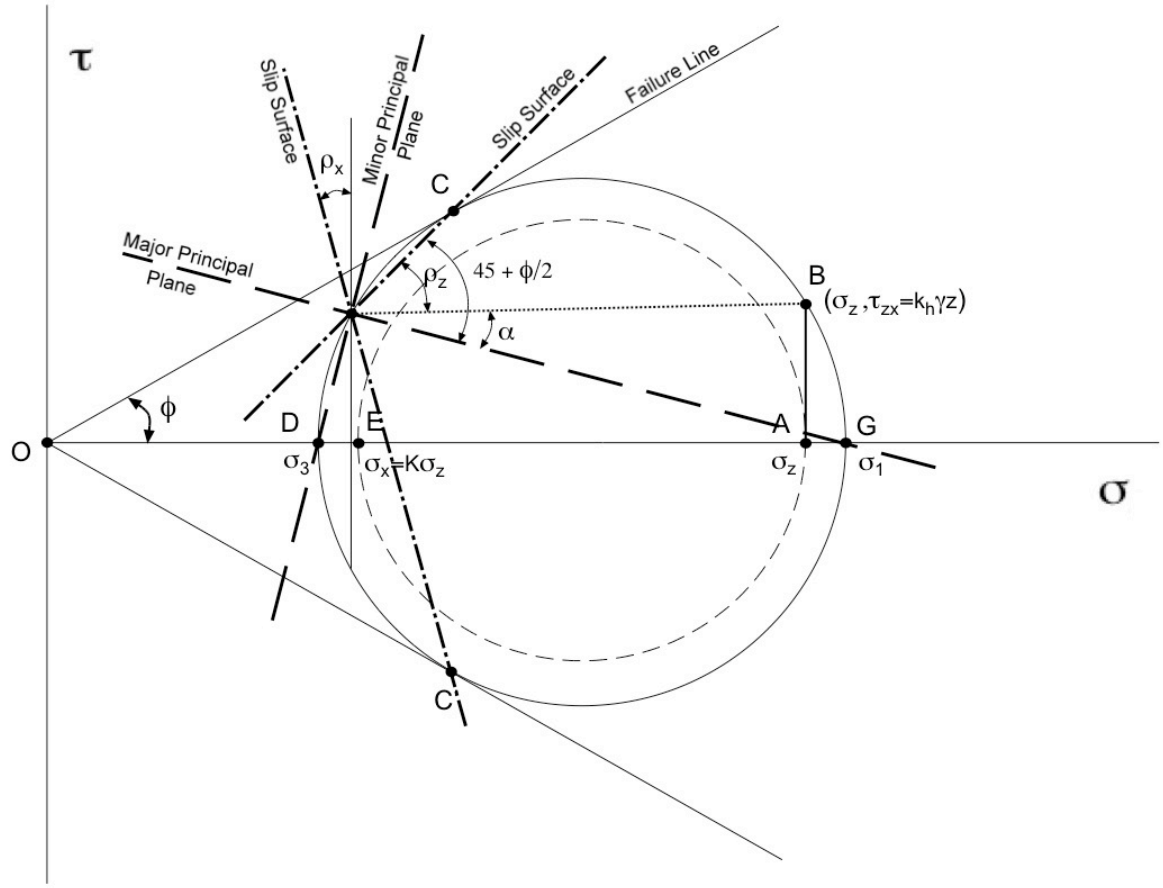



Figure 2.7. Orientation of slip surfaces and principle planes

2.2.2.2. Intermediate Fluidization: The potential slip surfaces in the free field at this condition are inclined with respect to the horizontal direction (Fig. 2.8), but due to the infinite lateral boundary, there is no failure surface possible at this yield condition and the shear stress in the soil continues to increase as the acceleration increases. Thus, the value of the lateral earth pressure coeffcient, K, must also increase with increasing horizontal acceleration to maintain equilibrium and to satisfy the Mohr-Coulomb yield criterion. Fig.2.9 shows the effect of increasing horizontal acceleration on the stress field.

As Mohr circle grows, stress on the horizontal plane will move on a plane vertically upward from point B. In intermediate fluidization stage, it reaches point B', that is the

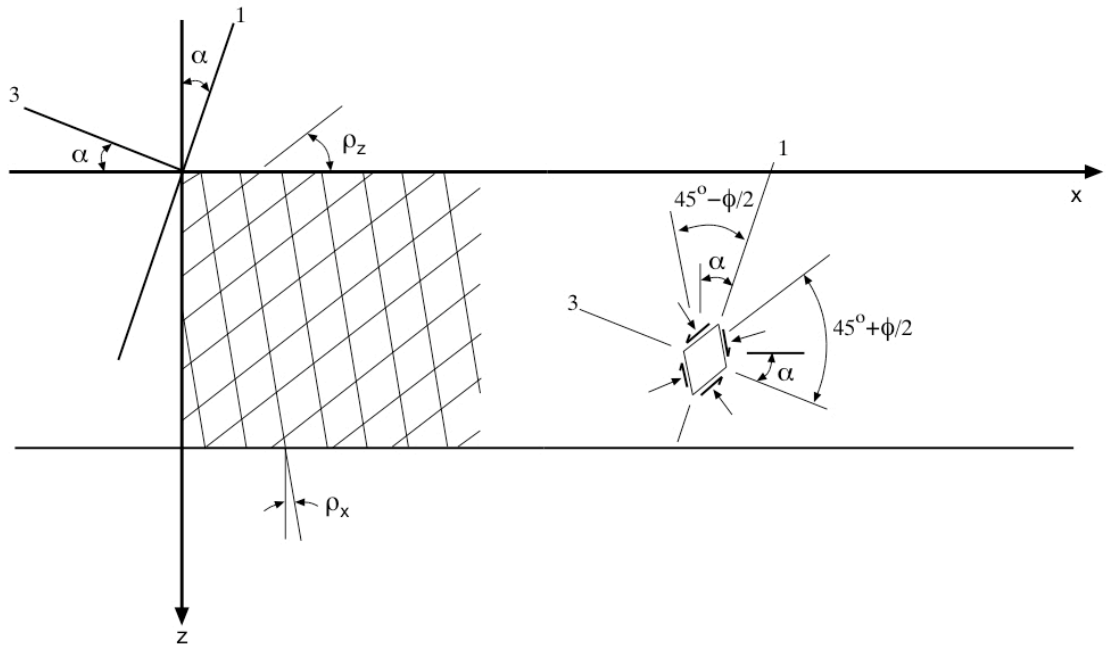



Figure 2.8. Initial slip field

top point of the circle and point A becomes the center of the circle. Here, K=1 and $\sigma_x = \sigma_z$. Slip surface direction lines have rotated clockwise as shown in Fig.2.9.

2.2.2.3. General Fluidization: Further increases in horizontal acceleration can only be sustained until the stress path reaches the failure line, which it does at point B" and slip surface direction lines continue to rotate clockwise as shown in Fig.2.10. The circle tangent to the failure line at B" is the largest circle possible. At this stage, one of the slip surfaceshas become horizontal. Any subsequent increase in horizontal acceleration of the underlying rock or subsrate merely leads to differential motion between it and the soil. The soil can not sustain any further acceleration. This stage is called general fluidization.[8]

At this point soil mass acts very much like a viscous fluid with bounds on the directions in which shear flow can occur. Horizontal acceleration and corresponding lateral earth coefficient at general fluidization can be calculated from the geometry of

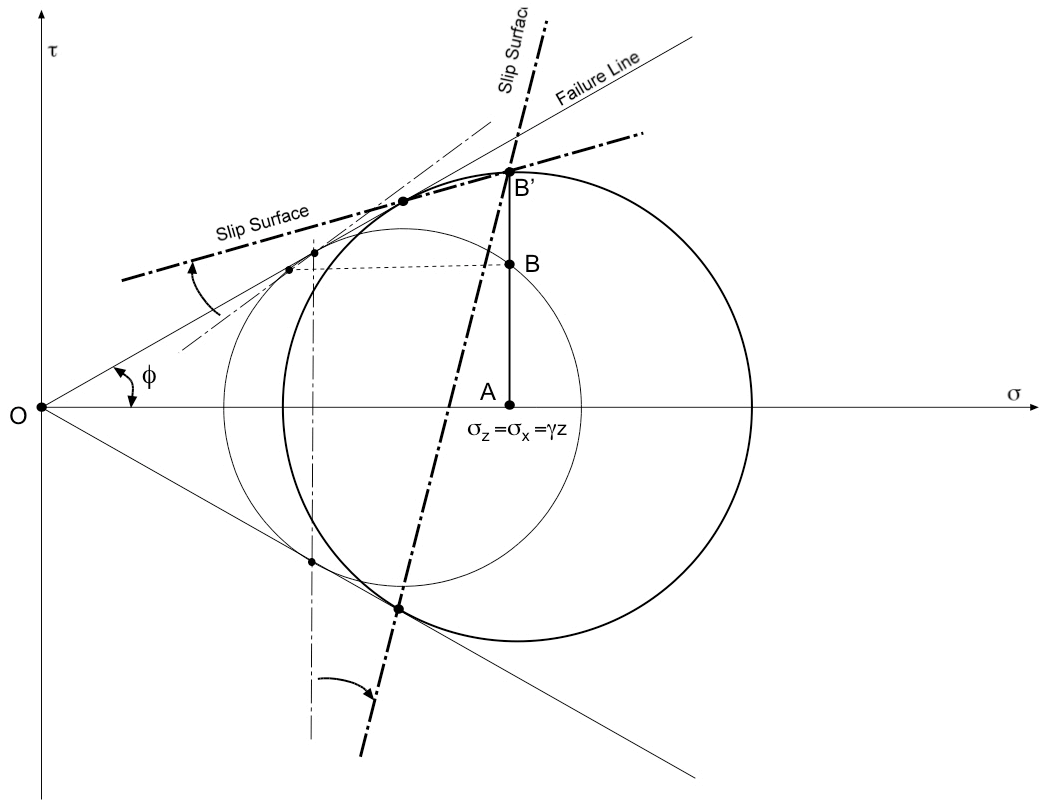



Figure 2.9. Intermediate fluidization

Mohr circle:

$$\tan\phi = \frac{|B''A|}{|OA|} = \frac{\tau_{zx}}{\gamma z} = \frac{k_h \gamma z}{\gamma z} = k_h \tag{2.16}$$

$$K_F = \frac{\sigma_x}{\sigma_z} = \frac{|EO|}{|OA|} = \frac{\frac{r}{\sin\phi} + r\sin\phi}{\frac{r}{\sin\phi} - r\sin\phi} = \frac{1+\sin^2\phi}{1-\sin^2\phi} = \frac{K_A + K_P}{2} \tag{2.17}$$

### 2.2.3. Fluidization of $c-\phi$ Soils

When the fluidization concept described in Section 2.4 is extended to $c-\phi$ soils, Mohr circle change will be as shown in Fig.2.11:

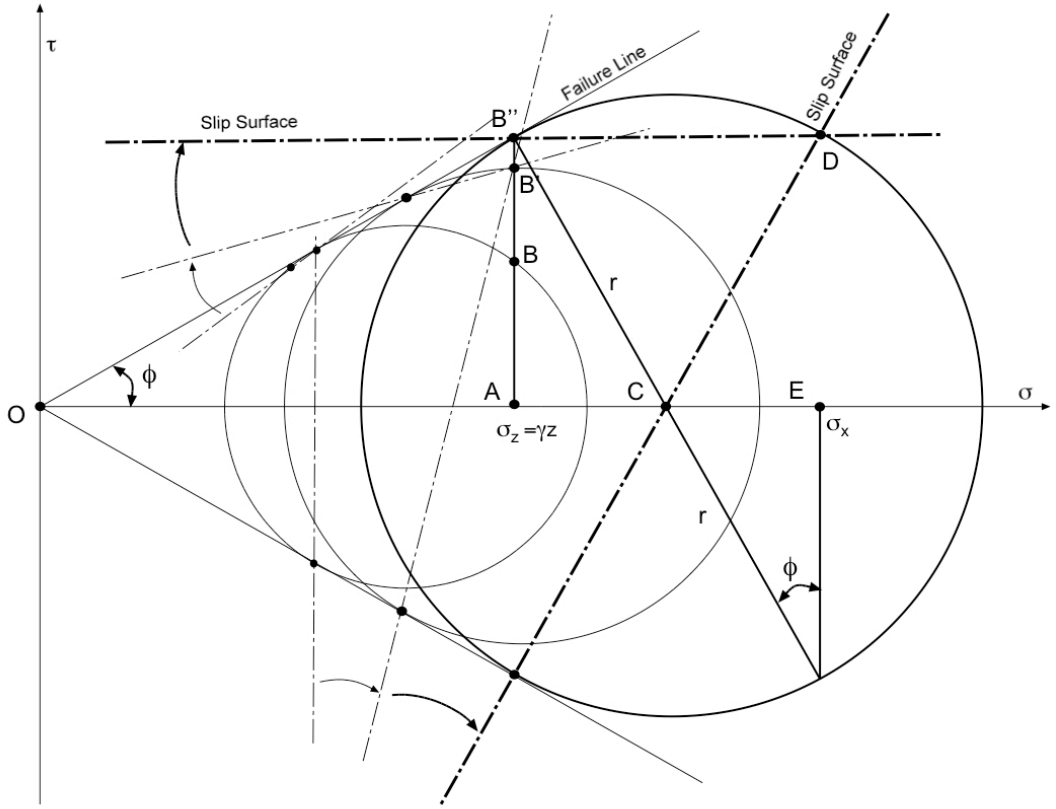



Figure 2.10. General fluidization

The lateral earth pressure coefficient $K$, can be calculated from Fig.2.11:

$$|HF| \sin\phi = \sqrt{|FA|^2 + |AB|^2} = r \tag{2.18}$$

in terms of $K$, $\gamma$, $z$, $k_h$, $\phi$ and $c$:

$$\left[c \cot\phi + \frac{1+K}{2}\gamma z\right]^2 \sin^2\phi = \left[\frac{1-K}{2}\gamma z\right]^2 + (k_h \gamma z)^2 \tag{2.19}$$

in open form:

$$\frac{c^2 \cos^2\phi}{\gamma^2 z^2} + \frac{c \cos\phi \sin\phi (1+K)}{\gamma z} + \left[\frac{1+K}{2}\right]^2 \sin^2\phi = \left[\frac{1-K}{2}\right]^2 + k_h^2 \tag{2.20}$$

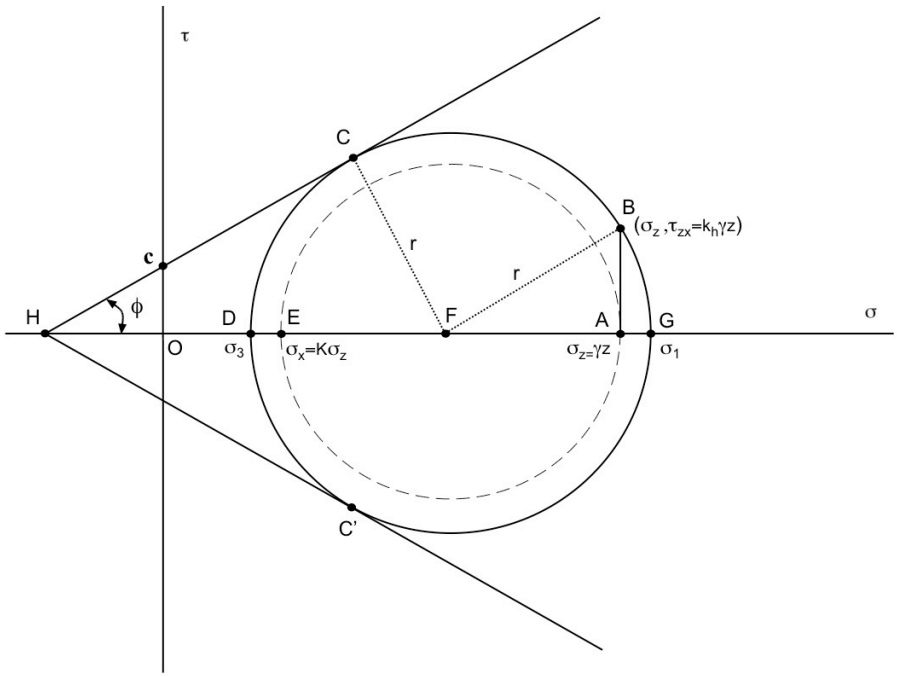



Figure 2.11. Mohr circle of $c-\phi$ soils under seismic loading

by rearranging Eq.2.20:

$$K^2 - K\left[\frac{4c\tan\phi}{\gamma z} + \frac{2(\sin^2\phi+1)}{\cos^2\phi}\right] - \left[\left[\frac{2c}{\gamma z}\right]^2 + \frac{4c}{\gamma z}\tan\phi - \frac{4k_h^2}{\cos^2\phi} - 1\right] = 0 \quad (2.21)$$

which when solved K gives:

$$\begin{aligned} K = {} & \frac{\sin^2\phi+1}{\cos^2\phi} + \frac{2c\tan\phi}{\gamma z} \\ & \pm\sqrt{\left[\frac{2c\tan\phi}{\gamma z} + \frac{\sin^2\phi+1}{\cos^2\phi}\right]^2 + \left[\frac{2c}{\gamma z}\right]^2 + \frac{4c}{\gamma z}\tan\phi - \frac{4k_h^2}{\cos^2\phi} - 1} \end{aligned} \quad (2.22)$$

The root with positive sign gives the value of passive earth pressure coefficient $K_{PE}$, and the root with negative sign gives the active earth pressure coefficient $K_{AE}$

at point B. [10]

$$K_{PE} = \frac{\sin^2\phi + 1}{\cos^2\phi} + \frac{2c\tan\phi}{\gamma z} + \sqrt{\left[\frac{2c\tan\phi}{\gamma z} + \frac{\sin^2\phi + 1}{\cos^2\phi}\right]^2 + \left[\frac{2c}{\gamma z}\right]^2 + \frac{4c}{\gamma z}\tan\phi - \frac{4k_h^2}{\cos^2\phi} - 1} \tag{2.23}$$

$$K_{AE} = \frac{\sin^2\phi + 1}{\cos^2\phi} + \frac{2c\tan\phi}{\gamma z} - \sqrt{\left[\frac{2c\tan\phi}{\gamma z} + \frac{\sin^2\phi + 1}{\cos^2\phi}\right]^2 + \left[\frac{2c}{\gamma z}\right]^2 + \frac{4c}{\gamma z}\tan\phi - \frac{4k_h^2}{\cos^2\phi} - 1} \tag{2.24}$$

Slip surface orientations to the horizontal and vertical planes $(\rho_z, \rho_x)$ can be found by using Eq.2.14 and Eq.2.15 respectively. From the geometry of Mohr circle in Fig. 2.11 $\alpha$ can be calculated.[10]

For the active case:

$$\tan\alpha_A = \frac{2k_h}{1 - K_{AE} + \sqrt{(1 - K_{AE})^2 + 4(k_h)^2}} \tag{2.25}$$

For the passive case:

$$\tan\alpha_P = \frac{2k_h}{K_{PE} - 1 + \sqrt{(K_{PE} - 1)^2 + 4(k_h)^2}} \tag{2.26}$$

## 2.3. Seismic Bearing Capacity

### 2.3.1. Static Bearing Capacity Calculations by Coulomb Mechanism

Richards et al. (1993) present a simple Coulomb mechanism to obtain seismic bearing capacity for cohesionless soils. In this analysis the seismic bearing capacity factors and their ratios to static values are calculated in order to get reduction in bearing capacity for a given horizontal acceleration. Reduction in bearing capacity is due to both seismic degradation of soil strength and the lateral inertial forces transmitted by shear to soil through the structure and surcharge. [11]

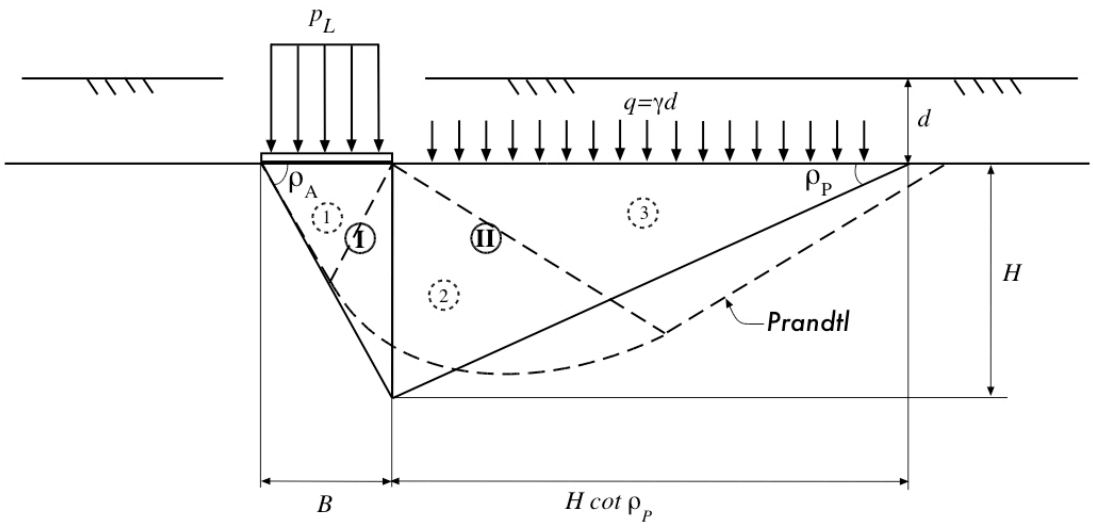



Figure 2.12. Comparison of Prandtl and Coulomb types failure mechanisms

The comparison of slip line fields obtained by Prandtl (1921) solution [2] and simple Coulomb type mechanism suggested by Lambe and Whitman (1969) [12] is shown in Fig.2.12. In addition to Lambe and Witman solution Richards et al. (1993) includes shear friction between two Coulomb wedges. The basic Prandtl failure pattern has three regions:

1. an active wedge of soil moving downward

2. a logaritmic radial-fan transition zone that rotates about point A,
3. a passive wedge that moves upward

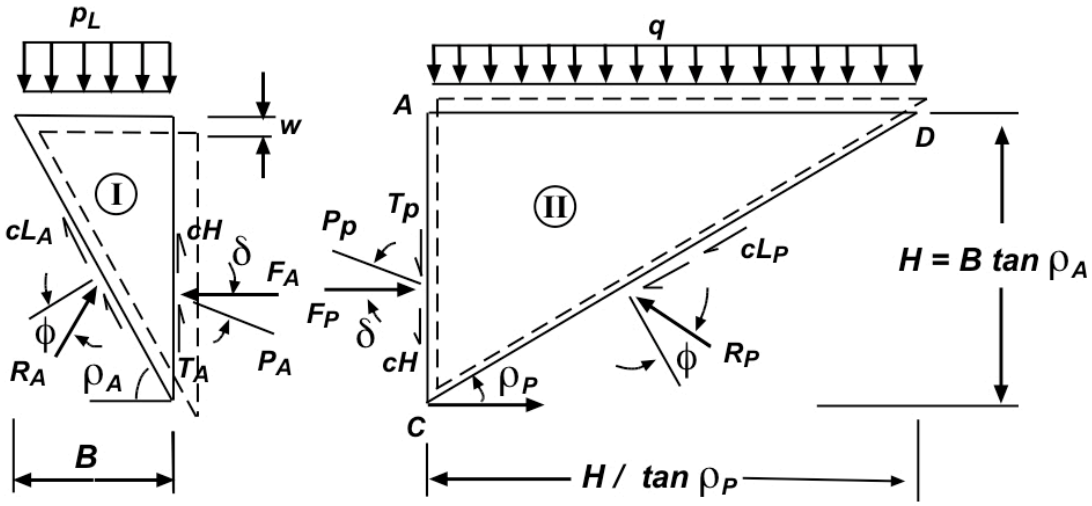



Figure 2.13. Static forces acting on Coulomb wedges

Coulomb type mechanism consists of two wedges, active (I) and passive (II) zones. By assuming an imaginary retaining wall between the wedges and from the force equilibrium of these two wedges (Fig.2.13), bearing capacity factors for each component of strength can be derived. Considering first only the surcharge by setting weight and cohesion of the soil to zero:[11]

For $c = \gamma = 0$ :

$$F_A^q = K_A \cdot p_L^q \cdot H \tag{2.27}$$

$$F_P^q = K_P \cdot q \cdot H \tag{2.28}$$

where $p_L^q$ is the ultimate foundation load when it is supported by only surcharge load $q$. $K_A$ and $K_P$ active and passive earth pressure coefficients respectively. At failure $F_A^q = F_P^q$ :

$$p_L^q = q\frac{K_P}{K_A} \tag{2.29}$$

for $p_L^q = q \cdot N_q$:

$$N_q = \frac{K_P}{K_A} \tag{2.30}$$

Similarly, considering only the contribution of the weight of the soil below footing and ignoring the surcharge and cohesion:

For $c = q = 0$ :

$$F_A^\gamma = K_A \cdot p_L^\gamma \cdot H + K_A \cdot \frac{1}{2} \cdot \gamma \cdot H^2 \tag{2.31}$$

$$F_P^\gamma = K_P \cdot \frac{1}{2} \cdot \gamma \cdot H^2 \tag{2.32}$$

where $p_L^\gamma$ is the ultimate foundation load when it is supported by only the weight of the soil. At failure $F_A^\gamma = F_P^\gamma$ and $H = B \cdot \tan \rho_A$:

$$p_L^\gamma = \frac{1}{2} \cdot \gamma \cdot B \cdot \tan \rho_A \cdot \left[ \frac{K_P}{K_A} - 1 \right] \tag{2.33}$$

where $\rho_A$ is the critical angle of rupture on active wedge. For $p_L^\gamma = \frac{1}{2} \cdot \gamma \cdot B \cdot N_\gamma$:

$$N_\gamma = \tan \rho_A \cdot \left[ \frac{K_P}{K_A} - 1 \right] \tag{2.34}$$

According to Richards et. al. (1993) there is friction between the wedges. If edge AC in Fig. 2.13 is considered as an imaginary wall, the friction between the edges can be regarded as wall friction ($\delta$). Using Tschebotarioff (1951) [13] method for determination of the lateral earth pressure coefficients with wall friction:

$$K_A = \frac{\cos^2 \phi}{\cos \delta \cdot \left[ 1 + \sqrt{\frac{\sin(\phi+\delta) \cdot \sin \phi}{\cos \delta}} \right]^2} \tag{2.35}$$

$$K_P = \frac{\cos^2 \phi}{\cos \delta \cdot \left[1 - \sqrt{\frac{\sin(\phi+\delta)\cdot \sin \phi}{\cos \delta}}\right]^2} \tag{2.36}$$

The angles of failure surfaces to the horizontal on active ($\rho_A$) and passive ($\rho_P$) wedges are [14]:

$$\rho_A = \phi + \tan^{-1}\left[\frac{[\tan\phi \cdot (\tan\phi + \cot\phi) \cdot (1 + \tan\rho \cdot \cot\phi]^{1/2} - \tan\phi}{1 + \tan\delta \cdot (\tan\phi + \cot\phi)}\right] \tag{2.37}$$

$$\rho_P = -\phi + \tan^{-1}\left[\frac{[\tan\phi \cdot (\tan\phi + \cot\phi) \cdot (1 + \tan\rho \cdot \cot\phi]^{1/2} + \tan\phi}{1 + \tan\delta \cdot (\tan\phi + \cot\phi)}\right] \tag{2.38}$$

The results of static bearing capacity factors $N_q$ and $N_\gamma$ for various $\phi$ and $\rho$ values and corresponding values for Prandtl type mechanism are shown in Table 2.5.

For correct Coulomb mechanism, $\delta$ should be equal to $\phi$. However, since the imaginary wall replace the fan-shaped transition zone, it should average the shear transfer. Therefore setting the frictional angle between the interface of the two wedges $\delta = \phi/2$ gives more reasonable results as shown in Table 2.5.

### 2.3.2. Seismic Bearing Capacity Calculations by Coulomb Mechanism

Richards et al. (1993) extend the static Coulomb failure mechanism to the seismic situations by applying uniform horizontal ($k_h g$) and vertical ($k_v g$) accelerations to the soil wedges and the structure as shown in Fig.2.14. The resulting force equilibrium equations are same except that the lateral earth pressure coefficients and the angles of rupture surfaces are replaced with seismic counterparts:

$$N_{qe} = \frac{K_{PE}}{K_{AE}} \tag{2.39}$$

Table 2.5. Comparison of Prandtl and Coulomb types mechanisms for $N_c$ and $N_q$

| $\phi$ | $\delta$ | $N_q$ | | $N_\gamma$ | |
|---|---|---|---|---|---|
| | | Prandtl | Coulomb | Prandtl | Coulomb |
| 0° | 0° | 1 | 1 | 0 | 0 |
| 10° | 0° | 2.47 | 2.02 | 1.22 | 1.21 |
| | 5° | 2.47 | 2.37 | 1.22 | 1.38 |
| | 10° | 2.47 | 2.73 | 1.22 | 1.54 |
| 20° | 0° | 6.40 | 4.16 | 5.39 | 4.51 |
| | 10° | 6.40 | 5.90 | 5.39 | 6.06 |
| | 20° | 6.40 | 8.26 | 5.39 | 8.10 |
| 30° | 0° | 18.40 | 9 | 22.40 | 13.85 |
| | 15° | 18.40 | 16.51 | 22.40 | 23.76 |
| | 30° | 18.40 | 33.97 | 22.40 | 45.96 |
| 40° | 0° | 64.20 | 21.15 | 109.41 | 43.21 |
| | 20° | 64.20 | 59.03 | 109.41 | 111.9 |
| | 40° | 64.20 | 44.05 | 109.41 | 774.4 |

$$N_{\gamma e} = \tan \rho_{AE} \cdot \left[ \frac{K_{PE}}{K_{AE}} - 1 \right] \tag{2.40}$$

where $\rho_{AE}$ is the angle of seismic rupture surface of the active wedge and $K_{AE}$ and $K_{PE}$ active and passive seismic earth pressure coefficients, respectively.

Mononabe-Okabe analysis gives the seismic earth pressure coefficients: [15],[16]

$$K_{AE} = \frac{\cos^2 a}{\cos\theta \cdot \cos(\delta + \theta) \cdot \left[ 1 + \sqrt{\frac{\sin(\phi+\delta)\cdot\sin a}{\cos(\delta+\theta)}} \right]^2} \tag{2.41}$$

$$K_{PE} = \frac{\cos^2 a}{\cos\theta \cdot \cos(\delta + \theta) \cdot \left[ 1 - \sqrt{\frac{\sin(\phi+\delta)\cdot\sin a}{\cos(\delta+\theta)}} \right]^2} \tag{2.42}$$

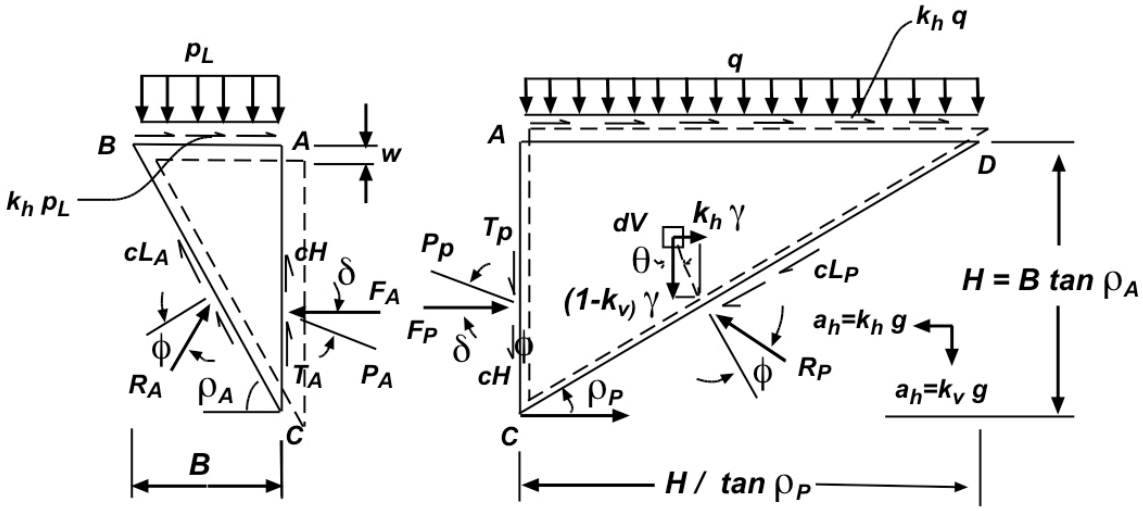



Figure 2.14. Seismic forces acting on Coulomb wedges

where $\theta = \tan^{-1}\left[k_h/(1-k_v)\right]$ and corresponding angles of rupture surfaces:[11]

$$\rho_{AE} = a + \tan^{-1}\left[\frac{\sqrt{(1+\tan^2 a\cdot[1+\tan(\delta+\phi)\cdot\cot a]} - \tan a}{1+\tan(\delta+\theta)\cdot[\tan a+\cot a]}\right] \tag{2.43}$$

$$\rho_{PE} = -a + \tan^{-1}\left[\frac{\sqrt{(1+\tan^2 a\cdot[1+\tan(\delta-\phi)\cdot\cot a]} + \tan a}{1+\tan(\delta+\theta)\cdot[\tan a+\cot a]}\right] \tag{2.44}$$

where $a = \phi - \theta$.

Equations 2.41, 2.42, 2.43 and 2.44 are plotted in Fig.2.15 for $\phi = 30$ and $\delta = 15°$ to show the siesmic effect on the active and passive leteral earth pressure coefficients and wedge angles and also the corresponding geometry of the foundation failure mechanism for $\tan\theta = 0.3$. As acceleration intensity increases, the active trust increases and passive trust decreases and the wedge angles become smaller. At $K_{AE} = K_{PE}$, $\rho_{AE} = \rho_{PE} = 0$, general fluidization takes place and soil simply flows from under the footing.

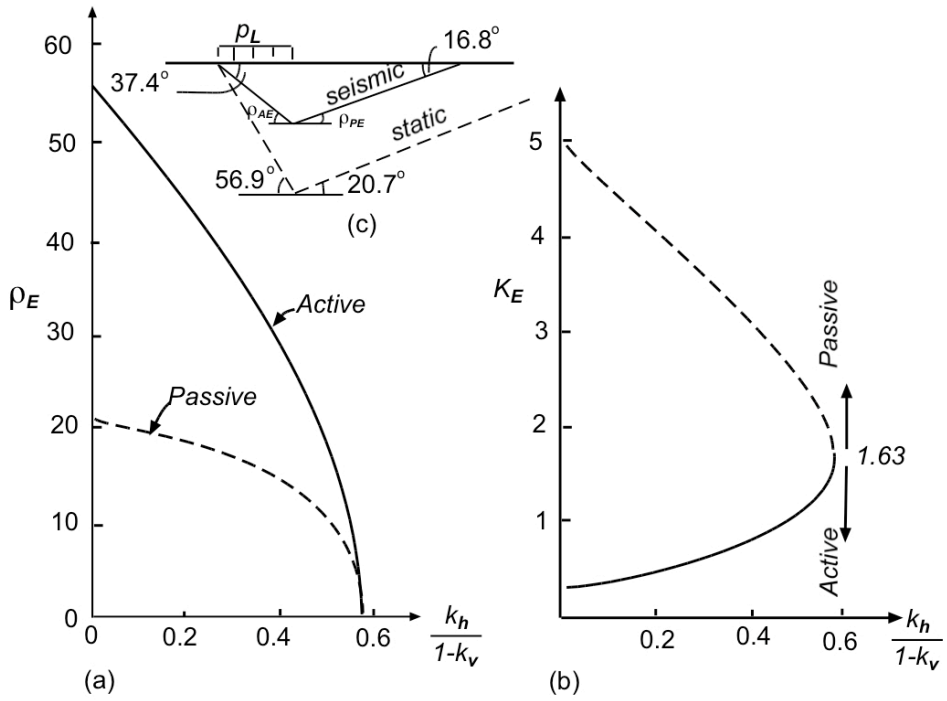



Figure 2.15. Coulomb analysis for $\phi = 30$ (a) failure surface inclination (b) seismic pressure coefficients (c) failure mechanism for $\tan\theta = 0.3$

As a result modified Terzaghi formulation for bearing capacity will be:

$$p_{LE} = cN_{cE} + \gamma dN_{qE} + \frac{1}{2}\gamma BN_{\gamma E} \tag{2.45}$$

Richards et al. (1993) use the same method, as in the static case, for the determination of $N_{cE}$ although its reliability is a moot point:

$$N_{cE} = (N_{qE} - 1)\cot\phi \tag{2.46}$$

In order to illustrate the seismic effect on the reduction of the bearing capacity factors, Richards at al. (1993) use the ratios of the seismic bearing capacity factors to static ones. Both factors are calculated by Coulomb mechanism and with an assumption of $\delta = \phi/2$. Table 2.6 shows the reduction in the values of bearing capacity factors for soils of $\phi = 30°$ with respect to various acceleration intensities.

Table 2.6. Comparison of seismic and static bearing capacity factors for $\phi = 30°$

| Acceleration Intensity $\theta = \tan^{-1}\left[\frac{k_h}{1-k_v}\right]$ | Seismic Bearing Capacity Factors | | | Ratios of Seismic to Static Factors | | |
|---|---|---|---|---|---|---|
| | $N_{qE}$ | $N_{\gamma E}$ | $N_{cE}$ | $N_{qE}/N_{qS}$ | $N_{\gamma E}/N_{\gamma S}$ | $N_{cE}/N_{cS}$ |
| 0 | 16.51 | 23.76 | 26.86 | 1.00 | 1.00 | 1.00 |
| 0.176 | 9.84 | 9.45 | 15.31 | 0.60 | 0.40 | 0.57 |
| 0.268 | 7.30 | 5.36 | 10.91 | 0.44 | 0.23 | 0.41 |
| 0.364 | 5.12 | 2.61 | 7.14 | 0.31 | 0.11 | 0.27 |
| 0.466 | 3.21 | 0.88 | 3.83 | 0.19 | 0.04 | 0.14 |
| 0.577 | 1.00 | 0.00 | 0.00 | 0.06 | 0.00 | 0.00 |

To better illustrate the decrease in the bearing capacity during an earthquake, the ratios of seismic to static bearing capacity factors for various $\phi$ values are shown in Fig.2.16.

### 2.3.3. Inclination Factors For Seismic Bearing Capacity Calculations

The classical approach of the determination of bearing capacity of foundations with inclined load is to introduce empirically derived inclination factors to reduce the cohesion, self weight and surcharge elements of the Terzaghi's bearing capacity equation. Fishman et al. (2003) [17] derived these factors using limit analysis of a simple Coulomb type mechanism and extended them for seismic case again for only cohesionless soils. In this seismic analysis, inclination of the load can be both due to seismic activity and the inclination in the foundation load independent of the seismic activity. However, the reduction in bearing capacity of soil is not only as a result of the inclination of the foundation load but also a consequence of the inertial loss of soil strength during seismic activity.

In the analysis only horizontal component of the seismic acceleration is considered

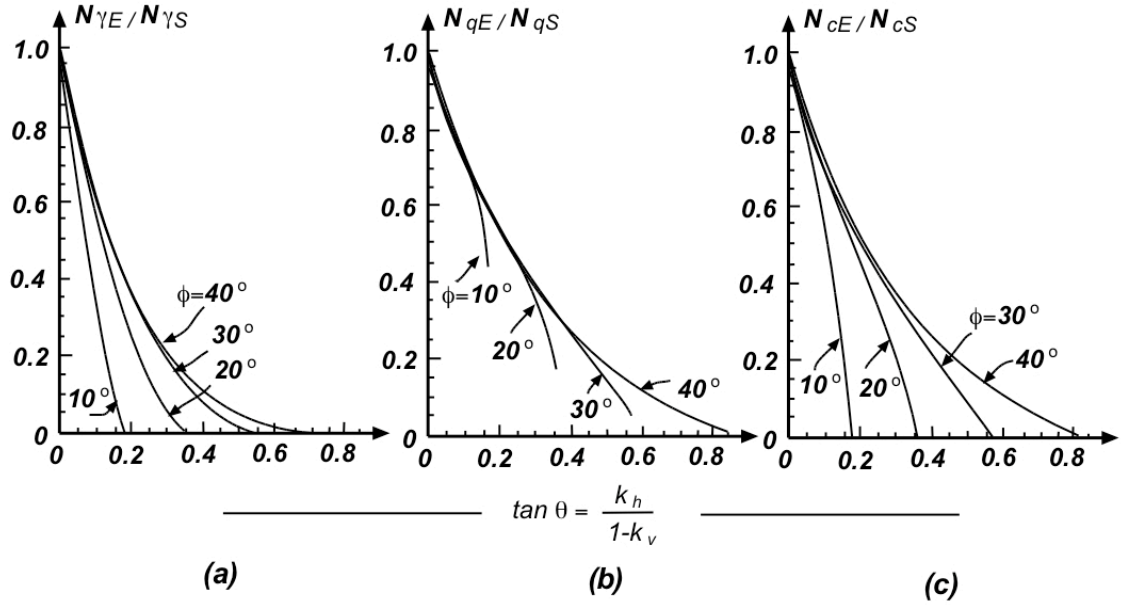



Figure 2.16. Seismic to static bearing capacity ratios

and inclination of the load is defined by seismic shear factor, $n$: [17]:

$$n = \frac{P_h}{P_v \tan \phi} \tag{2.47}$$

where $P_h$ and $P_v$ are resultant shear and vertical forces at the base of the foundation. Fishman et al. (2003) prefer to normalize the inclination with $\tan \phi$ in their analysis against sliding mode of failure.

From the free body diagram of Coulomb wedges (Fig.2.17) similar to the ones introduced by Richards et al. (1993), equilibrium equations in the active wedge will be as follows[17]:

$$R_A \sin(\rho_{AE} - \phi) + k_h W_A + P_h = P_{AE} \cos \delta \tag{2.48}$$

$$W_A + P_{LE} = R_A \cos(\rho_{AE} - \phi) + P_{AE} \sin \delta \tag{2.49}$$

where $P_{LE}$ is vertical force at the base of the foundation, $R_A$ is reaction load on the

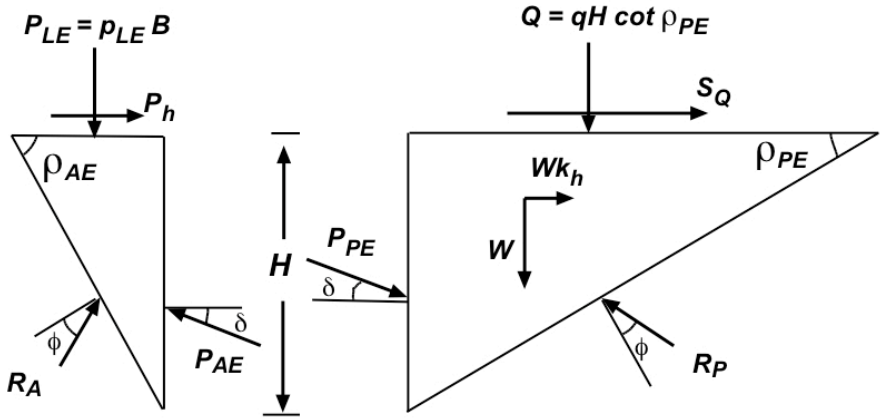



Figure 2.17. Forces acting on Coulomb weges

wedge, $P_{AE}$ is active thrust and $W_A$ is the weight of the active wedge at failure. Solving these two equations:

$$P_{AE} = \left[(P_{LE} + W_A)\tan(\rho_{AE} - \phi) + k_h W_A + P_h\right]\frac{\cos(\rho_{AE} - \phi)}{\cos(\rho_{AE} - \phi - \delta)} \tag{2.50}$$

substituting $P_h = nP_{LE}\tan\phi$, $P_{LE} = p_{LE}H\cot\rho_{AE}$, $W_A = 1/2\gamma H^2\cot\rho_{AE}$ :

$$P_{AE} = \left[\frac{2p_{LE}}{H} + \gamma\right]\frac{H^2}{2}R_1 + \frac{1}{2}\gamma H^2 k_h R_2 + np_{LE}H\tan\phi R_2 \tag{2.51}$$

where $p_{LE}$ is the ultimate vertical load, $H$ is the depth of the wedges as shown in Fig.2.17 and

$$R_1 = \frac{\sin(\rho_{AE} - \phi)\cot\rho_{AE}}{\cos(\rho_{AE} - \phi - \delta)} \tag{2.52}$$

$$R_2 = \frac{\cos(\rho_{AE} - \phi)\cot\rho_{AE}}{\cos(\rho_{AE} - \phi - \delta)} \tag{2.53}$$

For the passive wedge, horizontal component of the surcharge force $S_Q = Qk_h$

and the passive thrust $P_{PE}$ is

$$P_{PE} = \frac{1}{2}\gamma H^2 K_{PE} + qHK_{PE} \tag{2.54}$$

Recalling Mononabe-Okabe analysis for seismic lateral earth pressure coefficients:

$$K_{PE} = \frac{\cos^2 a}{\cos\theta \cdot \cos(\delta+\theta) \cdot \left[1 - \sqrt{\frac{\sin(\phi+\delta)\cdot\sin a}{\cos(\delta+\theta)}}\right]^2} \tag{2.41}$$

At failure, $P_{AE} = P_{PE}$:

$$\left[\frac{2p_{LE}}{H} + \gamma\right]\frac{H^2}{2}R_1 + \frac{1}{2}\gamma H^2 k_h R_2 + np_{LE}H\tan\phi R_2 = \frac{1}{2}\gamma H^2 K_{PE} + qHK_{PE} \tag{2.55}$$

Rearranging the equation:

$$p_{LE}(R_1 + n\tan\phi R_2) = \frac{1}{2}\gamma H(K_{PE} - R_1 - R_2 k_h) + qK_{PE} \tag{2.56}$$

and the ultimate load in terms of Terzaghi's bearing capacity factor for $c = 0$:

$$p_{LE} = qN_{qE} + \frac{1}{2}\gamma B N_{\gamma E} \tag{2.57}$$

So the seismic bearing capacity factors are [17]:

$$N_{\gamma E} = \frac{K_{PE} - R_1 - R_2 k_h}{R_1 + n\tan\phi R_2}\tan\rho_{AE} \tag{2.58}$$

$$N_{qE} = \frac{K_{PE}}{R_1 + n\tan\phi R_2} \tag{2.59}$$

Fishman et al. (2003) propose the iteration method for determination of angle of

seismic rupture surface for active wedge ($\rho_{AE}$). Since $P_{AE} = P_{PE}$ at failure and

$$P_{AE} = \frac{1}{2}\gamma H^2 K_{AE} + qHK_{AE} \tag{2.60}$$

$$K_{AE} = \frac{P_{PE}}{\frac{1}{2}\gamma H^2 + p_{LE}H} \tag{2.61}$$

and $\rho_{AE}$ is the angle giving maximum value of $K_{AE}$.

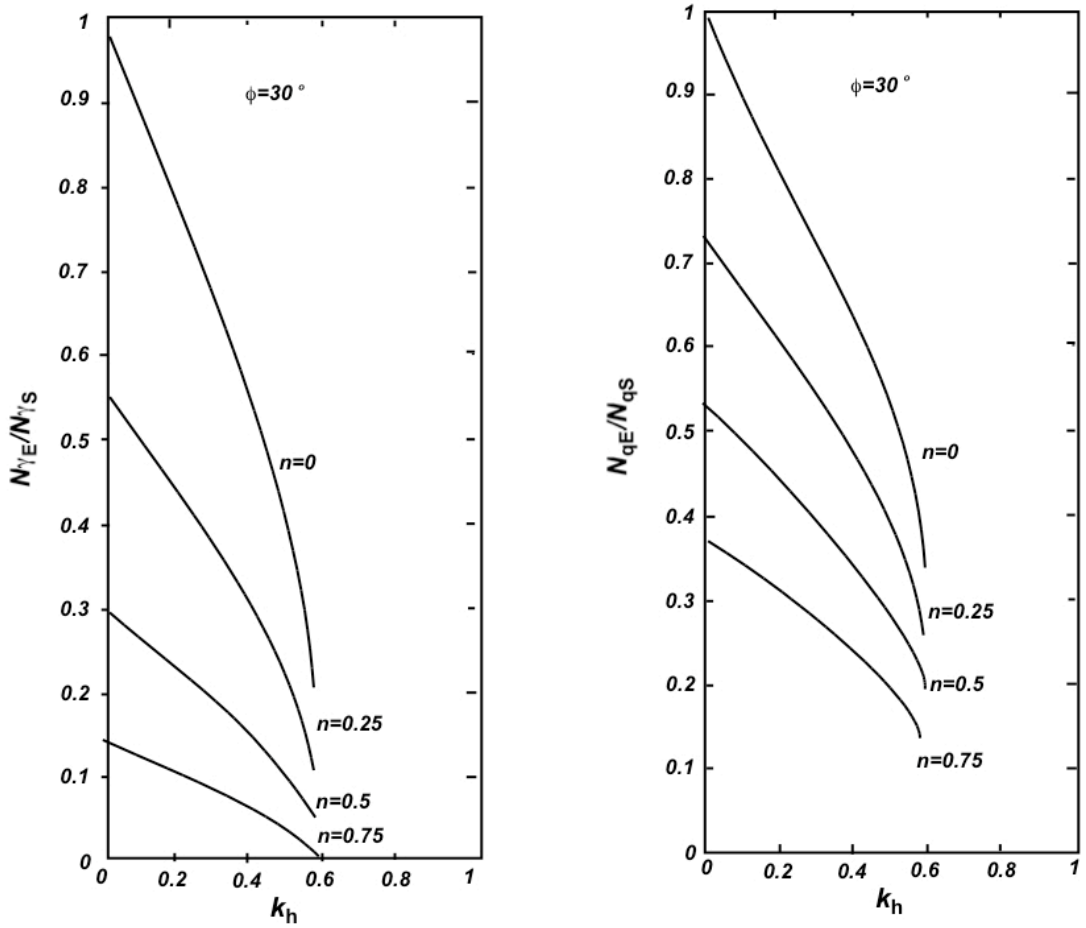



Figure 2.18. Bearing capacity reduction (a)$N_{\gamma E}/N_{\gamma S}$ (b)$N_{qE}/N_{qS}$

Fig.2.18 shows some results of Fishman et al. (2003) approach in reduction of bearing capacity for soils have internal friction angle of 30° for various $n$ values. Static bearing capacity factors $N_{qS}$ and $N_{\gamma S}$ are the factors obtained using same method but

by setting $k_h$ to zero. As it can be seen from the figure seismic bearing capacity goes to zero when $k_h$ reaches the general fluidization value of $\tan\phi$ (Eq.2.16) no matter what the horizontal force is. [17]

### 2.3.4. Seismic Bearing Capacity Calculations for Cohesive Soils

The Coulomb mechanism for seismic bearing capacity calculation of Richards et al. (1993) do not cover cohesive soils. Another approach to determine the seismic bearing capacity of soils is presented by Budhu and Al-Karni (1993) [10] which covers also cohesive soils. According to this approach seismic bearing capacity factors are derived within the framework of Mohr-Coulomb theory and using modified Vesic failure surface.

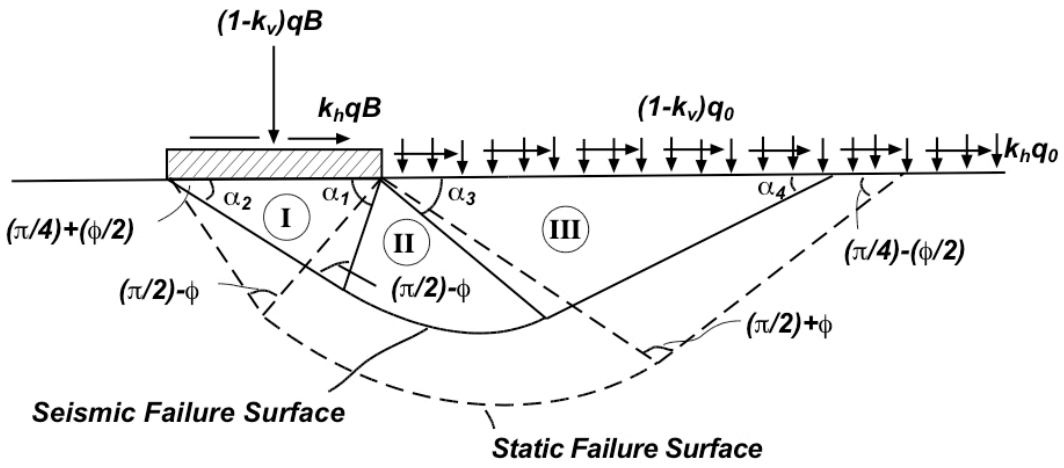



Figure 2.19. Static and seismic failure surfaces

Vesic's static failure surface, as shown in Fig.2.19 with dashed line consists of three zones: an inclined active zone I, a radial transition zone II, and a passive zone III. The accelerations of a seismic event produce a non-symetric failure surface which is assumed to compromise similar zones to static case, but these zones are now much shallower. The new angles of seismic failure surface will be:[10]

$$\alpha_1 = \pi/4 + \phi/2 + \alpha_A \tag{2.62}$$

$$\alpha_2 = \pi/4 + \phi/2 - \alpha_A \tag{2.63}$$

$$\alpha_3 = \pi/4 + \phi/2 + \alpha_P \tag{2.64}$$

$$\alpha_4 = \pi/4 + \phi/2 - \alpha_P \tag{2.65}$$

The values of $\alpha_A$ and $\alpha_B$ can be determined by Equations 2.25 and 2.25.

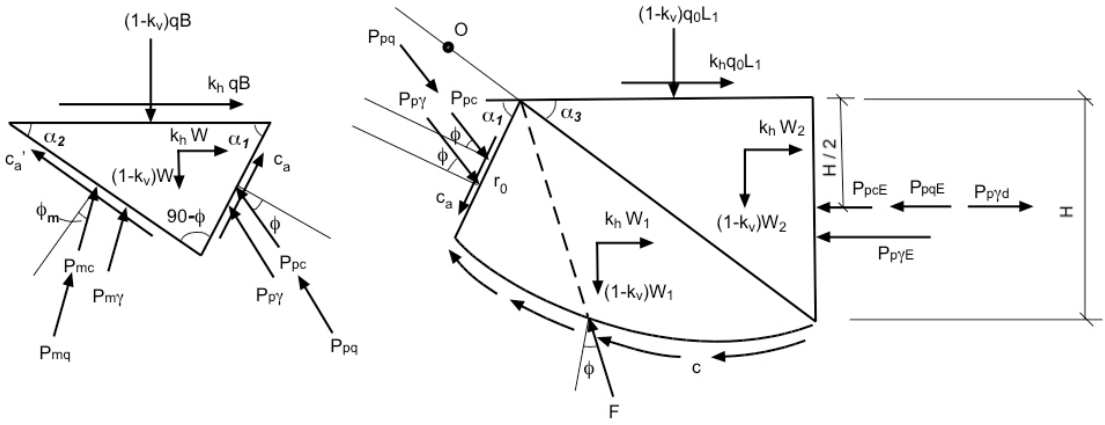



Figure 2.20. Forces acting on seismic failure surfaces

Budhu and Al-Karni (1993) derived equilibrium equations on free body diagrams as shown in Fig.2.20 for failure zones . The moment equilibrium about centre of the log spiral ($O$) gives:

$$\begin{aligned} P_{pc} = & \frac{2c\sqrt{K_{pE}}\sin^2\alpha_3}{\cos\phi} \times r_0 \\ & \times \exp\left[2(\pi - \alpha_1 - \alpha_3)\tan\phi\right] + \frac{cr_0}{\sin\phi} \\ & \times \left(\exp\left[2(\pi - \alpha_1 - \alpha_3)\tan\phi\right] - 1\right) \end{aligned} \tag{2.66}$$

$$P_{mc} = \frac{2mc\sqrt{K_{pE}}\sin^2\alpha_3}{\cos(m\phi)} \times r_0 \times \exp\left[2(\pi - \alpha_2 - \alpha_3)\tan(m\phi)\right] + \frac{mcr_0}{\sin(m\phi)} \times \left(\exp\left[2(\pi - \alpha_2 - \alpha_3)\tan\phi\right] - 1\right) \tag{2.67}$$

where $P_{pc}$ and $P_{mc}$ are passive earth pressures,$m$ is an assumed strength mobilization factor and

$$\phi_m = \tan^{-1}(m\tan\phi) \tag{2.68}$$

Resulting $N_{cE}$ equation for equilibrium in the horizontal direction:

$$N_{cE} = \frac{P_{pc}\cos(\alpha_1 - \phi) + P_{mc}\cos(\alpha_2 - \phi_m)}{cB} + \frac{(1+m)\sin\alpha_1\sin\alpha_2}{\sin(\alpha_1 + \alpha_2)} \tag{2.69}$$

and resulting $N_{cE}$ equation for equilibrium in the vertical direction:

$$N_{cE} = \frac{1}{k_h}\left[\frac{P_{pc}\sin(\alpha_1 - \phi) - P_{mc}\sin(\alpha_2 - \phi_m)}{cB} - \frac{\sin\alpha_2\cos\alpha_1 - m\sin\alpha_1\cos\alpha_2}{\sin(\alpha_1 + \alpha_2)}\right] \tag{2.70}$$

and the correct value of $N_{cE}$ is found from Eq.2.69 and Eq.2.70 by iteration for different values of $m$. Authors preferred to plot $N_{cE}$ values found by iteration with respect to various $\phi$ and $k$ values and to construct best fit curve. So that they derived a simple equation for calculating $N_{cE}$. And the final equation for cohesive component of the seismic bearing capacity is :

$$N_{cE} = N_{cS}\exp(-\beta_c) \tag{2.71}$$

where

$$\beta_c = 4.3k_h^{1+\frac{c}{\gamma H}} \tag{2.72}$$

Budhu and Al-Karni (1993) applied same procedure for determination of $N_{qE}$ and $N_{\gamma E}$ and proposed seismic bearing capacity factors of surcharge and soil weight components as follows:

$$N_{qE} = (1 - k_v)N_{qS}\exp(-\beta_q) \tag{2.73}$$

$$N_{\gamma E} = (1 - \frac{2}{3}k_v)N_{\gamma S}\exp(-\beta_\gamma) \tag{2.74}$$

where

$$\beta_q = \frac{5.3k_h^{1.2}}{1 - k_v} \tag{2.75}$$

$$\beta_\gamma = \frac{9k_h^{1.1}}{1 - k_v} \tag{2.76}$$

## 2.4. Mechanics of Vehicle-Soil Interaction (Terramechanics)

### 2.4.1. Introduction

Terramechanics is a relatively new engineering discipline that focuses on the performance of off-road vehicles in relation to terrain. This recent inbreed of mechanics has attracted considerable interest since World War II. In this period, *U.S. Army Corps of Engineers* developed various empirical formulas. This formulas have been used to correlate in-situ test results with "go" and "no go" performance of off-road vehicles. With the publication of *Theory of Land Locomotion*, by Bekker(1956) and the inception of the *Journal of Terramechanics*, the discipline has become an important field dealing with mobility problems of military, agricultural and lunar vehicles. Several researchers improved the semi-empirical models with various experiments such as bevameter (introduced by Bekker in 1960), cone penetration and plate penetration tests. Analytical models based on elasticity and plasticity theories and numerical methods have also been introduced to predict the mechanical behavior of vehicle-soil interaction.

### 2.4.2. Empirical Models

The procedure in utilizing empirical methods in predicting off-road performance of a vehicle is to conduct performance tests on selected vehicles over representative terrains and to correlate the obtained test results with terrain characteristics. Empirical methods are mainly based on the cone index (CI) and were developed during the World WAR II by US Army waterways Experiment Station (WES) to measure the trafficability of terrains on a "go or no go" basis.

In developing the WES model numerous tests were performed for a range of terrain types on primarily fine and coarse grained soils. The measured data for vehicle performance and terrain conditions were then empirically correlated, and a model known as the WES vehicle cone index (VCI) was proposed for predicting vehicle performance on fine and coarse grained inorganic soils. [18]

2.4.2.1. Tracked Vehicle Performance: According to WES model for predicting the tracked vehicle performance, an emprical equation is first used to calculate the mobility index (MI) of a given vehicle. MI is expressed by:[18]

$$MI = \left[\frac{F_{pressure} \times F_{weight}}{F_{track} \times F_{grouser}} + F_{bogie} - F_{clrn}\right] \times F_{engine} \times F_{trans} \tag{2.77}$$

where,

$$F_{pressure} : Contact\ Pressure\ Factor\ = \frac{gross\ weight, lb}{contact\ area\ of\ track\ with\ ground, in^2} \tag{2.78}$$

$$F_{weight} : Weight\ Factor : \begin{cases} less\ than\ 50\ 000\ lb\ (222.4\ kN) & = 1.0 \\ 50\ 000 - 69\ 999\ lb\ (222.4 - 311.4\ kN) & = 1.2 \\ 70\ 000 - 99\ 999\ lb\ (311.4 - 444.8\ kN) & = 1.4 \\ 100\ 000\ lb\ (444.8\ kN)\ or\ greater & = 1.8 \end{cases} \tag{2.79}$$

$$F_{track} : Track\ Factor\ = \frac{track\ width,\ in}{100} \tag{2.80}$$

Grouser Factor: [1]

$$F_{grouser} : \begin{array}{ll} grousers\ less\ than\ 1.5\ inch\ (38\ cm)\ high & = 1.0 \\ grousers\ more\ than\ 1.5\ inch\ (38\ cm)\ high & = 1.1 \end{array} \tag{2.81}$$

Bogie Factor[2] :

$$F_{bogie} = \frac{gross\ weight,\ lb,\ divided\ by\ 10}{\left[\begin{array}{c} total\ number\ of\ bogies\ on \\ tracks\ in\ contact\ with\ ground \end{array}\right] \times \left[\begin{array}{c} area\ of\ one \\ track\ shoe,\ in.^2 \end{array}\right]} \tag{2.82}$$

$$F_{clrn} : Clearance\ Factor\ = \frac{clearance,\ in}{10} \tag{2.83}$$

$$F_{engine} : Engine\ Factor : \begin{array}{ll} \geqslant\ 10\ hp/ton\ of\ vehicle & = 1.00 \\ \leqslant 10\ hp/ton\ of\ vehicle & = 1.05 \end{array} \tag{2.84}$$

$$F_{trans} : Transmission\ Factor : \begin{array}{ll} Automatic & = 1.00 \\ Manual & = 1.05 \end{array} \tag{2.85}$$

The vehicle cone index ($VCI$) is calculated based on mobility index ($MI$). The

[1] Grousers are the lugs on the track that penetrate the soil

[2] Bogie is a chassis or framework carrying wheels, attached to a vehicle.

$VCI$ is defined by The International Society for Terrain-Vehicle System(ISTVS) as "minimum soil strength in the critical soil layer, in terms of rating cone index (RCI) for fine grained soils or cone index (CI) for coarse grained soils, required for a specific number of passes of vehicle, usually one pass or 50 passes" [19]

The critical layer is the layer of soil that exerts the greatest influence on trafficability, and it is usually 15 cm for freely draining or clean sands. For fine-grained soils and poorly drained sands with fines, it is usually 15 cm for one pass and between 15-30 cm for 50 passes.[20]

RCI is an index of soil shear strength that includes consideration of the sensitivity of soil to strength losses under vehicular traffic, and it is related to both the bearing capacity and tractive resistance of soils. RCI is defined as the product of CI and remold index (RI) for a particular layer of soil, and these two constituent indexes are measured using trafficability equipments developed and standardized by US Army's Engineer Research and Development Center (ERDC). CI is an index of soil shear strength, and it is determined using a cone penetrometer. The CI measurement is the average of pressure readings taken at specified depths of penetration of the base of the cone into the soil. RI is an index of the sensitivity of soil to strength losses under vehicular traffic, and it is determined using a Hvorslev trafficability sampler and remolding equipment (Fig 2.21). The Hvorslev sampler is a piston-type device used to obtain undisturbed samples of soil, and remolding equipment consists of a cylindrical tube mounted on a steel base and a drop hammer. The RI measurement is defined as the measured CI in a sample taken after 100 blows of the drop hammer divided by the measured CI taken before 100 blows. [21]

For fine-grained soils the $VCI$ values for one pass ($VCI_1$) and 50 passes ($VCI_{50}$) may be calculated from the following empirical equations:

$$VCI_1 = 7.0 + 0.2MI - \left[\frac{39.2}{MI + 5.6}\right] \tag{2.86}$$

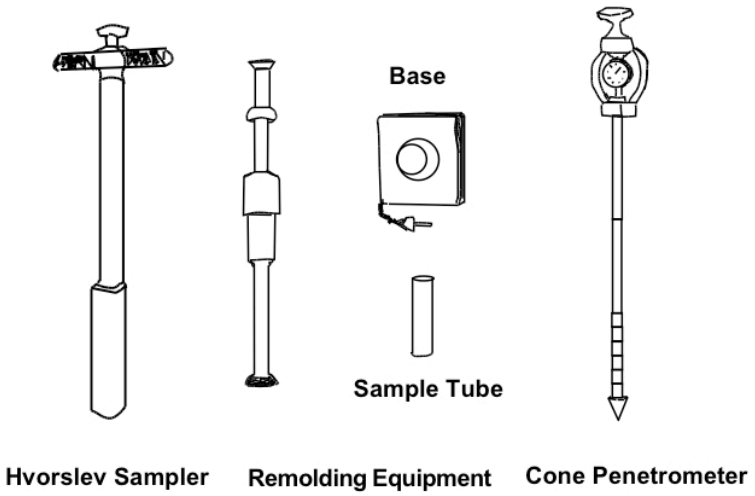



Figure 2.21. ERDC trafficability equipments

$$VCI_{50} = 19.27 + 0.43MI - \left[\frac{125.79}{MI + 7.08}\right] \tag{2.87}$$

The soil strength is described in terms of either the rating cone index (RCI) for fine grained soils or the cone index (CI) for coarse grained soils. After the VCI and soil strength have been determined, the excess of RCI over VCI (RCI-VCI) for fine grained soils or CI over VCI (CI-VCI) for coarse grained soils is calculated to evaluate the mobility performance.

2.4.2.2. Wheeled Vehicle Performance: According to WES model for predicting the wheeled vehicle performance, an empirical method similar to the one used in tracked vehicle mobility determination is used. The mobility index of a wheeled vehicle is given by:[18]

$$MI = \left[\frac{F_{pressure} \times F_{weight}}{F_{tire} \times F_{grouser}} + F_{wload} - F_{clrn}\right] \times F_{engine} \times F_{trans} \tag{2.88}$$

where,

$$F_{pressure}: \begin{bmatrix} Contact \\ Pressure \\ Factor \end{bmatrix} = \frac{gross\ weight,\ lb}{\begin{matrix} nominal\ tire \\ width,\ in \end{matrix} \times \begin{matrix} outside\ radius \\ of\ tire,\ in \end{matrix} \times \begin{matrix} no.\ of \\ tires \end{matrix}} \tag{2.89}$$

$F_{weight}$ :

| *weight range, lb* | *Weight Factor*($F_{weight}$) |
|---|---|
| *<2000 (8.9 kN)* | $0.533 \times X$ |
| *2000 - 13 500 (8.9 - 60 kN)* | $0.033 \times X + 1.050$ |
| *13 501 - 20 000 (60 - 88.9 kN)* | $0.142 \times X$ - 0.420 |
| *> 20 000 (88.9 kN)* | $0.278 \times X$ - 3.115 |

(2.90)

where:

$$X = \frac{gross\ weight,\ kips}{no.\ of\ axles}$$

$$F_{tire}: Tire\ Factor\ = \frac{10 + tire\ width,\ in}{100} \tag{2.91}$$

$$F_{grouser}: Grouser\ Factor: \begin{matrix} with\ chains & = 1.05 \\ without\ chains & = 1.00 \end{matrix} \tag{2.92}$$

$$F_{wload}: Wheel\ Load\ Factor\ = \frac{gross\ weight,\ kips}{no.\ of\ axles \times 2} \tag{2.93}$$

$$F_{clrn}: Clearance\ Factor\ = \frac{clearance,\ in}{10} \tag{2.94}$$

$$F_{engine} : Engine\ Factor : \begin{array}{ll} \geqslant 10\ hp/ton\ of\ vehicle & = 1.00 \\ \leqslant 10\ hp/ton\ of\ vehicle & = 1.05 \end{array} \tag{2.95}$$

$$F_{trans} : transmission\ Factor : \begin{array}{ll} Automatic & = 1.00 \\ Manual & = 1.05 \end{array} \tag{2.96}$$

The Vehicle Cone Index (VCI) is determined according to calculated Mobility Index (MI), similar to the method of tracked vehicles. For instance, for a self-propelled, wheeled vehicle, the vehicle cone index for fine-grained soils is related to the mobility index by the following equation: [20]

For 50 pass,

$$VCI_{50} = 28.23 + 0.43MI - \left[ \frac{92.67}{MI + 3.67} \right] \tag{2.97}$$

After the commercialization of radial tires, Deflection Correction Factor ($F_{def}$)has been introduced to account for the effect of tire deflection on VCI performance. The corrected value of VCI is obtained by multiplying Eq. 2.97 by correction factor and correction factor is calculated by: [21]

$$F_{def} = \sqrt[4]{\frac{0.15}{\delta/h}} \qquad \begin{array}{ll} \delta & is\ the\ deflection, \\ h & is\ the\ unloaded\ section\ height\ of\ the\ tire \end{array} \tag{2.98}$$

### 2.4.3. Semi-Empirical Models

Another method in constructing a soil-vehicle model is to design a device to collect specific data for evaluating the necessary parameters related to mobility problems and to use these results as inputs of the theoretical frameworks. Bekker's bevameter test is

the most relevant and reliable test for fulfilling the requirements of this semi-empirical approach to soil-vehicle interaction problems.

2.4.3.1. Bevameter Tests:

The bevameter[3] is developed by Bekker in 1960 and the it is still in use today. The purpose of this test is to develop loading conditions representing the soil-vehicle interaction behavior as much as possible. The test consists of two devices: One device performs the plate penetration test (Fig. 2.22 a) and the other device performs the shear test (Fig. 2.22 b).

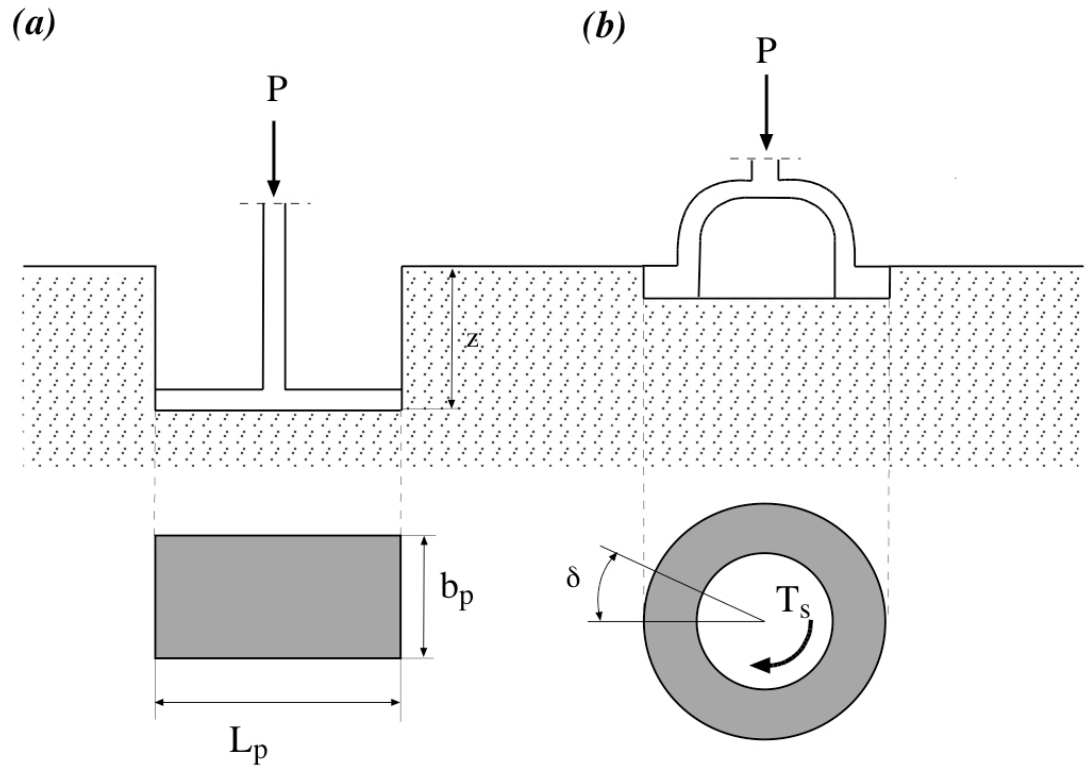



Figure 2.22. Schematic representation of bevameter tests (after Bekker 1969): (a)plate-penetration test, (b) shear test

In the plate-penetration test, the plate is used to simulate the pressure-penetration relationship between the vehicle running gear and the soil. A plate penetrates the soil to a depth, such as $z$, under pressure $p$. After the pressure-penetration data collected,

[3]The acronym (BEkker VAlue METER) was introduced in 1955 by S.J. Weiss

it is used for deducing widely used empirical parameters $k_c$, $k_\phi$ and $n$. Although $k_c$ and $k_\phi$ might appear to be related to cohesion and internal friction of Mohr-Columb yield condition, there is no clear relationship between these strength parameters.[20] The pressure-sinkage relationship can be characterized with these parameters by the following equation proposed by Bekker: [22]

$$p = \left[\frac{k_c}{b} + k_\phi\right] z^n \tag{2.99}$$

where $p$ is pressure in $kN/m^2$, $b_p$ is smaller dimension of the contact surface in meters, $z$ is the penetration depth in meters and $n$, $k_c$ and $k_\phi$ are pressure sinkage parameters having variable dimensions. At depth $z = 1\ m$, the parameter $n$ will have no effect on the pressure, so for the known pressure at sinkage depth $z = 1\ m$, at least two equations are needed to determine two unknown parameters, $k_c$ and $k_\phi$. So, a minimum of two tests are performed with two sizes of plates having different widths or radii. These tests produce two curves:

$$(p_1)_{z=1} = \frac{k_c}{b_1} + k_\phi = a_1 \tag{2.100}$$

$$(p_2)_{z=1} = \frac{k_c}{b_2} + k_\phi = a_2 \tag{2.101}$$

By solving the equation for $k_c$ and $k_\phi$:

$$k_\phi = \frac{a_2 b_2 - a_1 b_1}{b_2 - b_1} \tag{2.102}$$

$$k_c = \frac{(a_1 - a_2) b_1 b_2}{b_2 - b_1} \tag{2.103}$$

The parameter $n$ can be determined after redrawing the pressure-penetration curves in the logarithmic scale. On logarithmic scale, the equations 2.100 and 2.101 can be

rewritten as:

$$\log p_1 = \log \left[ \frac{k_c}{b_1} + k_\phi \right] + n \log z \tag{2.104}$$

$$\log p_1 = \log \left[ \frac{k_c}{b_1} + k_\phi \right] + n \log z \tag{2.105}$$

These equations represent two parallel straight lines on the log-log scale as shown in Fig 2.23. $n$ will be equal to the slopes of these straight lines.

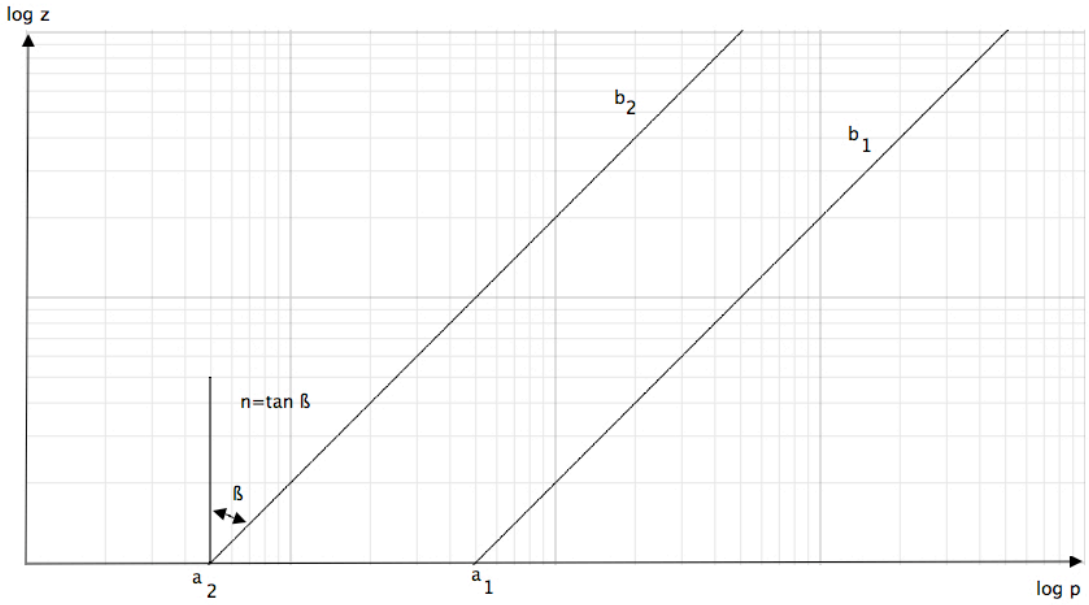



Figure 2.23. Method for determining sinkage moduli and exponent

The values of $n$, $k_c$ and $k_\phi$ for various terrains are given in Table 2.7[1]:

Onafeko and Reece (1967) [23] proposed a new equation for the pressure-penetration relationship that is more conceivable with dimensonless parameters ($k'_c$ and $k'_\phi$) and similarities with Terzaghi's bearing capacity equation :

$$p = (ck'_c + \gamma_s b k'_\phi) \left[ \frac{z}{b} \right]^n \tag{2.106}$$

Table 2.7. $n$, $k_c$ and $k_\phi$ values for various soil types

| **Terrain** | **Moist.** (%) | $n$ | $k_c$ ($kN/m^{n+1}$) | $k_\phi$ ($kN/m^{n+2}$) | $c$ kPa | $\phi$ deg |
|---|---|---|---|---|---|---|
| Dry Sand (LLL) | 0 | 1.1 | 0.99 | 1528.43 | 1.04 | $28^o$ |
| Sandy Loam | 15 | 0.7 | 5.27 | 1515.04 | 1.72 | $29^o$ |
| (LLL) | 22 | 0.2 | 2.56 | 43.12 | 1.38 | $38^o$ |
| Sandy Loam Michigan | 11 | 0.9 | 52.53 | 1127.97 | 4.83 | $20^o$ |
| (Strong, Buchele) | 23 | 0.4 | 11.42 | 808.96 | 9.65 | $35^o$ |
| Sandy Loam | 26 | 0.3 | 2.79 | 141.11 | 13.79 | $22^o$ |
| (Hanamoto) | 32 | 0.5 | 0.77 | 51.91 | 5.17 | $11^o$ |
| Clayey Soil | 38 | 0.5 | 13.19 | 692.15 | 4.17 | $13^o$ |
| (Thailand) | 55 | 0.7 | 16.03 | 1262.53 | 5.17 | $10^o$ |
| Heavy Clay | 25 | 0.13 | 12.70 | 1555.95 | 68.95 | $34^o$ |
| (WES) | 40 | 0.11 | 1.84 | 103.27 | 20.69 | $6^o$ |
| Lean Clay | 22 | 0.2 | 16.43 | 1724.69 | 68.95 | $20^o$ |
| (WES) | 32 | 0.15 | 1.52 | 119.61 | 13.79 | $11^o$ |
| LETE Sand (Wong) | | 0.79 | 102 | 5301 | 1.3 | $31.1^o$ |
| Upland Sandy Loam (Wong) | 51 | 1.10 | 74.6 | 2080 | 3.3 | $33.7^o$ |
| Rubicon Sandy Loam (Wong) | 43 | 0.66 | 6.9 | 752 | 3.7 | $29.8^o$ |
| North Gower Clayey Loam (Wong) | 46 | 0.73 | 41.6 | 2471 | 6.1 | $26.6^o$ |
| Grenville Loam (Wong) | 24 | 1.01 | 0.06 | 5880 | 3.1 | $29.8^o$ |
| sources: [22] and [20] | | | | | | |

where $n$, $k'_c$ and $k'_\phi$ are pressure penetration parameters, $\gamma_s$ is the weight of the soil and c is cohession.

The purpose of shear test in bevameter tests is to measure parameters relevant to the resistance of the soil to shear induced by running gear. The parameters $K$, $c_b$ and $\phi_b$ are determined from curve fitting data collected with the shear test and used in the equation originally proposed by Janosi and Hanamoto (1961)[24]:

$$\sigma_t = (c_b + \sigma_n \tan \phi_b)(1 - e^{-j/K}) \tag{2.107}$$

where $\sigma_t$ is the tangential contact stress; $\sigma_n$ is the normal contact stress, $j$ is the shear displacement and $K$ is the shear deformation modulus. $c$ and $\phi$ are referred to the cohesion and the angle of internal shearing resistance. However, these two parameters do not address the strength of soil mass itself, they pertaining to the interface between the soil and the running gear.

### 2.4.4. Analytical Methods

2.4.4.1. Theory of Elasticity Theory of elasticity describes the mechanical behavior of homogenous and isotropic materials which recover its original size and shape upon removal of applied stress. Soils are rarely homogenous and isotropic in situ because of their formation process. They are also rarely linearly elastic except over a narrow range of stress change. However, solutions using elasticity in soil vehicle interaction problems give reasonable predictions of local deformation for relatively small wheel loads and also to predict distribution of stresses in the soil under vehicular loads (Boussineq Equations).

The constitutive equations describing the mechanical response of ideal isotropic elastic body are given in the form of Hooke' s law:

$$\epsilon_x = \frac{1}{E_y} [\sigma_x - \nu(\sigma_y + \sigma_z)] \tag{2.108}$$

$$\epsilon_y = \frac{1}{E_y}\left[\sigma_y - \nu(\sigma_x + \sigma_z)\right] \tag{2.109}$$

$$\epsilon_z = \frac{1}{E_y}\left[\sigma_z - \nu(\sigma_x + \sigma_y)\right] \tag{2.110}$$

$$\epsilon_{xy} = \frac{1}{2G}\tau_{xy} \tag{2.111}$$

$$\epsilon_{yz} = \frac{1}{2G}\tau_{yz} \tag{2.112}$$

$$\epsilon_{xz} = \frac{1}{2G}\tau_{xz} \tag{2.113}$$

The elastic properties of a given soil are described in terms of elastic constants, namely the Young modulus $E_y$ and Poisson's ratio $\nu$. These moduli are assumed to be instinct properties of the material and therefore independent of the method of testing or the particular configuration of the material.

In cases where displacements are small, elastic solutions may give good approximations of soil behavior provided $E_y$ and $\nu$ are representative of values in the field. However, in cases where plastic yielding occurs, which are majority of cases of interest in vehicle mobility studies, other theories must be sought to determine stress states under applied load and to predict soil behavior as a result of these stress states.[1]

Stress distribution of a point load on a semi-infinite, homogenous, isotropic, elastic medium was determined by Boussinesq in 1885 referring the Fig. 2.24 by the following equations :

$$\sigma_z = \frac{3Q}{2\pi z^2}\left[\frac{1}{1+(r/z)^2}\right] \tag{2.114}$$

$$\sigma_r = \frac{Q}{2\pi}\left[\frac{3r^2 z}{(r^2+z^2)^{5/2}} - \frac{1-2\nu}{r^2+z^2+z(r^2+z^2)^{1/2}}\right] \tag{2.115}$$

$$\sigma_\theta = -\frac{Q}{2\pi}(1-2\nu)\left[\frac{z}{(r^2+z^2)^{3/2}} - \frac{1}{r^2+z(r^2+z^2)^{1/2}}\right] \tag{2.116}$$

$$\tau_{rz} = \frac{3Q}{2\pi}\left[\frac{rz^2}{(r^2+z^2)^{5/2}}\right] \tag{2.117}$$

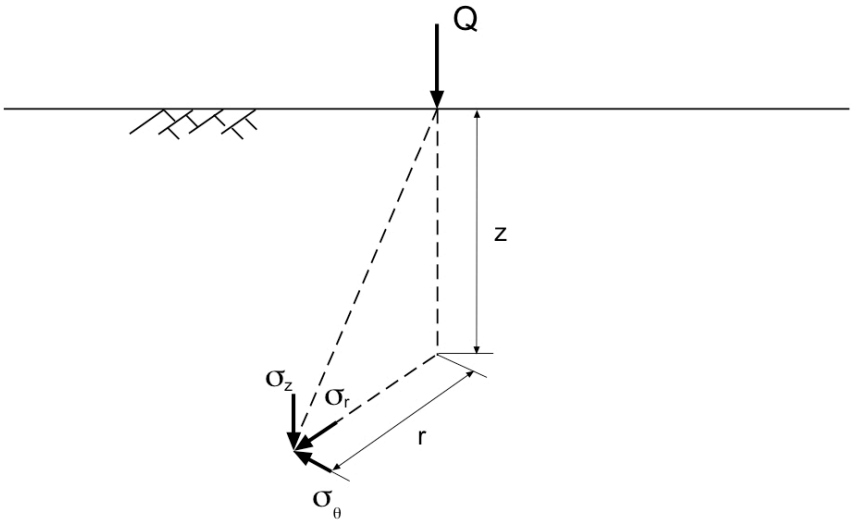



Figure 2.24. Stresses due to point load

Based on the analysis of the stress distribution from a point load and by using principle of superposition; distribution of stresses under various loading conditions may be predicted:

Referring the Fig.2.25, stress distribution due to a line load per unit length on the surface is:

$$\sigma_z = \frac{2Q}{\pi} \frac{z^3}{(x^2+z^2)^2} \tag{2.118}$$

$$\sigma_x = \frac{2Q}{\pi} \frac{x^2 z}{(x^2+z^2)^2} \tag{2.119}$$

$$\tau_{xz} = \frac{2Q}{\pi} \frac{xz^2}{(x^2+z^2)^2} \tag{2.120}$$

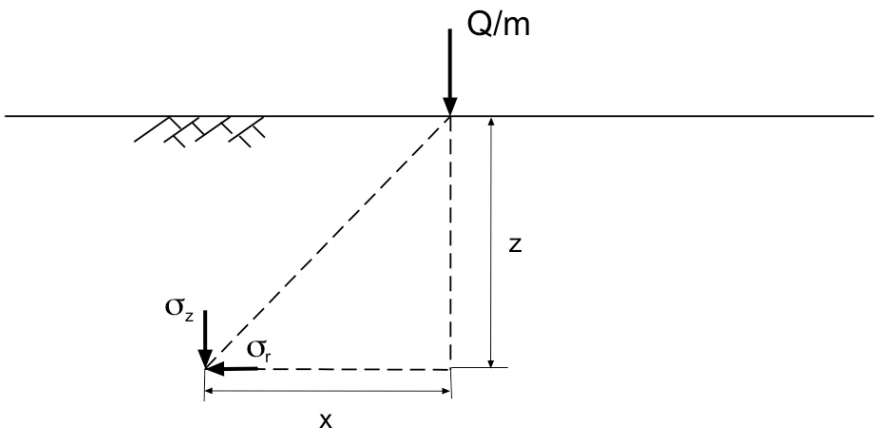



Figure 2.25. Stresses due to line load

From the vehicle-soil interaction viewpoint, soil under the action of uniform strip load is important. A tracked vehicle over a soil may be idealized as a strip load. Stress distribution due to a uniform pressure $q$ on a strip area of width $B$ and infinite length

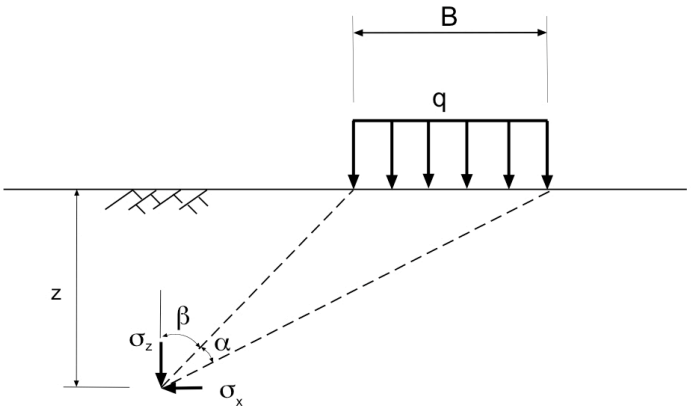



Figure 2.26. Stresses due to strip load

are given referring the Fig. 2.26:

$$\sigma_z = \frac{q}{\pi}\{\alpha + \sin\alpha\cos(\alpha + 2\beta)\} \tag{2.121}$$

$$\sigma_x = \frac{q}{\pi}\{\alpha - \sin\alpha\cos(\alpha + 2\beta)\} \tag{2.122}$$

$$\tau_{xz} = \frac{q}{\pi}\{\sin\alpha\sin(\alpha + 2\beta)\} \tag{2.123}$$

Distribution of vertical stresses under a tracked vehicle can be shown as in Fig.2.27 using equal vertical stress contours with respect to depth in tracked width $B$.

It should be pointed out that the use of theory of elasticity produces approximate results only. Measurements have shown that the stress distribution in a real soil deviates from that computed using Boussinesq's equations. [25]

2.4.4.2. Theory of Plasticity

Analyses of soil-vehicle interaction by theory of plasticity is based on the as-

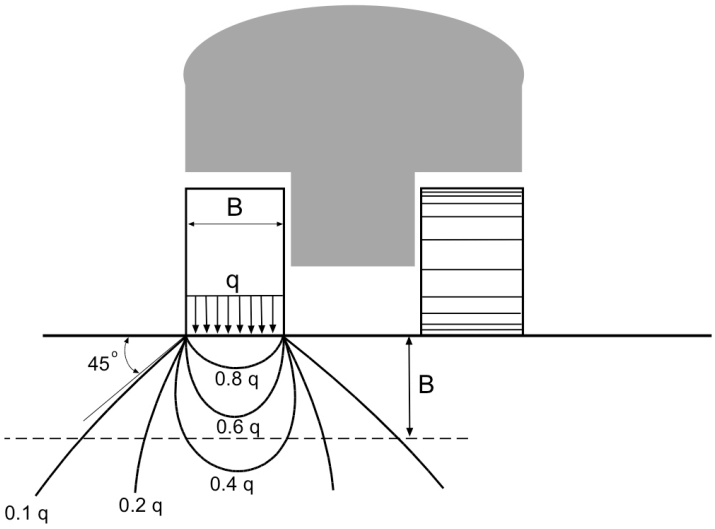



Figure 2.27. Equal vertical stress curves under tracked vehicles

sumption that the soil is a rigid-perfectly plastic material as shown in Figure 2.28. When the vehicular load applied to the soil exceeds a certain limit, the soil undergoes a non-reversible and rapid deformation which constitutes plastic flow. Plastic flow in soil-vehicle interaction represents failure of soil and subsequently loss of the mobility. There are various criteria proposed for failure of soils. One of the widely used criterion is Mohr-Coulomb.

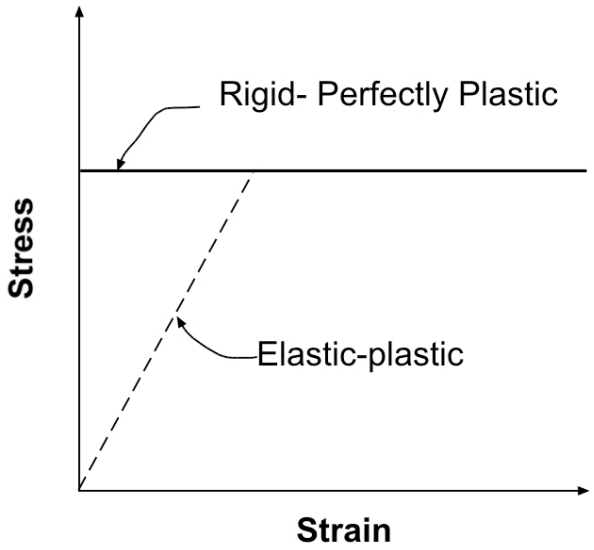



Figure 2.28. Rigid-perfectly plastic and elastic-plastic behavior of soils

In the Mohr-Coulomb yield criterion failure is defined in terms of stress conditions. The material at a point will fail if the shear stress at that point satisfies the following condition:

$$\tau = c + \sigma \tan \phi \tag{2.124}$$

where $\tau$ is the shear strength, $c$ is the cohesion, $\sigma$ is the normal stress on the sheared surface and $\phi$ is the internal friction angle of the soil.

In the graphical representation of Mohr-Coulomb criterion (Fig. 2.29), the line tangent to the Mohr circle is called the failure envelope. Any combination of normal and shear stress below this failure envelope can be sustained by the material without yielding or failure. The Mohr circle in the Fig. 2.29 shows one of the states of stress that cause shear failure with major ($\sigma_1$)and minor ($\sigma_3$) principle stresses. Failure occurs along a plane at an angle of $\theta$ to the major principle plane and it is equal to $(45 + \phi/2)$. The soil-wheel interaction problem can be considered as a modified soil-

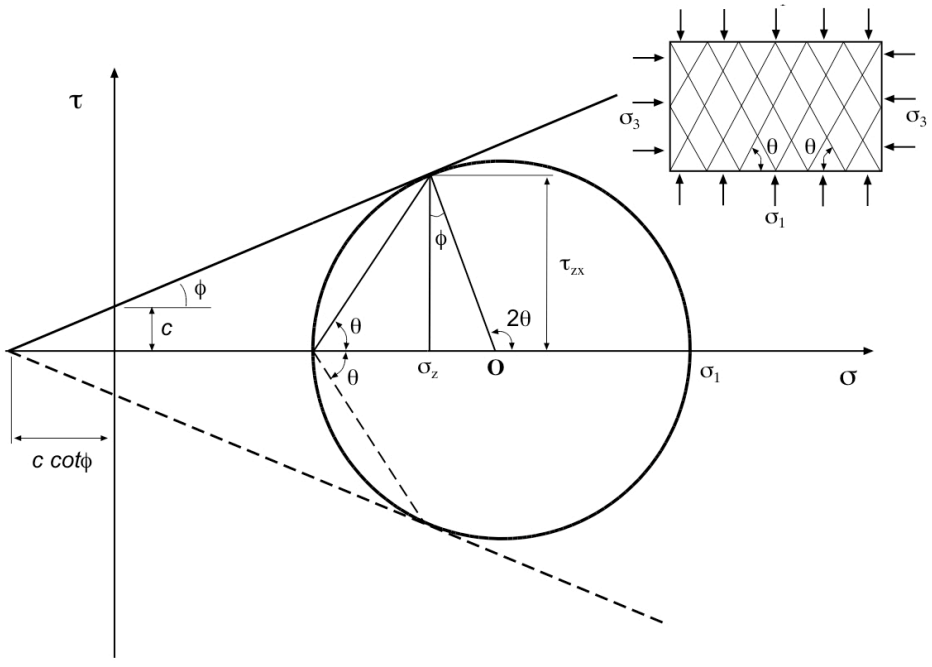



Figure 2.29. Principle stresses on mohr circle and failure planes

footing problem and studies about applications of plasticity theory to bearing capacity problems will be useful also in soil-wheel interaction problems.

As discussed in section 2.1, Terzaghi derived the basic expression of the bearing capacity of a strip footing. This equation has been modified for the geometric shape of the footing, inclination and eccentricity of the load etc. The resulted general equation is repeated here:

$$q_u = \frac{1}{2}\gamma B N_\gamma s_\gamma d_\gamma i_\gamma + c N_c s_c d_c i_c + q_0 N_q s_q d_q i_q \tag{2.3}$$

The shortcomings of this method are that the interaction between wheel and soil is much more complex than the bearing capacity theory assumes and unlike foundations, the contact region between the soil and wheel is not flat. Also contact area depends on the wheel deformability and sinkage.

### 2.4.5. Numerical Methods

By the advent and widespread availability of the high speed computers, various numerical techniques have become available for analysis of complex problems such as layering, complex geometries and stress boundary conditions, anisotropy and three-dimensional effects.

The finite element method (FEM)is one such technique. It was originally developed as a tool for structural analysis, but the theory and formulation have been progressively so refined and generalized that the method has been successfully applied to other field. The basis of the finite element method is the representation of a body or a structure by an assemblage of subdivisions called finite elements.

To initiate the solution process the distributions of the normal and shear stresses on the contact patch, as well as the load-unload stress-strain relations for the soil are required as input. The output of the analysis is given in terms of stress, strain rate, and velocity fields in soil.

It should be point out that in many cases, the assumption of linear elastic behavior

is unrealistic. Under vehicle load, soil usually undergoes large yielding and plastic deformation and does not behave elastically. Consequently, it appears unnecessary to use the finite element method in off-road mobility problems. [20]

### 2.4.6. Shearing Resistance Between Solids and Soil

Traction between the vehicles and soil is developed by shear stresses at the solid-soil interface. These shear stresses are limited by the shearing resistance between solid and soil.

The shearing resistance between solid and soils may be expressed in similar form as the Coulombic expression of shear strength for soils: [1]

$$s = a_{ss} + \sigma_n \tan \phi_s \tag{2.125}$$

where
$a_{ss}$=adhesion between solid and soil
$\phi_s$=friction angle between solid and soil

The adhesion is somehow equivalent to cohesion and includes molecular, electrical, Coulomb and capillary forces. The most important forces in off-road vehicle engineering are the capillary forces that arise if water menisci are formed in the space between a soil particle and solid surface.

Behavior of frictional component of the shearing resistance is similar to the internal shearing resistance of a frictional soil (Figure 2.3).

In dense state before shear failure interlocking between particles must be overcome in addition to the frictional resistance. In the case of loose sand there is no significant interlocking and the stress increases gradually to the ultimate value without a peak.

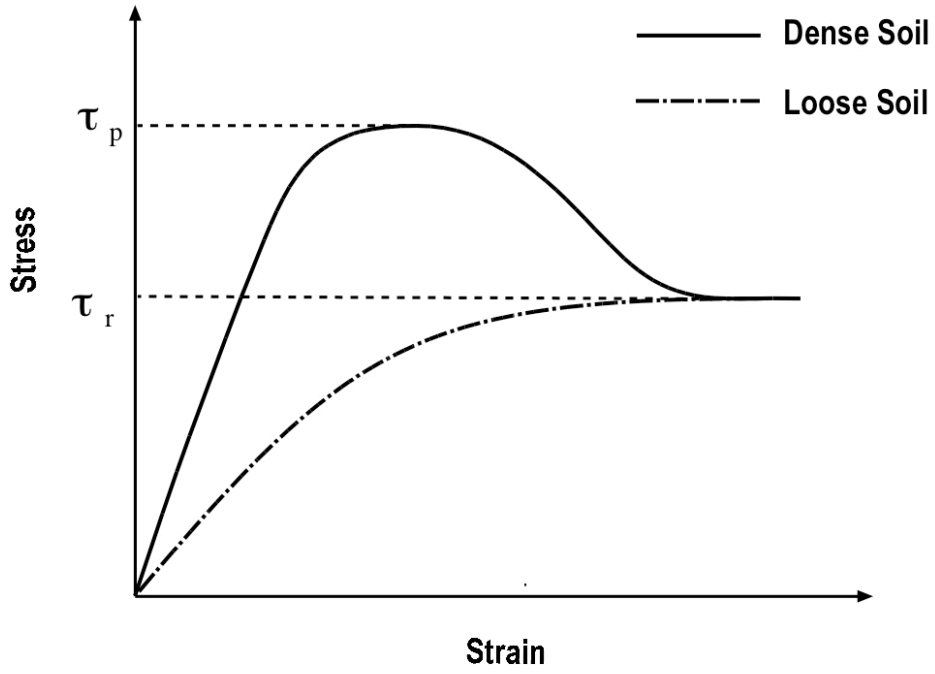



Figure 2.30. Shearing stress -strain relationship of frictional soils in loose and dense state

The shearing resistance between solid and soil can be determined with shear testing devices in the laboratory. The tests performed with dry and saturated flour showed the of friction angle of solid-soil to friction angle of soil-soil is in the range of 0.71 to 1.0 varying with the roughness of the surface of the solid material. Other tests performed with moist granular soils showed that the ratio of adhesion/cohesion was always much more lower than the ratio of friction angles.[26]

Al- Hussaini and Gilbert (1974) [27] performed tests for the purpose of studying the effect of wetting the solid surfaces on the solid-soil shearing resistance. Test results indicate that a small amount of water is sufficient to reduce solid-soil friction (about 50 % less) and causing slipperiness.

Ampera and Aydogmus (2005) [28] investigated friction between peat and silt soils with various construction materials. This study shows that peak shear stress increases as the solid surface roughness increases and the shear deformation required

to reach the peak value also increases with the surface roughness. The authors have analyzed the results of experimentation on the change of skin friction as a function of grain distribution of soils, moisture content, normal load, type of construction material, and difference of surface finish. The results confirm that in every case the skin friction was lower than the shearing strength of the soil.

# 3. INTRODUCTION TO THE METHOD OF SOLUTION

The mechanical behavior of vehicle-soil interaction is very complicated. However, in a situation that requires quick decision of mobility of a vehicle on a terrain, we need a simplified method that may include several assumptions to transform the problem into a comprehensible state. Here, the mobility problem is adapted to a well-known geotechnical problem, bearing capacity of soils, by following two basic assumptions:

1. Soil is homogenous, isotropic and has rigid-perfectly plastic behavior
2. Contact region between soil and the vehicle is flat and has a constant area even if the vehicle has tracks or wheels

The analysis of soil for mobility decision is focused on stresses at failure. So, the assumption of rigid-perfectly plastic behavior is adequate and acceptable. Flat contact region with constant area is an acceptable assumption for tracks but wheels have curved contact surface and variable contact area changing with stresses developed on the contact surface. However, when dealing the condition of total loss of mobility, using the value of flat contact area will be on the safe side.

Now, the mobility analysis problem can be adapted into soil bearing capacity problem. In order to determine the most critical situation in soil failure analysis, the shear force transmitted to the soil by the vehicle should be maximized. Accelerating vehicle climbing a slope or decelerating vehicle downward on a slope will be the most critical situations.

A vehicle moving in a horizontal pavement and with constant velocity transmits shear force to the ground only to overcome frictional loss of rolling resistance which has a negligible effect on required force. However, when off-road situation is considered, the force required to move the vehicle with constant velocity on horizontal ground becomes significant because of the sinkage of the wheels or tracks. The force required to overcome the sinkage is, in a sense, related to the force required to climb small slopes.

So a bearing capacity analysis that yields the maximum slope angle and maximum acceleration that vehicle can sustain without failure of underlying soil will be the most suitable mobility analysis when quick determination is needed .

The wheel or the track of an accelerating vehicle climbing a slope can be considered as an extraordinary footing on a slope with base parallel to the slope as shown in the Fig.3.1(a). When the horizontal and vertical axis transform to tangential and normal axis in order to adapt the base of the footing to an ordinary footing with base parallel to the horizontal, problem turns into a seismic bearing capacity problem with a foundation carrying inclined load as shown in Fig.3.1(b). The normal and tangential components of the soil weight are now acting as inertial forces of the soil similar to horizontal and vertical force components of earthquake loads. This is exactly the same problem discussed in Fishman et al. (2003); foundation carrying an inclined load on a soil that is under seismic activity .

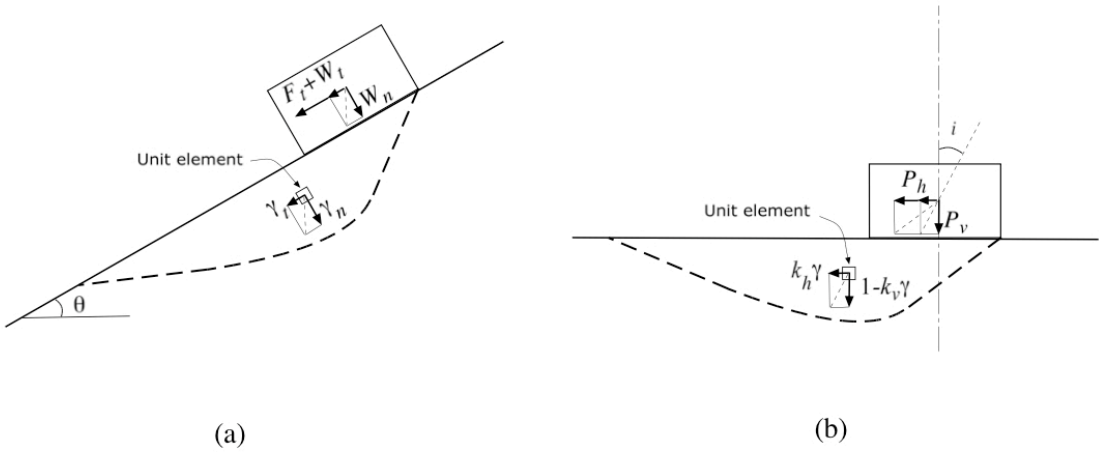



Figure 3.1. Footing and body forces exerted on (a) sloped soil (b) soil under seismic loads

In Fishman et al. (2003) approach, seismic loads are assumed as uniform loads, indeed they are not. However, when transforming a sloping ground to a horizontal ground by applying inertial forces to the soil, same assumption totally acceptable, because the force components of the soil weight are static as weight is a static load.

Adapting Fishman et al. (2003) approach to mobility analysis will be appropri-

ate but not adequate because it does not consider cohesive strength of the soil or in other words it is only for cohesionless soil. Budhu and Al-Karni (1993) approach is considering cohesive soils, however in that approach the geometry of seismic failure surface is determined by only considering the effect of seismic acceleration on soil, i.e. the inclination of the load is not considered. And in both approaches, there is not a solution for the cohesive component of the bearing capacity of frictional soils .

In this study, in order to determine the reduction in surcharge and soil weight components of the bearing capacity equation, Fishman et al. (2003) method will be used. However, for the cohesive component of the bearing capacity of frictional soils Budhu and Al-Karni (1993) method will be adapted to mobility problems. Moreover, a new method based on Coulomb wedge mechanism will be introduced to determine the cohesive component of the bearing capacity of frictionless soils.

The vehicle loads exerted to the soil will be investigated, then failure mechanism as a function of this load will be determined and finally, reduction factors will be introduced to the modified bearing capacity equation for mobility decision.

# 4. VEHICLE LOADS EXERTED TO THE GROUND

## 4.1. Introduction

The weight of the vehicle is transmitted to the ground through the tires or tracks of the vehicle. Equal sharing of the vehicle load between the tires or the tracks is a fair assumption when the vehicle stands on a horizontal ground. However, one can easily predict that for vehicles climbing a slope, rear tires will carry more load than front wheels and for vehicle moving downward on a slope vice versa. This phenomenon is quite important for mobility decision using bearing capacity solution, because accepting uniform distribution of the loads between tires will result in an unsafe solution.

The horizontal position of the center of gravity of a vehicle determines the load distribution between the wheels or through the tracks. The vertical position of the center of gravity does not have any effect on load distribution when the vehicle is on horizontal ground. However when the vehicle on a slope, height of the center of the gravity with respect to ground will create an additional moment arm in force equilibrium.

In order to solve this problem of load distribution in plane strain condition, equal sharing of the load between the wheels of an axle or between the tracks of the vehicle is assumed. So if the total weight of the vehicle is $W_v$:

$$w_v = \frac{W_v}{2E} \tag{4.1}$$

where $w_v$ is the weight of the vehicle in plane strain condition and E is the width of the wheel or the track.

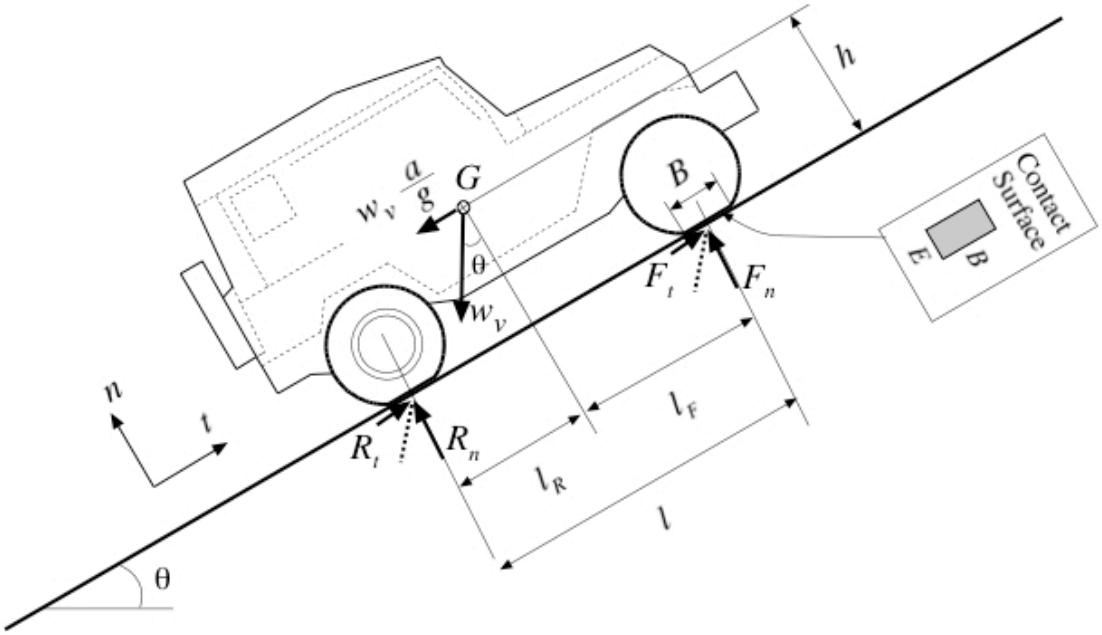



Figure 4.1. Forces acting on a wheeled vehicle on slope

## 4.2. Wheeled Vehicles

The forces acting on a vehicle that is climbing a slope with an acceleration of $a$ is shown in Fig.4.1. The horizontal distance between the center of the gravity and the rear axle is $l_R$, and front axle is $l_F$, the vertical distance between the center of gravity and the bottom of the wheel is $h$, the distance between the axles of the vehicle is $l$, the normal and the tangential components of the reaction force on the rear wheel are $R_n$ and $R_t$ and the normal and the tangential components of the reaction force on the front wheel are $F_n$ and $F_t$ respectively. These reaction force components constitute four unknowns, and the four equations for their solutions are:

1. Force equilibrium in the normal direction:

$$R_n + F_n = w_v \cos\theta \tag{4.2}$$

2. Force equilibrium in the tangential direction:

$$R_t + F_t = w_v \sin\theta + w_v \frac{a}{g} \tag{4.3}$$

3. Moment equilibrium about point G:

$$F_n \cdot l_F + F_t \cdot h + R_t \cdot h = R_n \cdot l_R \tag{4.4}$$

4. By the assumption of the reaction forces on the rear and the front wheel have the same inclination $i$:

$$i = \frac{F_t}{F_n} = \frac{R_t}{R_n} \tag{4.5}$$

Substituting Eq.4.2, Eq.4.3, into Eq.4.5:

$$F_t = \left[\tan\theta + \frac{a}{g\cos\theta}\right] F_n \tag{4.6}$$

so:

$$i = \left[\tan\theta + \frac{a}{g\cos\theta}\right] \tag{4.7}$$

by substituting Eq.4.2, Eq.4.3 and Eq.4.6 into Eq.4.4:

$$F_n \left[l_F + l_R\right] = w_v \cos\theta \left[l_R - ih\right] \tag{4.8}$$

and $l_F + l_R = l$:

$$F_n = w_v \cos\theta \left[\frac{l_R}{l} - \frac{h}{l} i\right] \tag{4.9}$$

Normal force on the rear wheel using Eq. 4.2:

$$R_n = w_v \cos\theta \left[1 - \frac{l_R}{l} + \frac{h}{l} i\right] \tag{4.10}$$

and $l - l_R = l_F$:

$$R_n = w_v \cos\theta \left[\frac{l_F}{l} + \frac{h}{l} i\right] \tag{4.11}$$

So tangential force components:

$$F_t = w_v \cos\theta \left[\frac{l_R}{l} - \frac{h}{l} i\right] i \tag{4.12}$$

$$R_t = w_v \cos\theta \left[\frac{l_F}{l} + \frac{h}{l} i\right] i \tag{4.13}$$

If $q_w$ is the uniform inclined load exerted to the ground trough the most critical wheel of the vehicle:

$$q_w = \frac{w_v \cos\theta}{B} \sqrt{R_n^2 + R_t^2} \tag{4.14}$$

$$q_w = \frac{w_v \cos\theta}{B} \left[\frac{l_F}{l} + \frac{h}{l} i\right] \sqrt{i^2 + 1} \tag{4.15}$$

## 4.3. Tracked Vehicles

The force distribution under a tracked vehicle can be determined by the procedure used in eccentrically loaded foundations. The eccentricity in $n - t$ axis for a tracked

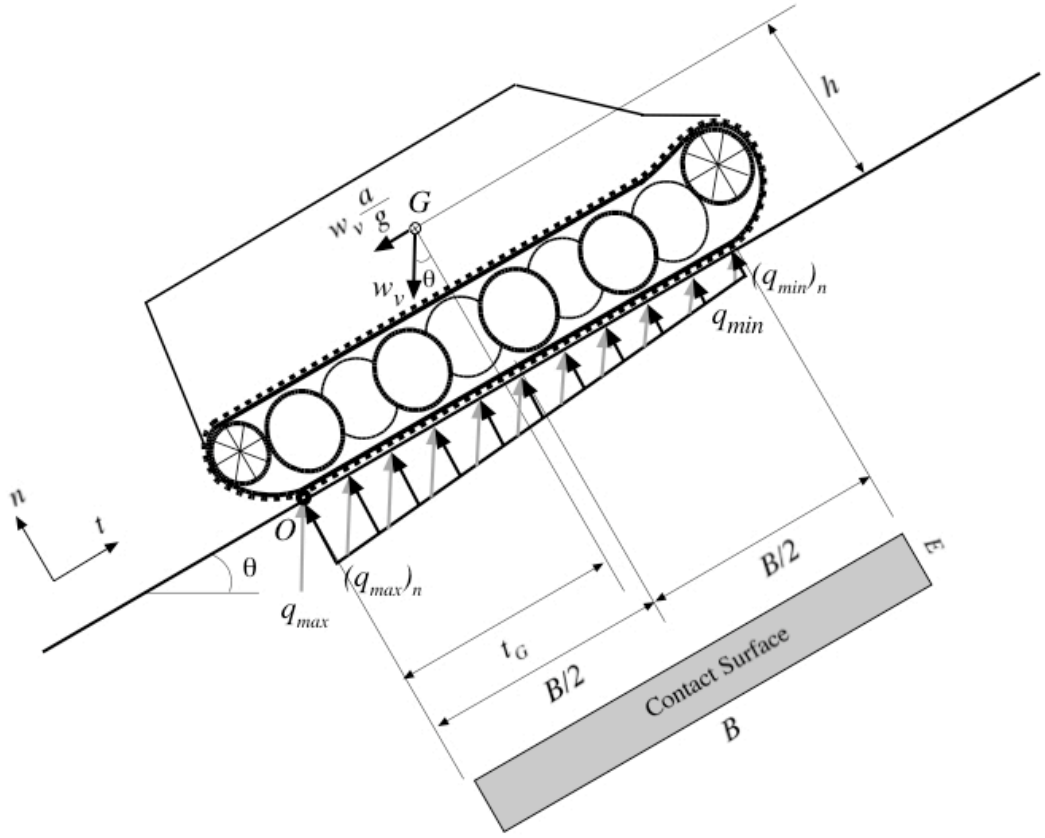



Figure 4.2. Forces acting on a tracked vehicle on slope

vehicle on a slope as shown in Fig.4.2:

$$e = \frac{M}{Q} = \frac{w_v \cos\theta \cdot \left[\frac{B}{2} - t_G\right] + w_v \frac{a}{g} \cdot h + w_v \sin\theta \cdot h}{w_v \cos\theta} \tag{4.16}$$

where $B$ is the length of the bottom track, $t_G$ is the horizontal distance between the center of gravity and the rear bottom of the track.

$$e = \frac{B}{2} - t_G + h\left[\frac{a}{g\cos\theta} + \tan\theta\right] \tag{4.17}$$

recalling Eq.4.7 and substituting $i$:

$$e = \frac{B}{2} - t_G + ih \tag{4.18}$$

The common method used for the foundations transmitting eccentric loads is also valid for tracked vehicles. Therefore, if the value of $e \leqslant B/6$:

$$(q_n)_{max} = \frac{w_v \cos\theta}{B}\left[1 + \frac{6e}{B}\right] \tag{4.19}$$

$$(q_n)_{min} = \frac{w_v \cos\theta}{B}\left[1 - \frac{6e}{B}\right] \tag{4.20}$$

However, if the value of $e \geqslant B/6$, tension will develop in the front side of the track which means there will be separation between the track and the soil in front part. Then the value of $(q_n)_{max}$:

$$(q_n)_{max} = \frac{4w_v \cos\theta}{3(B - 2e)} \tag{4.21}$$

The method of Mayerhof (1953) for bearing capacity determination of eccentrically loaded foundations suggests determining ultimate bearing capacity developed over an effective length of $B'$ and comparing with $(q_n)_{max}$ where:

$$B' = B - 2e \tag{4.22}$$

So, If $q_t$ is the maximum uniform inclined load exerted to the ground trough the tracks of the vehicle:

1. For $e \leqslant B/6$:

$$q_t = \frac{w_v \cos\theta}{B}\left[1 + \frac{6e}{B}\right]\sqrt{i^2 + 1} \tag{4.23}$$

2. For $e \geqslant B/6$:

$$q_t = \frac{4w_v \cos\theta}{3B'}\sqrt{i^2+1} \tag{4.24}$$

and the effective track length (effective foundation width) to be used in bearing capacity calculations is $B'$.

## 4.4. Summary

The normal and tangential components of the wheel load:

$$(q_w)_n = \frac{w_v \cos\theta}{B}\left[\frac{l_F}{l} + \frac{h}{l}i\right] \tag{4.25}$$

$$(q_w)_t = (q_w)_n i \tag{4.26}$$

The normal and tangential components of the track load:

1. For $e \leqslant B/6$:

$$(q_t)_n = \frac{w_v \cos\theta}{B}\left[1 + \frac{6e}{B}\right] \tag{4.27}$$

$$(q_t)_t = (q_t)_n i \tag{4.28}$$

2. For $e \geqslant B/6$:

$$(q_t)_n = \frac{4w_v \cos\theta}{3B'} \tag{4.29}$$

$$(q_t)_t = (q_t)_n i \tag{4.30}$$

where $i$ is the inclination of the load computed in Eq.4.7 and $e$ is the eccentricity of the load computed in Eq.4.18.

If $q_{w/t}$ is maximum uniform load exerted to the ground through wheels or tracks:

$$(q_{w/t})_n = \frac{w_v \cos\theta}{B} k \tag{4.31}$$

$$(q_{w/t})_t = (q_{w/t})_n i \tag{4.32}$$

where for wheeled vehicles

$$k = \frac{l_F + hi}{l} \tag{4.33}$$

for tracked vehicles with $e \leqslant B/6$:

$$k = \frac{B + 6e}{B} \tag{4.34}$$

for tracked vehicles with $e \geqslant B/6$:

$$k = \frac{4B}{3B'} \tag{4.35}$$

# 5. SLIPPING OF THE VEHICLES

If the shear stress developed on the vehicle- soil interaction surface exceeds shear resistance between soil and the wheel or the tracks, tracks or wheels will start to slip. In other words the shear stresses exerted to the ground through the vehicle is limited by the shearing resistance between the soil and the wheel or track. As discussed in Section 2.4.6, the shearing resistance between the materials used in tires or wheels and the soil is lower than the shearing strength of the soil. However the strength values obtained by the laboratory tests of various materials is not applicable to the surfaces having lugs and voids.

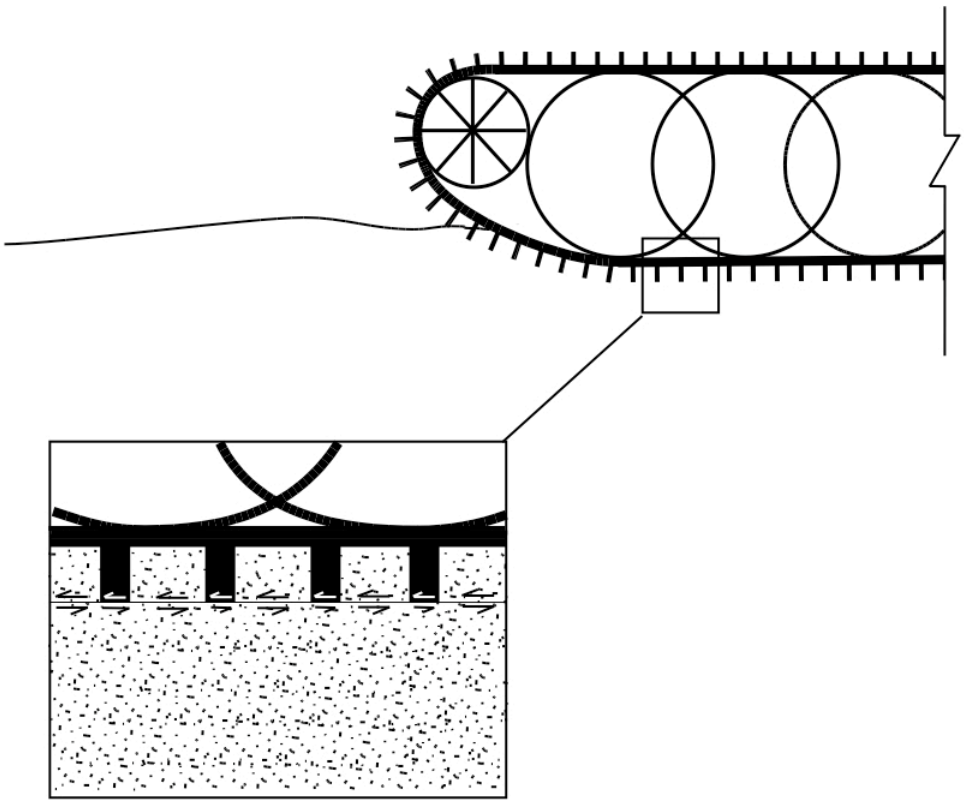


Figure 5.1. Shear forces between track and soil

In tracks, shear stress transmitted to the ground is mostly through the captured soil between the tracks. This means that the shear strength between the track and the

soil is almost equal to the shear strength of the soil (Fig. 5.1).

The tires of off-road vehicles also have lugs to increase traction. These lugs increase the interaction shear strength to a value between the shear strength of soil-rubber interface and shear strength of the soil within the gaps on surface of the tyre. This increase in strength is a function of the ratio of the gaps to lags on the surface of the track or the wheel. Shear strength between the tyre and the soil can be determined by some laboratory tests or by calculating the weighted averages of the soils internal and rubber-soil interface shear strengths according to gap ratio on surface of the tyre:

$$s_{ws} = \frac{A_l s_{rs} + A_v s}{A_t} \tag{5.1}$$

where $s_{ws}$ shear strength between soil and wheel, $s_{rs}$ shear strength between soil and rubber, $s$ shear strength of soil, $A_l$ area of the lugs, $A_v$ area of the gap between lugs, and $A_t$ is the total area of the tyre surface.

$$s_{ws} = a_{ws} + \frac{R_n}{B} \tan \phi_{ws} \tag{5.2}$$

$a_{ws}$ is the adhesion between the soil and tyre and

$$a_{ws} = \frac{A_l a_{rs} + A_v c}{A_t} \tag{5.3}$$

$a_{rs}$ is the adhesion between the soil and rubber, $c$ is the cohesion of the soil

$\phi_{ws}$=friction angle between the wheel and the soil:

$$\tan \phi_{ws} = \frac{A_l \tan \phi_{rs} + A_v \tan \phi}{A_t} \tag{5.4}$$

where $\phi_{rs}$ is the friction angle between the soil and the rubber, $\phi$ is the internal friction angle of the soil.

As the shear strength exerted to the ground can not exceed $s_{ws}$, tangential loads

exerted by the wheels are limited by:

$$R_t \leqslant s_{ws} B \tag{5.5}$$

$$iR_n \leqslant s_{ws} B \tag{5.6}$$

$$i\frac{R_n}{B} \leqslant a_{ws} + \frac{R_n}{B}\tan\phi_{ws} \tag{5.7}$$

and inclination is limited by:

$$i \leqslant \frac{a_{ws} B}{w_v \cos\theta \left[\frac{l_F}{l} + \frac{h}{l} i\right]} + \tan\phi_{ws} \tag{5.8}$$

For wheeled vehicles the $i$ value should be checked according to this inequality, if it does not satisfy the inequality, it will mean that vehicle can not pass the slope with specified slope angle and acceleration values independent from the bearing capacity of the soil. So, if the ultimate weight of the vehicle without slipping is $(W_v)_{all}$, substituting Eq.4.1 into Eq. 5.8:

$$(W_v)_{all} = \frac{a_{ws} 2BE}{\cos\theta \left[i - \tan\phi_{ws}\right] k} \tag{5.9}$$

# 6. MOBILITY ANALYSIS BY MODIFIED SEISMIC BEARING CAPACITY APPROACH

## 6.1. Introduction

Bearing capacity analysis by simple Coulomb mechanism is originally developed by Richards et al. (1993) for cohesionless soils under seismic activity. Fishman et al. (2003) improve this method and present inclination factors for bearing capacity equation that include reduction in strength of soil under seismic activity and also the reduction due to inclination of the load. However these methods are valid only for cohesionless soils. Budhu and Al-Karni (1993) approach as discussed in Section 2.3.4, proposed a solution for phi-c soils. However, in this approach the geometry of the failure surface is obtained by only considering the seismic effects. The effect of inclination of the load is not considered in the determination of the failure surface. Also, there is no solution for frictionless soils ($\phi = 0$) in both approaches.

In order to develop a complete and reasonable bearing capacity equation for mobility analysis, instead of following a single method with all shortcomings, a combination of the most reliable methods for each component should be used. Accordingly, chosen methods for each bearing capacity factor are summarized in Table 6.1:

Table 6.1. Analysis methods for bearing capacity factors

| Factor | Soil Type | Method |
|---|---|---|
| $N_q$ | All | Coulomb Wedge |
| $N_\gamma$ | All | Coulomb Wedge |
| $N_c$ | $\phi \neq 0$ | Budhu and Al-Karni (1993) |
| | $\phi = 0$ | Coulomb Wedge |

Section 6.2 describes the determination of mobility bearing capacity factor of surcharge ($N_{qm}$) and soil weight ($N_{\gamma m}$) on the basis of Coulomb wedge mechanism

proposed by Fishman et al. (2003).

Section 6.3 provides methods for the determination of of mobility bearing capacity factor of cohesion ($N_{cm}$). For frictional soils Budhu and Al-Karni (1993) method is adapted in Section 6.3.1, and for frictionless ($\phi = 0$) soils a new method is presented based on Coulomb analysis in Section 6.3.2.

In Section 6.4, reduction factors for mobility bearing capacity equations are defined.

In Section 6.5 the final equation for mobility bearing capacity is derived.

## 6.2. Determination of $N_{qm}$ and $N_{\gamma m}$

First cohesionless soil is considered to obtain mobility bearing capacity factors of surcharge ($N_{qm}$) and soil weight ($N_{\gamma m}$). The normal and tangential components of weight of a unit element on slope (Fig. 6.1):

$$\gamma_n = \gamma \cos\theta \tag{6.1}$$

$$\gamma_t = \gamma \sin\theta \tag{6.2}$$

The normal and tangential components of the surcharge load when the depth of footing base is $D$:

$$(q_0)_n = \gamma_n D \tag{6.3}$$

$$(q_0)_t = \gamma_t D \tag{6.4}$$

The normal and tangential components of the vehicle load:

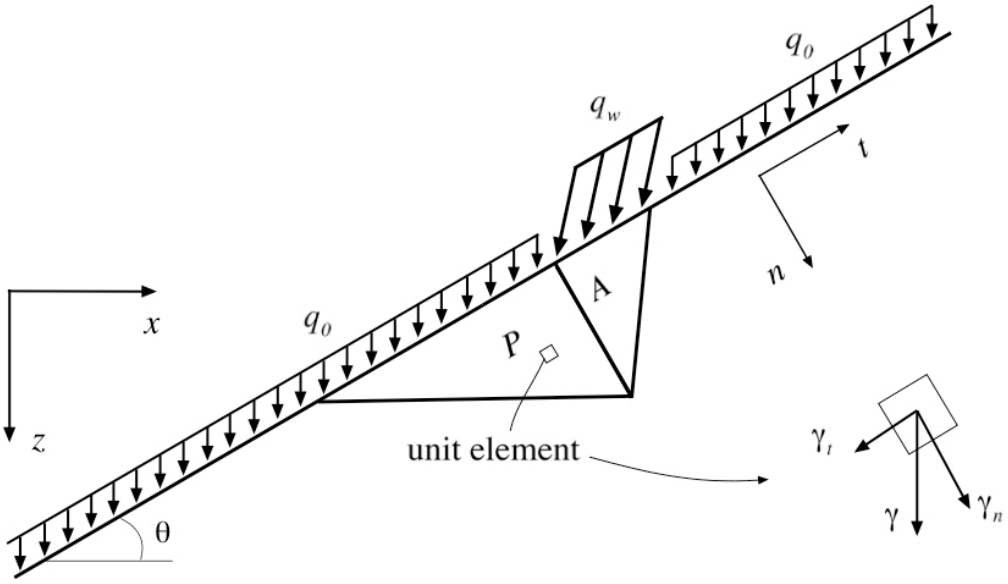



Figure 6.1. Loads and Coulomb wedges on a slope

$$(q_{w/t})_n = \frac{w_v \cos\theta}{B} k \tag{4.31}$$

$$(q_{w/t})_t = (q_{w/t})_n i \tag{4.32}$$

The forces acting on active and passive Coulomb wedges are shown in Fig.6.2. $W_A$ is the weight of the active wedge and $W_P$ is the weight of passive wedge:

$$W_{Pn} = W_p \cos\theta \tag{6.5}$$

$$W_{Pt} = W_p \sin\theta \tag{6.6}$$

$$W_{An} = W_a \cos\theta \tag{6.7}$$

$$W_{At} = W_a \sin\theta \tag{6.8}$$

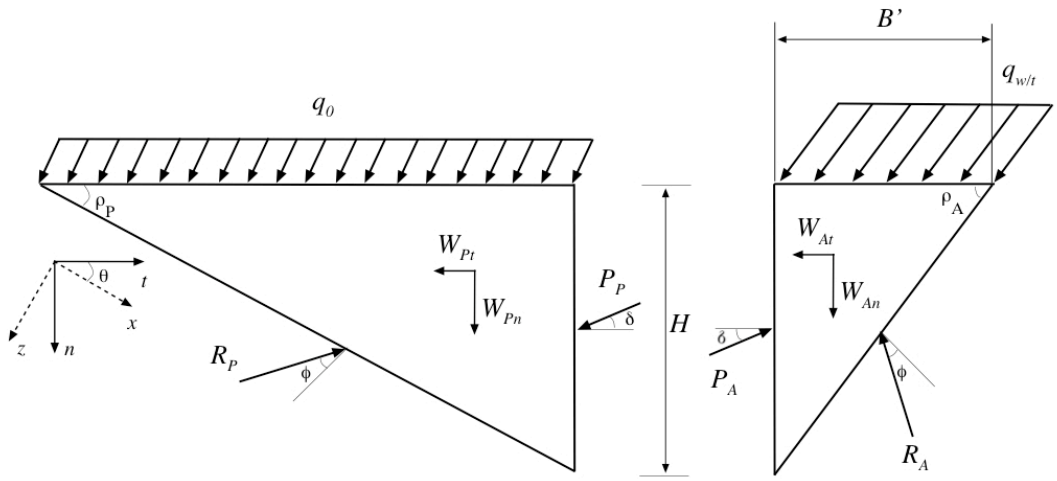



Figure 6.2. Coulomb's type failure mechanism for $c = 0$

The force equilibrium on the active wedges of Fig.6.2 can be written as follows:

$$R_A \cos(\rho_A - \phi) + P_A \sin\delta = W_{An} + (q_{w/t})_n B' \tag{6.9}$$

where $B'$ is the effective length of the contact area and $B' = B$ for wheeled vehicles, $B' = B - 2e$ for tracked vehicles:

$$R_A \sin(\rho_A - \phi) + W_{At} + (q_{w/t})_t B' = P_A \cos\delta \tag{6.10}$$

Substituting $R_A$ of Eq.6.10 to Eq.6.9:

$$\frac{P_A \cos\delta - W_{At} - (q_{w/t})_t B'}{\sin(\rho_A - \phi)} \cos(\rho_A - \phi) + P_A \sin\delta = W_{An} + (q_{w/t})_n B' \tag{6.11}$$

and rearranging for $P_A$:

$$P_A \frac{\cos\delta\cos(\rho_A-\phi)+\sin\delta\sin(\rho_A-\phi)}{\sin(\rho_A-\phi)} = \left[W_{At}+(q_{w/t})_t B'\right]\frac{\cos(\rho_A-\phi)}{\sin(\rho_A-\phi)}+W_{An}+(q_{w/t})_n B' \tag{6.12}$$

when we use the trigonometric equation:

$$\cos\delta\cos(\rho_A-\phi)+\sin\delta\sin(\rho_A-\phi)=\cos(\rho_A-\phi-\delta) \tag{6.13}$$

Eq.6.12 becomes:

$$P_A = \left[\left[W_{At}+(q_{w/t})_t B'\right]\frac{\cos(\rho_A-\phi)}{\sin(\rho_A-\phi)}+W_{An}+(q_{w/t})_n B'\right]\frac{\sin(\rho_A-\phi)}{\cos(\rho_A-\phi-\delta)} \tag{6.14}$$

substituting $(q_{w/t})_t = i(q_{w/t})_n$, $W_{An} = (1/2)\gamma_n B' H$, $W_{At} = (1/2)\gamma_t B' H$, $B' = H\cot\rho_A$, $\gamma_n = \gamma\cos\theta$ and $\gamma_t = \gamma\sin\theta$ :

$$P_A = \left[\frac{1}{2}\gamma H^2\sin\theta + i(q_{w/t})_n H\right]R_1 + \left[\frac{1}{2}\gamma H^2\cos\theta+(q_{w/t})_n H\right]R_2 \tag{6.15}$$

where:

$$R_1 = \frac{\cos(\rho_A-\phi)\cot\rho_A}{\cos(\rho_A-\phi-\delta)} \tag{6.16}$$

$$R_2 = \frac{\sin(\rho_A-\phi)\cot\rho_A}{\cos(\rho_A-\phi-\delta)} \tag{6.17}$$

Passive trust can be obtained using Eq.2.54 and corresponding passive earth pressure coefficient can be calculated using Eq.2.41. So,

$$P_P = \frac{1}{2}\gamma H^2 K_{PE} + qHK_{PE} \tag{6.18}$$

where $K_{PE}$ is equal to $K_P$ with an imaginary seismic acceleration ratio of $\theta$ which is equal to $\tan^{-1}[k_h/(1-k_v)]$. This $\theta$ value exactly fit our slope angle. In seismic situation $\tan\theta$ is equal to $k_h/(1-k_v)$ and in sloping ground $\tan\theta$ is equal to $\gamma_t/\gamma_n$. In a seismic activity the vectorial summation of the seismic and gravitational acceleration creates, in a sense, an imaginary slope where the horizontal and normal soil weight components correspond to the horizontal and vertical loads on the unit element during a seismic activity (Fig. 3.1).

So adapting the seismic lateral earth pressure coefficient into our case:

$$K_P = K_{PE} = \frac{\cos^2 a}{\cos\theta \cdot \cos(\delta+\theta) \cdot \left[1-\sqrt{\frac{\sin(\phi+\delta)\cdot\sin a}{\cos(\delta+\theta)}}\right]^2} \tag{2.41}$$

At failure, $P_A = P_P$:

$$\left[(\frac{1}{2}\gamma H^2 \sin\theta + i(q_{w/t})_n H)\right] R_1 + \left[\frac{1}{2}\gamma H^2 \cos\theta + (q_{w/t})_n H\right] R_2 = \frac{1}{2}\gamma H^2 K_P + qHK_P \tag{6.19}$$

Rearranging the equation for $(q_{w/t})_n$:

$$(q_{w/t})_n (R_1 + iR_2) = \frac{1}{2}\gamma H(K_P - R_1\sin\theta - R_2\cos\theta) + qK_P \tag{6.20}$$

Here, the $(q_{w/t})_n$ value shows the maximum normal load that can be transmitted from the vehicle to the ground without failure. In order to obtain the ultimate vehicle weight that can move on a given slope with a specified acceleration and without causing soil failure, equation of load distribution of tracked and wheeled vehicles (Eq. 4.31) should be substitute in Eq. 6.20:

$$\frac{w_v \cos\theta}{B} k = \frac{1}{2}\gamma H \frac{K_P - R_1\sin\theta - R_2\cos\theta}{R_1 + iR_2} + q\frac{K_P}{R_1 + iR_2} \tag{6.21}$$

and the ultimate vehicle weight in plane strain condition in terms of Terzaghi's bearing

capacity factor for $c = 0$:

$$\frac{(w_v)_{all}}{B} = qN_{qm} + \frac{1}{2}\gamma B N_{\gamma m} \tag{6.22}$$

where $N_{qm}$ and $N_{\gamma m}$ are mobility bearing capacity factors:

$$N_{\gamma m} = \left[\frac{K_P - R_1 \sin\theta - R_2 \cos\theta}{(R_1 + iR_2)\cos\theta}\right] \frac{\tan\rho_A}{k} \tag{6.23}$$

$$N_{qm} = \frac{K_P}{k(R_1 + iR_2)\cos\theta} \tag{6.24}$$

Angle of rupture surface for active wedge ($\rho_A$) can be found by iteration. $P_A = P_P$ at failure:

$$P_A = P_P = \frac{1}{2}\gamma H^2 K_A + qHK_A \tag{6.25}$$

$$K_A = \frac{P_P}{\frac{1}{2}\gamma H^2 + p_n H} \tag{6.26}$$

and $\rho_A$ is the angle giving maximum value of $K_A$.

### 6.3. Determination of $N_{cm}$

The method of Fishman et al. (2003), Coulomb wedge analysis for seismic bearing capacity, does not suggest a solution for the reduction in cohesive component of bearing capacity equation. Budhu and Al-Karni (1993) approach has a solution for $\phi$-$c$ soils but it is also limited by non zero internal shearing strength values.

Therefore, in order to overcome these shortcomings for mobility analysis, Budhu

and Al-Karni (1993) approach will be adapted for determination of reduction in $N_{cm}$ of frictional soils in Section 6.3.1 and Coulomb analysis will be extended to calculate the reduction in $N_{cm}$ of frictionless soils in Section 6.3.2.

### 6.3.1. Determination of $N_{cm}$ for Frictional Soils

The failure of soil under the vehicle is now assumed to be as shown in Fig.6.3. The geometry of the failure surface corresponds to modified Vesic's failure surface as discussed in Secion 2.3.4.

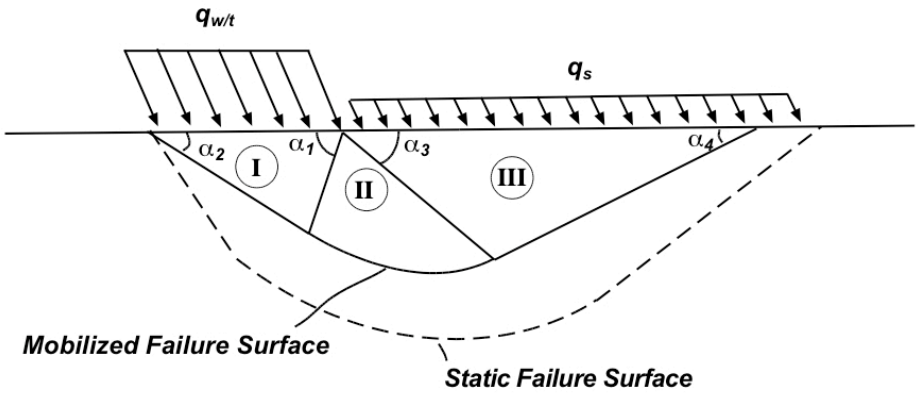



Figure 6.3. Modified Vesic's surface for mobility analysis

Recalling the term $\theta$, which is equal to $\tan^{-1}\left[k_h/(1-k_v)\right]$ in dynamic fludization concept and corresponds to slope angle in mobility analysis as discussed in Section 2.2.2, the equations of lateral earth pressure coefficients and rotation angle of the principle planes (2.23,2.24, 2.25 and 2.26) can be modified as follows when $k_v$ is equal to zero:

$$K_{PM} = \frac{\sin^2\phi + 1}{\cos^2\phi} + \frac{2c\tan\phi}{\gamma z} + \sqrt{\left[\frac{2c\tan\phi}{\gamma z} + \frac{\sin^2\phi+1}{\cos^2\phi}\right]^2 + \left[\frac{2c}{\gamma z}\right]^2 + \frac{4c}{\gamma z}\tan\phi - \frac{4\tan^2\theta}{\cos^2\phi} - 1} \tag{6.27}$$

$$K_{AM} = \frac{\sin^2\phi + 1}{\cos^2\phi} + \frac{2c\tan\phi}{\gamma z} - \sqrt{\left[\frac{2c\tan\phi}{\gamma z} + \frac{\sin^2\phi+1}{\cos^2\phi}\right]^2 + \left[\frac{2c}{\gamma z}\right]^2 + \frac{4c}{\gamma z}\tan\phi - \frac{4\tan^2\theta}{\cos^2\phi} - 1} \tag{6.28}$$

$$\tan\alpha_A = \frac{2\tan\theta}{1 - K_{AE} + \sqrt{(1-K_{AE})^2 + 4(\tan\theta)^2}} \tag{6.29}$$

$$\tan\alpha_P = \frac{2\tan\theta}{K_{PE} - 1 + \sqrt{(K_{PE}-1)^2 + 4(\tan\theta)^2}} \tag{6.30}$$

The angles of failure surface are:

$$\alpha_1 = \pi/4 + \phi/2 + \alpha_A \tag{2.62}$$

$$\alpha_2 = \pi/4 + \phi/2 - \alpha_A \tag{2.63}$$

$$\alpha_3 = \pi/4 + \phi/2 + \alpha_P \tag{2.64}$$

$$\alpha_4 = \pi/4 + \phi/2 - \alpha_P \tag{2.65}$$

By deriving equilibrium equations by following same procedure with Budhu and Al-Karni (1993), $N_{cm}$ equation for equilibrium in the horizontal direction is found as:

$$N_{cm1} = \frac{P_{pc}\cos(\alpha_1 - \phi) + P_{mc}\cos(\alpha_2 - \phi_m)}{cB} + \frac{(1+m)\sin\alpha_1\sin\alpha_2}{\sin(\alpha_1+\alpha_2)} \tag{6.31}$$

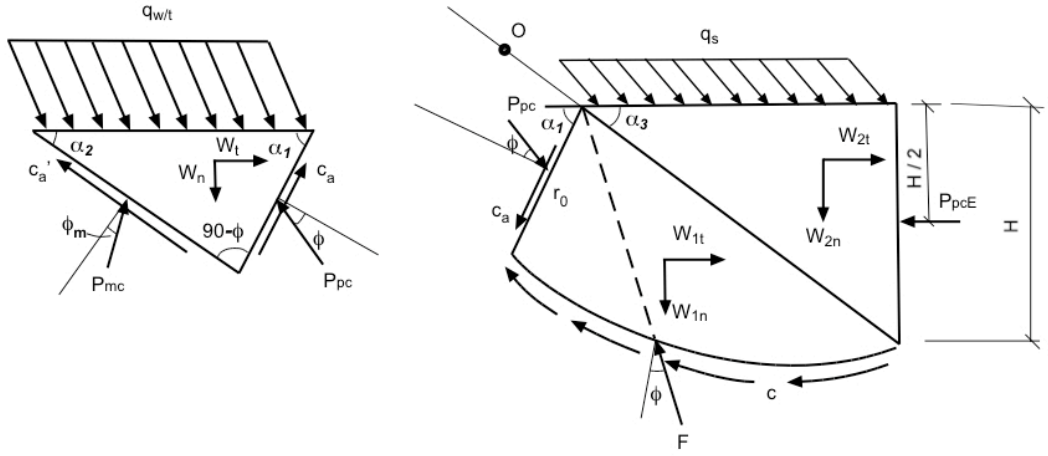



Figure 6.4. Forces acting on failure surfaces

and $N_{cm}$ equation for equilibrium in the vertical direction:

$$N_{cm2} = \frac{1}{i}\left[\frac{P_{pc}\sin(\alpha_1 - \phi) - P_{mc}\sin(\alpha_2 - \phi_m)}{cB} - \frac{\sin\alpha_2\cos\alpha_1 - m\sin\alpha_1\cos\alpha_2}{\sin(\alpha_1 + \alpha_2)}\right] \tag{6.32}$$

As described in Section 2.3.4, by iterating these two equations for different $m$ values, $N_{cm}$ can be found by the $m$ value when $N_{cm1} = N_{cm2}$:

$$N_{cm} = \frac{N_{cm1}}{k\cos\theta} \tag{6.33}$$

### 6.3.2. Determination of $N_{cm}$ for Frictionless Soils

Cohesive factor of mobility bearing capacity for frictionless soil can be determined with Coulomb analysis . First by setting $\gamma$ and $q_s$ values to zero, the force equilibriums on the passive wedge of Fig.6.5 will be:

$$R_P\cos\rho_P = 2cH \tag{6.34}$$

$$R_P\sin\rho_P + cH/\tan\rho_P = P_P \tag{6.35}$$

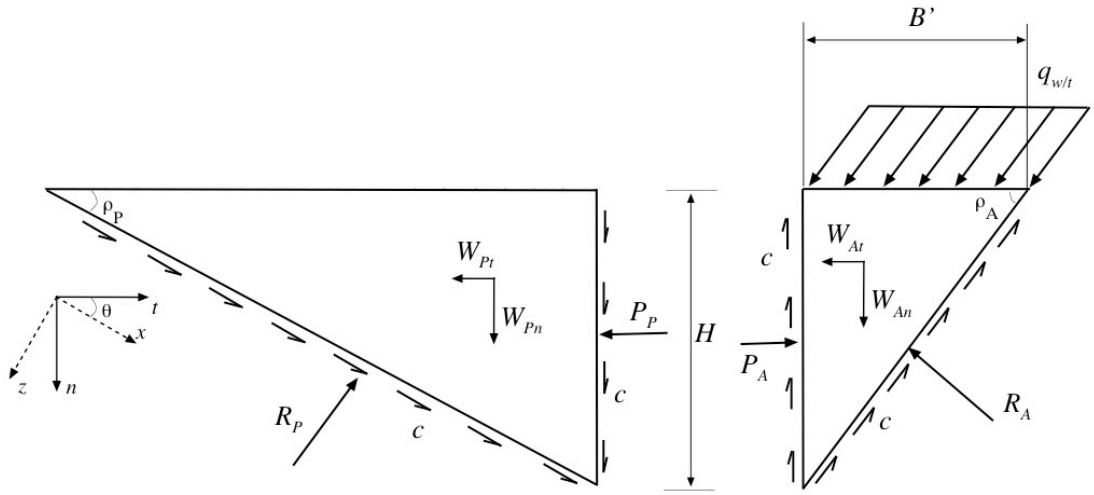



Figure 6.5. Coulomb's failure mechanism for $\phi = 0$ $q_s = 0$

and solving for $P_P$:

$$P_P = 2cH \tan \rho_P + \frac{cH}{\tan \rho_P} \tag{6.36}$$

The minimum value of $P_P$ corresponds to failure. Therefore, the value of $\rho_P$ that makes the derivative of the function $P_P(\rho_P)$ is equal to zero will be the angle of rupture surface at failure:

$$P'_P(\rho_P) = \frac{2cH}{\cos^2 \rho_P} - \frac{cH}{\sin^2 \rho_P} = 0 \tag{6.37}$$

when $\rho_P = 35.264°$ $P_P$ has minimum value of 2.83 $cH$.

The force equilibrium in the passive wedge:

$$R_A \cos \rho_A + 2cH = (q_{w/t})_n B \tag{6.38}$$

$$R_A \sin \rho_P + (q_{w/t})_t B = cB + P_A \tag{6.39}$$

solving for $P_A$ when $B = H \cot \rho_A$:

$$P_A = (q_{w/t})_t H \cot \rho_A - cH \cot \rho_A + \frac{(q_{w/t})_n H \cot \rho_A - 2cH}{\cos \rho_A} \sin \rho_A \quad (6.40)$$

$$P_A = H \left[ \cot \rho_A ((q_{w/t})_t - c) + (q_{w/t})_n - \frac{2c}{\cot \rho_A} \right] \quad (6.41)$$

$(q_{w/t})_t = i(q_{w/t})_n$ and at failure $P_A = P_P = 2.83\ cH$:

$$2.83cH = H \left[ \cot \rho_A (i(q_{w/t})_n - c) + (q_{w/t})_n - \frac{2c}{\cot \rho_A} \right] \quad (6.42)$$

solving for $(q_{w/t})_n$:

$$(q_{w/t})_n (i \cot \rho_A + 1) = 2.83c + \frac{2c}{\cot \rho_A} + \cot \rho_A c \quad (6.43)$$

substituting $(q_{w/t})_n = k w_v \cos \theta / B$ :

$$\frac{w_v \cos \theta}{B} k = c \left[ \frac{2.83 + 2 \tan \rho_A + \cot \rho_A}{i \cot \rho_A + 1} \right] \quad (6.44)$$

and the ultimate vehicle weight in plane strain condition in terms of Terzaghi's bearing capacity factor for $\phi = 0$ and $\gamma = 0$:

$$\frac{(w_v)_{all}}{B} = c N_{cm} \quad (6.45)$$

So, mobility bearing factor for cohesion:

$$N_{cm} = \frac{2.83 + 2 \tan \rho_A + \cot \rho_A}{k \cos \theta (i \cot \rho_A + 1)} \quad (6.46)$$

$\rho_A$ value that makes the $N_{cm}$ minimum will be the angle of rupture surface at failure and it can be found by iteration.

## 6.4. Reduction Factors for Bearing Capacity Analysis of Mobile Vehicles

In addition to factors in Hansen equation

$$q_f = \frac{1}{2}\gamma B N_\gamma s_\gamma d_\gamma i_\gamma + c N_c s_c d_c i_c + q_0 N_q s_q d_q i_q \tag{2.41}$$

where $s_\gamma$, $s_c$, $s_q$ are shape factors, $d_\gamma$, $d_c$, $d_q$ are depth factors and $i_\gamma$, $i_c$, $i_q$ are inclination factors, mobility reduction factors can be inserted:

$$m_\gamma = \frac{N_{\gamma m}}{N_{\gamma(m=0)}} \tag{6.47}$$

$$m_q = \frac{N_{qm}}{N_{q(m=0)}} \tag{6.48}$$

$$m_c = \frac{N_{cm}}{N_{c(m=0)}} \tag{6.49}$$

where $m_\gamma$, $m_q$ and $m_c$ are mobility reduction factors of soil weight, surcharge and cohesion factors of standard bearing capacity equation in order. $N_{\gamma m}$ and $N_{qm}$ are the calculated bearing capacity factors by Coulomb wedge analysis for an accelerating vehicle on a slope and $N_{\gamma(m=0)}$ and $N_{q(m=0)}$ are bearing capacity factors calculated by Coulomb analysis when the vehicle stops on horizontal ground with same soil parameters. For frictionless soil, $N_{cm}$ and $N_{c(m=0)}$ again calculated by Coulomb wedges when vehicle is accelerating vehicle on a slope and when vehicle stops on horizontal ground respectively. However, for frictional soils, $N_{cm}$ is calculated by Budhu and Al-Karni (1993) method which best describes the decreasing in the seismic failure surface in cohesive soils. In this method, $N_{c(m=0)}$ is equal to $N_c$ used in classic bearing capacity equation.

## 6.5. Modified Bearing Capacity Equation for Off-Road Mobility

Now, reduction factors for mobility analysis can be inserted in classical bearing capacity equation: Inclination factor included in mobility reduction factor and depth factor is negligible in mobility analysis. So ultimate vehicle weight that can be supported by the soil can be found by:

$$q_{ult} = \left[\frac{1}{2}\gamma B N_\gamma s_\gamma m_\gamma + c N_c s_c m_c + q N_q s_q m_q\right] \tag{6.50}$$

so, for wheeled vehicles:

$$(W_v)_{all} = \left[\frac{1}{2}\gamma B N_\gamma s_\gamma m_\gamma + c N_c s_c m_c + q N_q s_q m_q\right] 4BE \tag{6.51}$$

and tracked vehicles

$$(W_v)_{all} = \left[\frac{1}{2}\gamma B N_\gamma s_\gamma m_\gamma + c N_c s_c m_c + q N_q s_q m_q\right] 2BE \tag{6.52}$$

# 7. COMPUTATION SCHEME FOR MOBILITY DECISION

The methods used in the determination of mobility bearing capacity are discussed in details in previous sections. Since the solutions are based on iterations, a computer program is required to handle the calculations. The computation procedures are described briefly in this section in order to construct a scheme for a computer program and to summarize the whole solution method.

Since there is no direct solution, each required parameter has a different computation method. However, in a mobility decision problem, there are mainly three different cases:

- What is the maximum weight of the vehicle that can pass through a specified route?
- What is the allowable slope angle along the vehicle's route?
- What is the maximum acceleration of the vehicle that does not result in failure of soil?

Among these three cases, the most useful one is the case in which the slope angle is required. If the topography and the soil characteristics of the terrain are known, the most suitable route can be easily determined in a very short time. The computation procedures for maximum vehicle weight, maximum slope angle and maximum acceleration are described in the following sections.

The computer algorithm has four main parts:

- Analysis Type: The user chooses the desired parameter; allowable weight, allowable slope or allowable acceleration. Accordingly, the program will continue on the corresponding module.
- Data Input: User enters the vehicle, terrain and vehicle-soil interaction parameters.

- Calculation Parts: Direct calculations are made in these parts.
- Iteration Parts: Iterative calculations in specified increments and limits are made in these parts. After the completion of the iteration, the result will be an array. The element of the array which is providing the defined condition (e.g. the element of the $\rho_A$ array which makes $K_A$ value maximum) will be used in following calculations.

### 7.1. Computation Scheme for Allowable Vehicle Weight

The maximum vehicle weight that soil can carry is computed in this part (Table 7.3). Vehicle type (wheeled or tracked), the location of center of gravity and maximum acceleration of the vehicle are the input data for the vehicle characteristics.

Maximum slope angle on the route, internal friction angle, unit weight and cohesive strength of the soil are the input data for terrain characteristics. The width and the length of the contact surface between soil and the vehicle, the ruth depth and interface shear strength parameters of the interaction are the input data for the interaction characteristics.

There are three different calculation method for bearing capacity factors: The Fishman et. al.(2003) method for calculation of $N_{qm}$ and $N_{\gamma m}$, Budhu and Al-Karni (1993) method for $N_{cm}$ for frictional soils and new proposed method for $N_{cm}$ for frictionless soils.

To determine $N_{qm}$ and $N_{\gamma m}$, $i$, $k$ and $K_P$ are calculated. Then by defining an array for $\rho_A$ angle with the elements between $0^o$ and $45^o$, the $R_1$, $R_2$, $P_P$, $(q_{w/t})_n$, $H$ and $K_A$ arrays are calculated. The element of the $\rho_A$ array which corresponds to the element of the maximum value of the array $K_A$ is the $\rho_A$ value to be used in calculations of $N_{qm}$ and $N_{\gamma m}$. Then setting $a$ and $\theta$ values to zero same procedure is applied to get the values of bearing capacity factors when vehicle is at rest in horizontal position ($N_{qm=0}$, $N_{\gamma m=0}$).

In determination of $N_{cm}$ for frictionless soils, after the calculation of $i$ and $k$ values, again $\rho_A$ array is used for the calculation of $N_{cm}$ array. And this time $\gamma$ value is set to zero and the element of the $N_{cm}$ array which has minimum value is the correct $N_{cm}$ value. By following same procedure, but now setting $a$ and $\theta$ values to zero, $N_{qm=0}$ is calculated. For frictional soils, after the calculation of $i$, $k$, $K_M$ and $\alpha_{1:4}$ values; $P_{pc}$, $P_{mc}$ and $N_{cm}$ arrays with changing $m$ are calculated as described in Budhu and Al-Karni (1993) method. The $m$ value which makes the $N_{cm}$ values (derived from the horizontal and the vertical force equilibriums) gives the correct $N_{cm}$ value. $N_{cm=0}$ for the frictional soils has the same value with $N_c$ found by Meyerhof (1953)'s equation. The next step is the calculations of mobility reduction factors: $m_q$, $m_\gamma$ and $m_c$, and the shape factors. $s_q$, $s_\gamma$ and $s_c$. Then the capacity of soil for vehicle mobility can be determined .

The minimum of the vehicle weights calculated by the bearing capacity and the slip analyses will be the allowable vehicle weight ($[W_v]_{all}$).

## 7.2. Computation Scheme for Allowable Slope Angle

The computation method is very similar to the allowable vehicle computation method. Here, user enters the vehicle weight. However, the program performs the same computations as if the vehicle weight is an unknown and whole structure goes into iteration with changing slope angle value. And the slope angle which gives the closest vehicle weight value to the value defined by user, will be the allowable slope angle (Table 7.2).

## 7.3. Computation Scheme for Allowable Acceleration

Same approach is valid also for the acceleration computation. User enters the vehicle weight, then the program goes into iteration on acceleration values and the acceleration value which gives the closest vehicle weight value to the value defined by the user, will be the allowable acceleration (Table 7.3).

Table 7.1. Computer program scheme for determination of allowable vehicle weight

| | | | | | |
|---|---|---|---|---|---|
| Unknown | Allowable Vehicle Weight ($(W_v)_{all}$) | | | | |
| Input Data | Vehicle | | Terrain | Interaction | |
| | Vehicle Type (W/T) | | Max slope ($\theta$) | Width of contact surface ($E$) | |
| | Center of Gravity ($l_f$,$h$,$l$,$t_g$) | | Int. friction ($\phi$) | Length of Contact Surface($B$) | |
| | Acceleration ($a$) | | Unit weight ($\gamma$) | Ruth depth ($D$) | |
| | | | Cohesion ($c$) | Interface Strength ($a_{ws}$,$\phi_{ws}$) | |
| Calculations | $N_{qm}$ and $N_{\gamma m}$ | | $N_{cm}$ | | |
| | | | if $[\phi = 0]$ | | if $[\phi \neq 0]$ |
| | $c = 0$ | $a = c = \theta = 0$ | $\gamma = 0$ | $a = \gamma = \theta = 0$ | $i$ (Eq.4.7) |
| | $i$ (Eq.4.7) | $i$ (Eq.4.7) | $i$ (Eq.4.7) | $i$ (Eq.4.7) | $k$ (Eq.4.33-4.35) |
| | $k$ (Eq.4.33-4.35) | $k$ (Eq.4.33-4.35) | $k$ (Eq.4.33-4.35) | $k$ (Eq.4.33-4.35) | $K_M$ (Eq.2.23-2.24) |
| | $K_P$ (Eq.2.41) | $K_P$ (Eq.2.41) | | | $\alpha$ (Eq.2.62-2.65) |
| Iterations | $R_1$ (Eq.6.16) | $P_P$ (Eq.6.18) | | | $P_{pc}(Eq.2.66)$ |
| | $R_2$ (Eq.6.17) | $(q_{w/t})_n$(Eq.6.20) | $N_{cm}$ (Eq.6.46) | $N_{cm=0}$ | $P_{mc}(Eq.2.67)$ |
| | $H = B' \cot \rho_A$ | $K_A$ (Eq.4.33) | | (Eq.6.46) | $N_{cm}$(Eq.6.31-6.32) |
| Calculations | $N_{\gamma m}$ (Eq. 6.23) | $N_{\gamma m=0}$ (Eq. 6.23) | $N_{cm}$ | $N_{cm=0}$ | $N_{cm}$ |
| | $N_{qm}$ (Eq. 6.24) | $N_{qm=0}$ (Eq. 6.23) | | | $N_{cm=0} = N_c$ |
| | $m_\gamma$ (Eq. 6.47) | | $m_q$ (Eq. 6.48) | $m_c$ (Eq. 6.49) | |
| | $s_\gamma$ (Table 2.2) | | $s_q$ (Table 2.2) | $s_c$ (Table 2.2) | |
| | Capacity of Soil | | Slip Check | | |
| | $(W_v)_{all}$ (Eq. 6.51) | | $(W_v)_{all}$ (Eq. 5.9) | | |
| Result | Allowable Vehicle Weight ($(W_v)_{all}$) | | | | |

Table 7.2. Computer program scheme for determination of allowable slope angle

| | | | | | |
|---|---|---|---|---|---|
| Unknown | Allowable Slope Angle ($\theta$) | | | | |
| Input Data | Vehicle | | Terrain | Interaction | |
| | Vehicle Type (W/T) | | Int. friction ($\phi$) | Width of contact surface ($E$) | |
| | Center of Gravity ($l_f$,$h$,$l$,$t_g$) | | Unit weight ($\gamma$) | Length of Contact Surface($B$) | |
| | Acceleration ($a$) | | Cohesion ($c$) | Ruth depth ($D$) | |
| | Vehicle Weight ($W_v$) | | | Interface Strength ($a_{ws}$,$\phi_{ws}$) | |
| ITERATION on $\theta$ ∧ Calculations | $N_{qm}$ and $N_{\gamma m}$ | | | $N_{cm}$ | |
| | | | | if [$\phi = 0$] | if [$\phi \neq 0$] |
| | $c = 0$ | $a = c = \theta = 0$ | | $\gamma = 0$ | $a = \gamma = \theta = 0$ | $i$ (Eq.4.7) |
| | $i$ (Eq.4.7) | $i$ (Eq.4.7) | | $i$ (Eq.4.7) | $i$ (Eq.4.7) | $k$ (Eq.4.33-4.35) |
| | $k$ (Eq.4.33-4.35) | $k$ (Eq.4.33-4.35) | | $k$ (Eq.4.33-4.35) | $k$ (Eq.4.33-4.35) | $K_M$ (Eq.2.23-2.24) |
| | $K_P$ (Eq.2.41) | $K_P$ (Eq.2.41) | | | | $\alpha$ (Eq.2.62-2.65) |
| Iterations | $R_1$ (Eq.6.16) | $P_P$ (Eq.6.18) | | | | $P_{pc}(Eq.2.66)$ |
| | $R_2$ (Eq.6.17) | $(q_{w/t})_n$(Eq.6.20) | | $N_{cm}$ (Eq.6.46) | $N_{cm=0}$ | $P_{mc}(Eq.2.67)$ |
| | $H = B' \cot \rho_A$ | $K_A$ (Eq.4.33) | | | (Eq.6.46) | $N_{cm}$(Eq.6.31-6.32) |
| Calculations | $N_{\gamma m}$ (Eq. 6.23) | $N_{\gamma m=0}$ (Eq. 6.23) | | $N_{cm}$ | $N_{cm=0}$ | $N_{cm}$ |
| | $N_{qm}$ (Eq. 6.24) | $N_{qm=0}$ (Eq. 6.23) | | | | $N_{cm=0} = N_c$ |
| | $m_\gamma$ (Eq. 6.47) | | $m_q$ (Eq. 6.48) | $m_c$ (Eq. 6.49) | | |
| | $s_\gamma$ (Table 2.2) | | $s_q$ (Table 2.2) | $s_c$ (Table 2.2) | | |
| | Capacity of Soil | | Slip Check | | | |
| | $(W_v)_{all}$ (Eq. 6.51) | | $(W_v)_{all}$ (Eq. 5.9) | | | |
| | $(W_v)_{all} - W_v$ | | | | | |
| Result | Allowable Slope Angle ($\theta$) at min $[(W_v)_{all} - W_v]$ | | | | | |

Table 7.3. Computer program scheme for determination of allowable acceleration

| | | | | | |
|---|---|---|---|---|---|
| Unknown | Allowable Acceleration ($a$) | | | | |
| Input Data | Vehicle | | Terrain | | Interaction |
| | Vehicle Type (W/T) | | Int. friction ($\phi$) | | Width of contact surface ($E$) |
| | Center of Gravity ($l_f$,$h$,$l$,$t_g$) | | Unit weight ($\gamma$) | | Length of Contact Surface($B$) |
| | Vehicle Weight ($W_v$) | | Cohesion ($c$) | | Ruth depth ($D$) |
| | | | Max slope ($\theta$) | | Interface Strength ($a_{ws}$,$\phi_{ws}$) |
| ITERATION on $a$ ∧ | Calculations | $N_{qm}$ and $N_{\gamma m}$ | | $N_{cm}$ | |
| | | | | if $[\phi = 0]$ | if $[\phi \neq 0]$ |
| | | $\underline{c = 0}$ | $\underline{a = c = \theta = 0}$ | $\underline{\gamma = 0}$ | $\underline{a = \gamma = \theta = 0}$ | $i$ (Eq.4.7) |
| | | $i$ (Eq.4.7) | $i$ (Eq.4.7) | $i$ (Eq.4.7) | $i$ (Eq.4.7) | $k$ (Eq.4.33-4.35) |
| | | $k$ (Eq.4.33-4.35) | $k$ (Eq.4.33-4.35) | $k$ (Eq.4.33-4.35) | $k$ (Eq.4.33-4.35) | $K_M$ (Eq.2.23-2.24) |
| | | $K_P$ (Eq.2.41) | $K_P$ (Eq.2.41) | | | $\alpha$ (Eq.2.62-2.65) |
| | Iterations | $R_1$ (Eq.6.16) | $P_P$ (Eq.6.18) | | | $P_{pc}(Eq.2.66)$ |
| | | $R_2$ (Eq.6.17) | $(q_{w/t})_n$(Eq.6.20) | $N_{cm}$ (Eq.6.46) | $N_{cm=0}$ | $P_{mc}(Eq.2.67)$ |
| | | $H = B' \cot \rho_A$ | $K_A$ (Eq.4.33) | | (Eq.6.46) | $N_{cm}$(Eq.6.31-6.32) |
| | Calculations | $N_{\gamma m}$ (Eq. 6.23) | $N_{\gamma m=0}$ (Eq. 6.23) | $N_{cm}$ | $N_{cm=0}$ | $N_{cm}$ |
| | | $N_{qm}$ (Eq. 6.24) | $N_{qm=0}$ (Eq. 6.23) | | | $N_{cm=0} = N_c$ |
| | | $m_\gamma$ (Eq. 6.47) | | $m_q$ (Eq. 6.48) | $m_c$ (Eq. 6.49) | |
| | | $s_\gamma$ (Table 2.2) | | $s_q$ (Table 2.2) | $s_c$ (Table 2.2) | |
| | | $\underline{\text{Capacity of Soil}}$ | | $\underline{\text{Slip Check}}$ | | |
| | | $(W_v)_{all}$ (Eq. 6.51) | | $(W_v)_{all}$ (Eq. 5.9) | | |
| | | $(W_v)_{all} - W_v$ | | | | |
| Result | Allowable Acceleration ($a$) at min $[(W_v)_{all} - W_v]$ | | | | |

# 8. DISCUSSION OF RESULTS

In this thesis basically two new methods are proposed: First, the coulomb wedge analysis for frictionless soils is presented for the determination of the reduction in $N_c$ under seismic activity. Then, seismic bearing capacity calculation methods are adapted to mobility problems. The results and discussions of both methods are presented in this section.

## 8.1. Seismic Reduction in $N_c$

As mentioned in previous sections, there is not any solution for seismic cohesive factor of bearing capacity of frictionless soils in previous studies. In proposed mobility method, when $k = 1$, $i = 0$ and $\theta = \frac{k_h}{1-k_v}$ in mobility bearing factor for cohesion equation (Eq.6.46) becomes seismic bearing capacity factor for cohesion (Eq.8.1) which is alternate to Budhu and Al-Karni (1993) equation. Although the method proposed by Budhu and Al-Karni (1993) can not give a solution when $\phi = 0$, the equation of best fit curve (Eq. 2.71) is valid for all $\phi$ values. In new method:

$$N_{cE} = \frac{2.83 + 2\tan\rho_A + \cot\rho_A}{\cos\theta} \tag{8.1}$$

the $\rho_A$ angle which makes $N_{cE}$ value minimum is the angle of the rupture surface and the seismic cohesive component of the bearing capacity is the corresponding $N_{cE}$ value. Therefore, it is possible to compare the results of two approaches.

In order to decrease the number of the variables, the $c/\gamma z$ component of the equations of the lateral earth pressure coefficients of Budhu and Al-Karni (1993) method is defined by a factor $\kappa$ and the results of two approaches for three different values of $\kappa$ ($\kappa = 0.1$, $\kappa = 0.5$ and $\kappa = 1.0$) are compared in Table 8.1 and Figures 8.1, 8.2 and 8.3.

As it can be seen in the graphs, the ratios of the seismic to the static values of the cohesive component of the bearing capacity equation have values between 1.0000 and

Table 8.1. Comparison of the results of Coulomb wedge method with Budhu and Al-Karni (1993) method

| $k_h = \tan\theta$ | Budhu Al-Karni Method | | | Coulomb Wedges Method |
|---|---|---|---|---|
| | $N_{cE}/N_c$ | | | $N_{cE}/N_c$ |
| | $\kappa = 0.1$ | $\kappa = 0.5$ | $\kappa = 1.0$ | |
| 0.0 | 1.0000 | 1.0000 | 1.0000 | 1.0000 |
| 0.1 | 0.7107 | 0.8729 | 0.9579 | 0.8615 |
| 0.2 | 0.4809 | 0.6807 | 0.8420 | 0.7247 |
| 0.3 | 0.3186 | 0.4933 | 0.6791 | 0.5806 |
| 0.4 | 0.2082 | 0.3369 | 0.5026 | 0.4535 |
| 0.5 | 0.1345 | 0.2187 | 0.3413 | 0.3783 |
| 0.6 | 0.0862 | 0.1355 | 0.2127 | 0.3297 |
| 0.7 | 0.0548 | 0.0806 | 0.1216 | 0.2964 |
| 0.8 | 0.0346 | 0.0461 | 0.0638 | 0.2726 |
| 0.9 | 0.0217 | 0.0254 | 0.0307 | 0.2548 |
| 1.0 | 0.0136 | 0.0136 | 0.0136 | 0.2413 |

0.0136. The $\kappa$ value only change the shape of the curve and as it approaches 1.0, the shape of the curve diverges from the original fitted curve which Budhu and Al-Karni proposed.

The decrease of the seismic cohesive component found by wedge analysis is slower than the one found by the Budhu and Al-Karni (1993) method.

The other difference between the methods is; when the horizontal acceleration of the earthquake becomes equal to gravitational acceleration of earth, $N_{cE}$ has approximately zero value in Budhu and Al-Karni method. However, in Coulomb wedge analysis, $N_{cE}$ still has a considerable value. In order to clarify the difference between these two results, to remind the analogy between the sloped soil and soil under the seismic loading will be useful. Fluidization of cohesionless soils is an expected result when the horizontal acceleration factor ($k_h$) is equal to $\tan\phi$. It also means that cohesionless soils can not form a slope which has an inclination angle bigger than its internal friction

angle. However, same situation is not valid for cohesive soils, i.e. cohesive soils can form a slope without any inclination limit. When the results are checked within this perspective, it can be easily seen that proposed method gives more reasonable results.

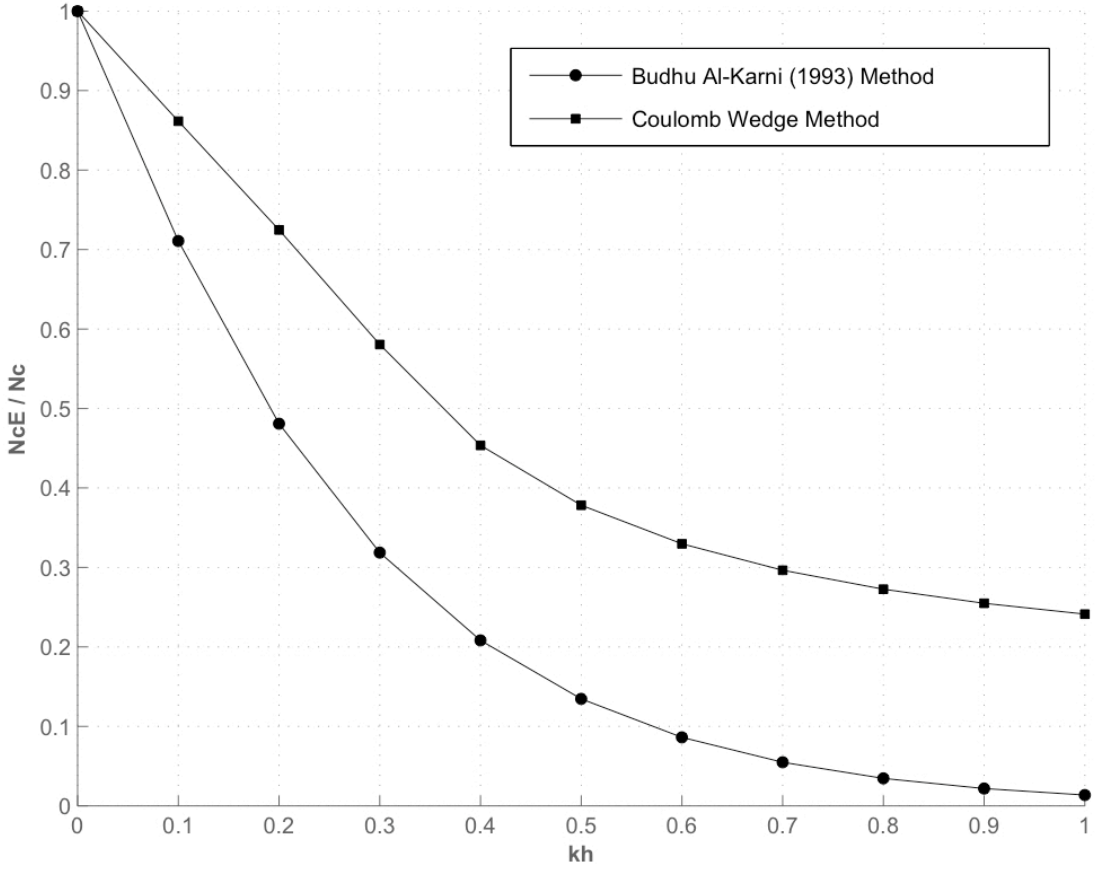



Figure 8.1. Comparison of the results of Coulomb wedge method with Budhu and Al-Karni (1993) method for $\kappa = 0.1$

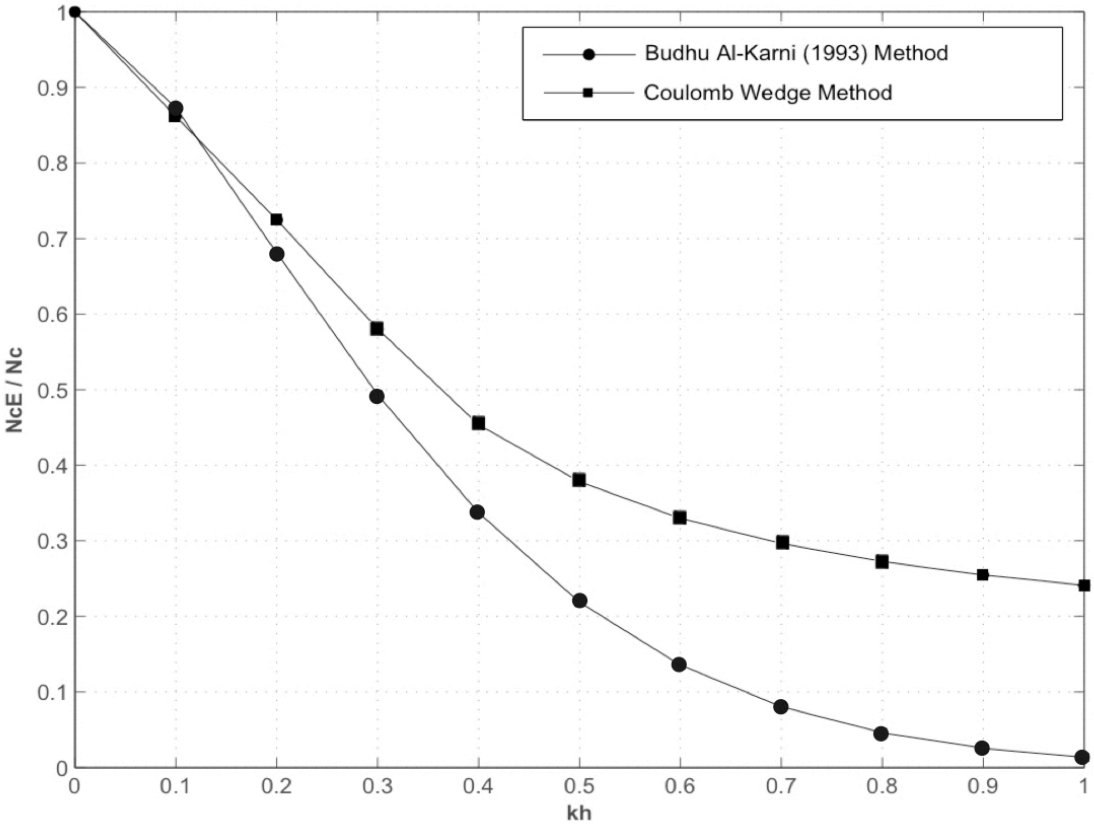



Figure 8.2. Comparison of the results of Coulomb wedge method with Budhu and Al-Karni (1993) method for $\kappa = 0.5$

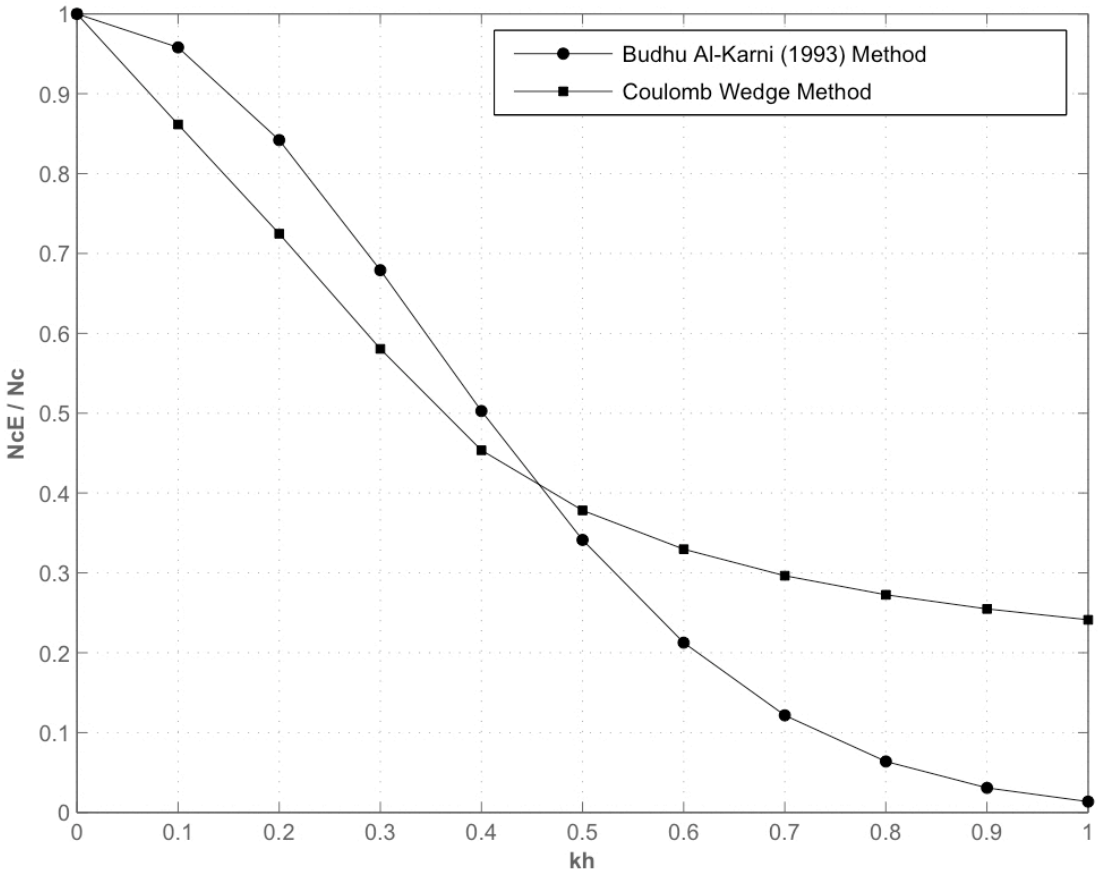



Figure 8.3. Comparison of the results of Coulomb wedge method with Budhu and Al-Karni (1993) method for $\kappa = 1.0$

## 8.2. Example Cases to Illustrate the Proposed Mobility Model

### 8.2.1. Allowable Weight Determination of a Wheeled Vehicle

Table 8.2 shows the results of the allowable weight analysis of a 2008 Jeep Grand Cherokee SRT8 with various terrain and interaction characteristics.

Case I: The mobility bearing capacity is less than the vehicle load with a very small difference and the soil fails before slipping occurs according to given vehicle and terrain parameters.

Case II: Only the acceleration of vehicle is reduced 1 $m/s^2$ according to the first case and the vehicle can pass safely without slipping of vehicle or failure of soil.

Case III: If the friction angle between soil and the wheels is reduced 10 degrees and maximum slope on the route is increase 10 degrees according the second case, the vehicle will slip before failure occurs.

Case IV: In this case the internal friction angle is made equal to the friction between the wheel and the soil when the other parameters in case III are not changed, and this time there is not slip failure but soil fails.

Case V: Adhesion of the wheel and soil interaction and cohesion of the soil is reduced according to the second case and soil failure occurs.

Case VI: In this case the allowable weight of a stopped vehicle on a horizontal ground is determined and the result is much more than the actual vehicle weight.

Table 8.2. Allowable weight determination of a wheeled vehicle

| Parameter | Unit | Case I | Case II | Case III | Case IV | Case V | Case VI |
|---|---|---|---|---|---|---|---|
| $W_v$ | $kN/m$ | 27.46 | 27.46 | 27.46 | 27.46 | 27.46 | 27.46 |
| $l$ | $m$ | 2.8 | 2.8 | 2.8 | 2.8 | 2.8 | 2.8 |
| $l_F$ | $m$ | 1.26 | 1.26 | 1.26 | 1.26 | 1.26 | 1.26 |
| $h$ | $m$ | 0.78 | 0.78 | 0.78 | 0.78 | 0.78 | 0.78 |
| $a$ | $m/s^2$ | 2 | 1 | 1 | 1 | 1 | 0 |
| $a_{ws}$ | $kN/m^2$ | 10 | 10 | 10 | 10 | 5 | 5 |
| $\phi_{ws}$ | $^o$ | 25 | 25 | 20 | 20 | 25 | 25 |
| $B$ | $m$ | 0.21 | 0.21 | 0.21 | 0.21 | 0.21 | 0.21 |
| $E$ | $m$ | 0.297 | 0.297 | 0.297 | 0.297 | 0.297 | 0.297 |
| $D$ | $m$ | 0.05 | 0.05 | 0.05 | 0.05 | 0.05 | 0.05 |
| $\theta$ | $^o$ | 10 | 10 | 20 | 20 | 10 | 0 |
| $\phi$ | $^o$ | 25 | 25 | 25 | 20 | 25 | 25 |
| $c$ | $kN/m^2$ | 10 | 10 | 10 | 10 | 5 | 5 |
| $\gamma$ | $kN/m^3$ | 18 | 18 | 18 | 18 | 18 | 18 |
| $(W_v)_{all}$ | $kN/m$ | 26.28 | 33.26 | 10.00 | 0.68 | 18.36 | 42.87 |
| Result | | No Slip Failure | No Slip Pass | Slip No Pass | No Slip Failure | No Slip Failure | No Failure at Rest |

### 8.2.2. Allowable Slope Angle Determination of a Wheeled Vehicle

Table 8.3 shows the results of the allowable weight analysis of a 2008 Jeep Grand Cherokee SRT8 with various terrain and interaction characteristics.

Case I: The vehicle and terrain parameters of the Case I in allowable weight determination are entered in this analysis and the result gives the maximum allowable value 9.5 degrees. So, in the first case of allowable weight analysis, the soil fails because the maximum slope angle exceeds the allowable slope angle with 0.5 degree. Also, the failure at limiting slope is soil bearing failure.

Case II: Here also, the same parameters of the Case II in allowable weight analysis are entered and the result of allowable slope angle on the route analysis is 12.5 degrees that is limited by soil bearing capacity.

Case IV: In this case, the acceleration is increased up to 4 $m/s^2$ and friction angle between soil and tyre is reduced to 20 degrees and the slipping of the vehicle limits the allowable slope with the value of 2 degrees.

Case V: Cohesive strength of the soil and adhesion between the tyre and soil is reduced to 5 $kN/m^2$ to see the effect of the cohesion in mobility capacity of soil. So, when the result is compared with the first case, 6 degrees reduction in the allowable slope angle can be observed .

Case V: The vehicle moves with a constant velocity in this case. The allowable slope angle increases up to 16.5 degrees without acceleration.

Table 8.3. Allowable slope angle determination of a wheeled vehicle

| Parameter | Unit | Case I | Case II | Case III | Case IV | Case V | Case VI |
|---|---|---|---|---|---|---|---|
| $W_v$ | $kN/m$ | 27.46 | 27.46 | 27.46 | 27.46 | 27.46 | 27.46 |
| $l$ | $m$ | 2.8 | 2.8 | 2.8 | 2.8 | 2.8 | 2.8 |
| $l_F$ | $m$ | 1.26 | 1.26 | 1.26 | 1.26 | 1.26 | 1.26 |
| $h$ | $m$ | 0.78 | 0.78 | 0.78 | 0.78 | 0.78 | 0.78 |
| $a$ | $m/s^2$ | 2 | 1 | 4 | 1 | 1 | 0 |
| $a_{ws}$ | $kN/m^2$ | 10 | 10 | 10 | 10 | 5 | 5 |
| $\phi_{ws}$ | $^o$ | 25 | 25 | 20 | 20 | 25 | 25 |
| $B$ | $m$ | 0.21 | 0.21 | 0.21 | 0.21 | 0.21 | 0.21 |
| $E$ | $m$ | 0.297 | 0.297 | 0.297 | 0.297 | 0.297 | 0.297 |
| $D$ | $m$ | 0.05 | 0.05 | 0.05 | 0.05 | 0.05 | 0.05 |
| $\phi$ | $^o$ | 25 | 25 | 25 | 20 | 25 | 25 |
| $c$ | $kN/m^2$ | 10 | 10 | 10 | 10 | 5 | 10 |
| $\gamma$ | $kN/m^3$ | 18 | 18 | 18 | 18 | 18 | 18 |
| $\theta$ | $^o$ | 9.5 Bearing | 12.5 Bearing | 2 Slip | 7 Bearing | 3.5 Bearing | 16.5 Bearing |

### 8.2.3. Allowable Acceleration Determination of a Wheeled Vehicle

Table 8.4 shows the results of the allowable acceleration analysis of a 2008 Jeep Grand Cherokee SRT8 with various terrain and interaction characteristics.

Case I: The vehicle and terrain parameters of the Case I in allowable slope angle determination are entered in this analysis also and the result gives the maximum allowable acceleration value of 1.96 $m/s^2$ and this acceleration is limited by bearing capacity of soil.

Case II: Again corresponding parameters of allowable slope analysis are entered here and the result is $1m/s^2$.

Table 8.4. Allowable acceleration determination of a wheeled vehicle

| Parameter | Unit | Case I | Case II | Case III | Case IV | Case V | Case VI |
|---|---|---|---|---|---|---|---|
| $W_v$ | $kN/m$ | 27.46 | 27.46 | 27.46 | 27.46 | 27.46 | 27.46 |
| $l$ | $m$ | 2.8 | 2.8 | 2.8 | 2.8 | 2.8 | 2.8 |
| $l_F$ | $m$ | 1.26 | 1.26 | 1.26 | 1.26 | 1.26 | 1.26 |
| $h$ | $m$ | 0.78 | 0.78 | 0.78 | 0.78 | 0.78 | 0.78 |
| $a_{ws}$ | $kN/m^2$ | 10 | 10 | 10 | 10 | 5 | 5 |
| $\phi_{ws}$ | $^o$ | 25 | 25 | 20 | 20 | 25 | 25 |
| $B$ | $m$ | 0.21 | 0.21 | 0.21 | 0.21 | 0.21 | 0.21 |
| $E$ | $m$ | 0.297 | 0.297 | 0.297 | 0.297 | 0.297 | 0.297 |
| $D$ | $m$ | 0.05 | 0.05 | 0.05 | 0.05 | 0.05 | 0.05 |
| $\theta$ | $^o$ | 9.5 | 12.5 | 2 | 7 | 3.5 | 0 |
| $\phi$ | $^o$ | 25 | 25 | 25 | 20 | 25 | 25 |
| $c$ | $kN/m^2$ | 10 | 10 | 10 | 10 | 5 | 10 |
| $\gamma$ | $kN/m^3$ | 18 | 18 | 18 | 18 | 18 | 18 |
| $a$ | $m/s^2$ | 1.96 Bearing | 1.08 Bearing | 4.00 Slip | 0.98 Bearing | 0.98 Bearing | 5.00 Slip |

Case III - IV and V: The reverse check for the two analysis is performed by entering same parameters and the results are comply with each other.

Case VI: The allowable acceleration analysis is performed for a route without slope in this case. There is approximately 3 $m/s^2$ increase in the acceleration according to the first case with a slope of 9.5 degrees.

### 8.2.4. Allowable Weight Determination of a Tracked Vehicle

Table 8.5 shows the results of the allowable weight analysis of a a tracked M60 Patton Battle Tank with various terrain and interaction characteristics. When the results are compared with the analysis of the wheeled vehicle, it can be easily seen that the tracked vehicles are much more suitable for off-road terrains.

Case I: Arbitrary terrain parameters are entered for analysis and the result shows that the vehicle can pass safely.

Case II: The weight analysis is performed for the same vehicle but in a cohesionless soil and internal friction angle is increased 5 degrees. The result is failure of soil.

Case III: Here, the internal friction angle is reduced below the slope angle. The result of the analysis is a complex number which means soil fluidizes and can not take any load.

Case IV: The acceleration and slope angle are increased and the failure is occurred.

Case V: In this case the allowable weight of a stopped vehicle on a horizontal ground is determined and the resulting allowable weight is approximately 55 times heavier than the actual vehicle weight.

Table 8.5. Allowable weight determination of a tracked vehicle

| Parameter | Unit | Case I | Case II | Case III | Case IV | Case V |
|---|---|---|---|---|---|---|
| $W_v$ | $kN/m$ | 528 | 528 | 528 | 528 | 528 |
| $t_g$ | $m$ | 2 | 2 | 2 | 2 | 2 |
| $h$ | $m$ | 1.8 | 1.8 | 1.8 | 1.8 | 1.8 |
| $a$ | $m/s^2$ | 1 | 1 | 1 | 3 | 0 |
| $B$ | $m$ | 4.8 | 4.8 | 4.8 | 4.8 | 4.8 |
| $E$ | $m$ | 0.6 | 0.6 | 0.6 | 0.6 | 0.6 |
| $D$ | $m$ | 0.1 | 0.1 | 0.1 | 0.1 | 0.1 |
| $\theta$ | $^o$ | 10 | 10 | 10 | 15 | 0 |
| $\phi$ | $^o$ | 15 | 20 | 8 | 20 | 20 |
| $c$ | $kN/m^2$ | 5 | 0 | 10 | 10 | 5 |
| $\gamma$ | $kN/m^3$ | 18 | 18 | 18 | 18 | 18 |
| $(W_v)_{all}$ | $kN/m$ | 545.5 | 347.7 | Fluidization | 472.1 | 29353.5 |
| Result | | Pass | Failure | Failure | Failure | At Rest |

### 8.2.5. Allowable Slope Angle Determination of a Tracked Vehicle

Table 8.6 shows the results of the allowable slope analysis of a tracked M60 Patton Battle Tank with various terrain and interaction characteristics.

Case I: The vehicle and terrain parameters of the Case I in allowable weight determination are entered in this analysis and the result gives the maximum allowable value 10.5 degrees. So, in the first case of allowable weight analysis, the vehicle can move because the maximum slope on route is 0.5 degree less than the allowable slope angle.

Case II: The slope analysis is performed for cohesionless soil and internal friction angle is increased 5 degrees. The result gives 0 degree which means vehicle can pass only on horizontal ground or the analysis is invalid because soil fails whatever the value of the slope. In this situation the weight analysis should be performed in order to see

if the vehicle can pass through on a horizontal ground.

Case III: The same parameters of corresponding case of weight analysis are entered except slope angle. The allowable slope angle is found 6.5 degrees which is 3.5 degrees less than the value entered in the weight analysis.

Case IV: In the fourth case of the vehicle weight analysis, the soil failed in when slope angle is 15 degrees. In order to calculate the critical slope angle, same soil parameters are entered in this case also and the result is 14.5 degrees.

Case V: The calculation of the allowable slope angle when there is no acceleration is performed . The result is 19 degrees which shows the importance of the acceleration magnitude.

Table 8.6. Allowable slope angle determination of a tracked vehicle

| Parameter | Unit | Case I | Case II | Case III | Case IV | Case V |
|---|---|---|---|---|---|---|
| $W_v$ | $kN/m$ | 528 | 528 | 528 | 528 | 528 |
| $t_g$ | $m$ | 2 | 2 | 2 | 2 | 2 |
| $h$ | $m$ | 1.8 | 1.8 | 1.8 | 1.8 | 1.8 |
| $a$ | $m/s^2$ | 1 | 1 | 1 | 3 | 0 |
| $B$ | $m$ | 4.8 | 4.8 | 4.8 | 4.8 | 4.8 |
| $E$ | $m$ | 0.6 | 0.6 | 0.6 | 0.6 | 0.6 |
| $D$ | $m$ | 0.1 | 0.1 | 0.1 | 0.1 | 0.1 |
| $\phi$ | $^o$ | 15 | 20 | 8 | 20 | 20 |
| $c$ | $kN/m^2$ | 5 | 0 | 10 | 10 | 5 |
| $\gamma$ | $kN/m^3$ | 18 | 18 | 18 | 18 | 18 |
| $\theta$ | $^o$ | 10.5 | 0 | 6.5 | 14.5 | 19 |
| Result | | Pass | Failure | Pass | Pass | At Rest |

### 8.2.6. Allowable Acceleration Determination of a Tracked Vehicle

Table 8.7 shows the results of the allowable acceleration analysis of a tracked M60 Patton Battle Tank with various terrain and interaction characteristics.

Case I: The reverse check of the weight and slope results are performed by entering same parameters used in previous analyses.

Case II: In cohesionless soil acceleration is in the minimum value according to defined interval and limits in the program which means which means additional vehicle weight analysis is required to ensure if the vehicle can pass or can not pass.

Case III and Case IV: These cases are the reverse check of the corresponding cases in the slope angle analysis. The results agrees with each other.

Case V: The allowable acceleration increases up to 6.3 $m/s^2$ when there is no slope on route.

Table 8.7. Allowable acceleration determination of a tracked vehicle

| Parameter | Unit | Case I | Case II | Case III | Case IV | Case V |
|---|---|---|---|---|---|---|
| $W_v$ | $kN/m$ | 528 | 528 | 528 | 528 | 528 |
| $t_g$ | $m$ | 2 | 2 | 2 | 2 | 2 |
| $h$ | $m$ | 1.8 | 1.8 | 1.8 | 1.8 | 1.8 |
| $B$ | $m$ | 4.8 | 4.8 | 4.8 | 4.8 | 4.8 |
| $E$ | $m$ | 0.6 | 0.6 | 0.6 | 0.6 | 0.6 |
| $D$ | $m$ | 0.1 | 0.1 | 0.1 | 0.1 | 0.1 |
| $\theta$ | $^o$ | 10 | 10 | 6.5 | 15 | 0 |
| $\phi$ | $^o$ | 15 | 20 | 8 | 20 | 20 |
| $c$ | $kN/m^2$ | 5 | 0 | 10 | 10 | 5 |
| $\gamma$ | $kN/m^3$ | 18 | 18 | 18 | 18 | 18 |
| $a$ | $^o$ | 1.08 | 0.1 | 0.7 | 2.7 | 6.3 |
| Result | | Pass | Failure | Pass | Pass | No Slope |

# 9. CONCLUSION

This thesis presents a new analytical method for quick determination of off-road vehicle mobility. The motivations for this research were the lack of simple geomechanical approaches to the off-road mobility problems and the high amount of empricism inherent in the existing methods. Accordingly, a theoretical model is proposed by satisfying the comprising equilibrium between the theory and simplicity. The new model is based on the total loss mobility as a result of bearing failure under the action of the stresses that the vehicle imposes on the soil.

A new term, namely, mobility bearing capacity was assigned for defining bearing capacity of soils beneath off-road vehicles. Mobility bearing capacity equation was obtained by introducing mobility reduction factors for each components of the classical bearing capacity equation. These mobility reduction factors are similar to shape, depth and inclination factors of the common bearing capacity theories and they include the reduction resulting from both traction loads of vehicle and slope of the terrain.

The mobility reduction factors for each bearing capacity components were determined by a new method which is based on the approaches of seismic bearing capacity of fluidized soil [11], [10], [17]. According to this point of view, the theoretical framework of fluidization provides a relationship between two seemingly different mechanisms when bearing capacity is concerned. These are (Fig. 3.1):

1. an extraordinary foundation on a slope with its base parallel to the slope
2. a foundation carrying an inclined load during seismic activity

The interaction between the soil and a vehicle which moves on a sloped ground was modeled as a foundation on a slope with its base parallel to the slope as mentioned in the first case. Consequently, the studies about the seismic bearing capacity based on fluidization concept in literature have been reviewed and discussed thoroughly in order to adapt them into mobility analysis model. It was observed that the studies either

consider Coulomb wedge mechanism or modified Vesic's failure surface but there is not an individual method for calculation of seismic reduction in bearing capacity which is applicable to all types of soils. Therefore each bearing capacity factor has been determined separately using the most appropriate method depending on the corresponding soil type. Moreover, a new method based on Coulomb wedge mechanism was introduced for determination of seismic reduction in the cohesive factor of bearing capacity for frictionless soils to overcome the common deficiency of the present methods.

The new method and the presently available methods of calculating bearing capacity factors are discussed briefly and a comparison of these methods are provided in the discussion of results.

Consequently, the mobility reduction factors for each bearing capacity components were derived either using Coulomb wedge mechanism or modified Vesic's failure surface as done in the seismic bearing capacity analysis . The calculations of mobility reduction factors have an iterative structure. Therefore, several computational schemes for computer programs and a Matlab code was provided. The allowable vehicle weight, allowable acceleration and allowable slope angle analysis can be performed by utilizing these schemes or the Matlab code.

Some illustrative examples were performed for several cases for different types of vehicles, terrains and unknowns and the results of the analyses are presented in discussion of results.

# APPENDIX A: MATLAB CODE FOR MOBILITY DECISION

## A.1. Main Body

```
clear all
%determination of analysis type
unknown = input('Required data ("w" for vehicle weight, "s" for slope
    angle, "a" for acceleration): ','s');
if unknown=='w'

%inputs for vehicle charasteristics
vehicle_type = input('Vehicle Type ("w" for wheeled, "t" for tracked
    vehicles): ','s');
if vehicle_type=='w'
    lf=input('The horizontal distance between the center of the gravity
        and the front axle -lf-(m): ');
    h=input('The vertical distance between the center of the gravity and
        the bottom of the wheel -h- (m): ');
    l=input('The distance between the wheels -l- (m): ');
    a = input('Acceleration of the vehicle -a- (m/s^2): ');
    as=input('Adhession between the tyre and the soil -as- (kN/m^2): ');
    phis=input('Friction angle between the tyre and the soil -phis-(
        degree): ')*pi()/180;
elseif vehicle_type=='t'
    tg=input('The horizontal distance between the center of the gravity
        and rear bottom of the track -tg-(m): ');
    h=input('The vertical distance between the center of the gravity and
        the bottom of the track -h-(m): ');
    a = input('Acceleration of the vehicle -a- (m/s^2): ');
else
     disp(sprintf('wrong entry'))
end


%inputs for interaction charasteristics
B=input('The length of the contact surface -B-(m) ');
```

```
E=input('The width of a one tyre or track -E-(m)');
d= input('The rut depth (m) -D-');


%inputs for terrain charasteristics
theta =input('max slope on route -theta-(degree)')*pi()/180;
phi=input('Internal friction angle of the soil -phi-(degree)')*pi()/180;
gamma= input('The unit weight of the soil -gamma-(kN/m3)');
c=input('The cohesion of the soil -c-(kN/m^2)');

%calculation of delta
delta=phi/2;

%calculations of Nq, Ng and Nc
Nq= (tan(pi()/4+phi/2))^2*exp(pi()*tan(phi));
Ng= 2*(Nq+1)*tan(phi);
if phi==0
    Nc=5.7;
else
    Nc=(Nq-1)*cot(phi);
end

%calculations of shape factors:
sq= 1+sin(phi)*B/E;
sc= 1+Nq/Nc*B/E;
sgcond=1-0.4*B/E*sin(phi);
if sgcond<=0.6
    sg=0.6;
else
sg=sgcond;
end

%calculations of i and Kp
in=tan(theta)+a/cos(theta)/9.81;
Kp=cos(phi-theta)^2/(cos(theta)*cos(delta+theta)*(1-sqrt(sin(phi+delta)*
    sin(phi-theta)/cos(delta+theta)))^2);
ins=in;
```

```
%calculation of k
cal_k

%calculations of Nqm and Ngm
cal_NqmNgm

%calculation of Ncm
if c==0
    Ncm=0
else
cal_Ncm
end
thetas=theta;
ks=k;

%calculations of Nqmo and Ngmo
theta=0;
a=0;
in=tan(theta)+a/cos(theta)/9.81;
Kpo=cos(phi-theta)^2/(cos(theta)*cos(delta+theta)*(1-sqrt(sin(phi+delta)*
    sin(phi-theta)/cos(delta+theta)))^2);
cal_k
cal_NqmoNgmo

%calculation of Ncmo
cal_Ncmo

%calculations of mq, mg, mc:
if phi==0
mq= Nqm/Nqo;
mg= 0;
mc= Ncm/Ncmo;
else

mq= Nqm/Nqo;
mg= Ngm/Ngo;
mc= Ncm/Ncmo;
end
```

```
%calculation of bearing capacity:
qult=c*Nc*mc*sc+gamma*d*Nq*mq*sq+0.5*gamma*B*Ng*mg*sg;

%calculation of weight:
if vehicle_type=='w'
    Wv=qult*4*B*E;
        if ins<= as*2*B*E/(Wv*cos(thetas)*ks)+tan(phis)
        disp(sprintf('no slip, allowable weight of the vehicle (kN):'))
        Wv
   else
        Wv= as*2*B*E/((ins-tan(phis))*cos(thetas)*ks);
        disp(sprintf('slip governs the weight, allowable weight of the
            vehicle (kN):'))
    Wv
    end
else
    Wv=qult*2*B*E;
    disp(sprintf('allowable weight of the vehicle (kN):'))
    Wv
end


      else


    if unknown=='s'

  %inputs for vehicle charasteristics
vehicle_type = input('Vehicle Type ("w" for wheeled, "t" for tracked
    vehicles): ','s');
Wv = input('Weight of the vehicle:');
if vehicle_type=='w'
    lf=input('The horizontal distance between the center of the gravity
        and the front axle -lf-(m):');
    h=input('The vertical distance between the center of the gravity and
        the bottom of the wheel -h- (m):');
    l=input('The distance between the wheels -l- (m):');
    a = input('Acceleration of the vehicle -a- (m/s^2): ');
    as=input('Adhession between the tyre and the soil -as-(kN/m^2): ');
```

```
    phis=input('Friction angle between the tyre and the soil -phis-(
        degree): ')*pi()/180;
elseif vehicle_type=='t'
    tg=input('The horizontal distance between the center of the gravity
        and rear bottom of the track -tg-(m): ');
    h=input('The vertical distance between the center of the gravity and
        the bottom of the track -h-(m): ');
    a = input('Acceleration of the vehicle -a- (m/s^2): ');
else
     disp(sprintf('wrong entry'))
end
aa=a;

%inputs for interaction charasteristics
B=input('The length of the contact surface -B-(m) ');
E=input('The width of a one tyre or track -E-(m) ');
d= input('The rut depth (m) -d-');

%inputs for terrain charasteristics
phi=input('Internal friction angle of the soil -phi-(degree) ')*pi()/180;
gamma= input('The unit weight of the soil -gamma- (kN/m^3) ');
c=input('The cohesion of the soil -c-(kN/m^2) ');

%calculation of delta
delta=phi/2;

%calculations of bearing capacity factors:
Nq= (tan(pi()/4+phi/2))^2*exp(pi()*tan(phi));
Ng= 2*(Nq+1)*tan(phi);
if phi==0
    Nc=5.7;
else
    Nc=(Nq-1)*cot(phi);
end

%calculations of shape factors:
sq= 1+sin(phi)*B/E;
sc= 1+Nq/Nc*B/E;
```

```
sgcond=1-0.4*B/E*sin(phi);
if sgcond<=0.6
    sg=0.6;
else
sg=sgcond;
end

  for o=1:180
    theta(o)=pi()*o/360;

%calculations of i and Kp
in(o)=tan(theta(o))+a/cos(theta(o))/9.81;
Kp(o)=cos(phi-theta(o))^2/(cos(theta(o))*cos(delta+theta(o))*(1-sqrt(sin(
    phi+delta)*sin(phi-theta(o))/cos(delta+theta(o))))^2);
ins(o)=tan(theta(o))+a/cos(theta(o))/9.81;

%calculation of k
iter_k
ks=k;

%calculations of Nqm and Ngm
iterl_NqmNgm

%calculation of Ncm
     if c==0
    for i=1:180
     Ncm(i)=0;
    end
else
iter_Ncm
end

  end

%calculations of Nqmo and Ngmo
a=0;
in=a/9.81;
Kpo=cos(phi)^2/(cos(delta)*(1-sqrt(sin(phi+delta)*sin(phi)/cos(delta)))
```

```
    ^2);
cal_k
iterl_NqmoNgmo

%calculation of Ncmo
iter_Ncmo

%calculations of mq, mg, mc:
for o=1:180

 mq(o)= Nqm(o)/Nqo;
 if phi==0
    mg(o)=0;
else
        mg(o)= Ngm(o)/Ngo;
  end
         mc(o)= Ncm(o)/Ncmo;

%calculation of bearing capacity:
qult(o)=c*Nc*mc(o)*sc+gamma*d*Nq*mq(o)*sq+0.5*gamma*B*Ng*mg(o)*sg;

%calculation of weight:
if vehicle_type=='w'
   W(o)=qult(o)*4*B*E;
else
   W(o)=qult(o)*2*B*E;
end
dw(o)=Wv-W(o);
end
xx=min(abs(dw));
for j=1:180
 if abs(dw(j))== xx
    yy(j)=j;
else
    yy(j)=0;
end
end
maxslope=theta(max(yy))*180/pi();
```

```
kss=ks(max(yy));
INS=ins(max(yy));
if vehicle_type=='w'
    if INS<= as*2*B*E/(Wv*cos(theta(max(yy)))*kss)+tan(phis)
        disp(sprintf('no slip ,maximum slope angle on the route:'))
        maxslope
    else
        for t=1:180
            thetaslip(t)=t/360*pi();
            islip(t)=tan(thetaslip(t))+aa/cos(thetaslip(t))/9.81;
            kslip(t)=(lf+h*islip(t))/l;
            Wv3(t)=as*2*B*E/(cos(thetaslip(t))*(islip(t)-tan(phis))*kslip
                (t));
            dws(t)=Wv-Wv3(t);
        end
        ss=min(abs(dws));
for j=1:180
 if abs(dws(j))== ss
    sss(j)=j;
else
    sss(j)=0;
 end
end
maxslope=theta(max(sss))*180/pi();
        disp(sprintf('slip governs the slope angle ,maximum slope angle
            on the route:'))
    maxslope
    end
else
    disp(sprintf('maximum slope angle on the route:'))
maxslope

end

elseif unknown=='a'

 %inputs for vehicle charasteristics
vehicle_type = input('Vehicle Type ("w" for wheeled ," t" for tracked
```

```
    vehicles): ','s');
Wv = input('Weight of the vehicle:');
if vehicle_type=='w'
    lf=input('The horizontal distance between the center of the gravity
        and the front axle -lf-(m):');
    h=input('The vertical distance between the center of the gravity and
        the bottom of the wheel -h- (m):');
    l=input('The distance between the wheels -l- (m):');
   as=input('Adhession between the tyre and the soil -as-(kN/m^2): ');
    phis=input('Friction angle between the tyre and the soil -phis-(
        degree): ')*pi()/180;
elseif vehicle_type=='t'
    tg=input('The horizontal distance between the center of the gravity
        and rear bottom of the track -tg-(m):');
    h=input('The vertical distance between the center of the gravity and
        the bottom of the track -h-(m):')
else
     disp(sprintf('wrong entry'))
end


%inputs for interaction charasteristics
B=input('The length of the contact surface -B-(m)');
E=input('The width of a one tyre or track -E-(m)');
d= input('The rut depth (m) -d-');


%inputs for terrain charasteristics
theta =input('max slope on route -theta-(degree)')*pi()/180;
phi=input('Internal friction angle of the soil -phi-(degree)')*pi()/180;
gamma= input('The unit weight of the soil -gamma-(kN/m^3)');
c=input('The cohesion of the soil -c-(kN/m^2)');

%calculation of delta
delta=phi/2;

%calculations of bearing capacity factors:
Nq= (tan(pi()/4+phi/2))^2*exp(pi()*tan(phi));
```

```
Ng= 2*(Nq+1)*tan(phi);
if phi==0
    Nc=5.7;
else
    Nc=(Nq-1)*cot(phi);
end

%calculations of shape factors:
sq= 1+sin(phi)*B/E;
sc= 1+Nq/Nc*B/E;
sgcond=1-0.4*B/E*sin(phi);
if sgcond<=0.6
    sg=0.6;
else
sg=sgcond;
end
 for o=1:100
    a(o)=o/100*9.81;

%calculations of i and Kp
in(o)=tan(theta)+a(o)/cos(theta)/9.81;
Kp=cos(phi-theta)^2/(cos(theta)*cos(delta+theta)*(1-sqrt(sin(phi+delta)*
    sin(phi-theta)/cos(delta+theta)))^2);
ins(o)=tan(theta)+a(o)/cos(theta)/9.81;

%calculation of k
k_a

%calculations of Nqm and Ngm
a_NqmNgm

%calculation of Ncm
if c==0
    for i=1:180
     Ncm(i)=0;
    end
else
a_Ncm
```

```
end
  end
%calculations of Nqmo and Ngmo
ao=0;
in=ao/9.81;
Kpo=cos(phi)^2/(cos(delta)*(1-sqrt(sin(phi+delta)*sin(phi)/cos(delta)))
    ^2);
cal_k
iterl_NqmoNgmo

%calculation of Ncmo
iter_Ncmo

%calculations of mq, mg, mc:
for o=1:100
        mq(o)= Nqm(o)/Nqo;
    if phi==0
    mg(o)=0;
    else
        mg(o)= Ngm(o)/Ngo;
    end
        mc(o)= Ncm(o)/Ncmo;

%calculation of bearing capacity:
qult(o)=c*Nc*mc(o)*sc+gamma*d*Nq*mq(o)*sq+0.5*gamma*B*Ng*mg(o)*sg;

%calculation of weight:
if vehicle_type=='w'
W(o)=qult(o)*4*B*E;
else
W(o)=qult(o)*2*B*E;
end
dw(o)=Wv-W(o);
end
xx=min(abs(dw));
for j=1:100
 if abs(dw(j))== xx
    yy(j)=j;
```

```
else
    yy(j)=0;
end
end
maxacc=a(max(yy));
kss=ks(max(yy));
INS=ins(max(yy));
if vehicle_type=='w'
    if INS<= as*2*B*E/(Wv*cos(theta)*kss)+tan(phis)
        disp(sprintf('no slip, maximum acceleration:'))
        maxacc
    else
        for t=1:100
            aslip(t)=t;
            islip(t)=tan(theta)+aslip(t)/cos(theta)/9.81;
            kslip(t)=(lf+h*islip(t))/l;
            Wv3(t)=as*2*B*E/(cos(theta)*(islip(t)-tan(phis))*kslip(t));
            dws(t)=Wv-Wv3(t);
        end
        ss=min(abs(dws));
for j=1:100
 if abs(dws(j))== ss
    sss(j)=j;
else
    sss(j)=0;
 end
end
        maxacc= aslip(max(sss));
        disp(sprintf('slip governs the max acc, maximum acceleration (m/s
            ^2):'))
    maxacc
    end
else
    disp(sprintf('maximum acceleration (m/s^2):'))
maxacc
end
else
disp(sprintf('wrong entry'))
```

```
end
```

## A.2. Calculation of $N_{qm}$ and $N_{\gamma m}$

```
for i=1:180
    roA(i)=pi()*i/360;
H(i)=b(o)*tan(roA(i));
R1(i)=cos(roA(i)-phi)*cot(roA(i))/cos(roA(i)-phi-delta);
R2(i)=sin(roA(i)-phi)*cot(roA(i))/cos(roA(i)-phi-delta);
Pp(i)=0.5*gamma*H(i)^2*Kp(o)+gamma*d*H(i)*Kp(o);
Ngxx(i)=(Kp(o)-R1(i)*sin(theta(o))-R2(i)*cos(theta(o)))/((R1(i)+in(o)*R2(
    i))*cos(theta(o)))*tan(roA(i))/k(o);
Nqxx(i)=Kp(o)/((R1(i)+in(o)*R2(i))*k(o)*cos(theta(o)));
q(i)=0.5*gamma*b(o)*Ngxx(i)+gamma*d*Nqxx(i);
Ka(i)=Pp(i)/(0.5*gamma*H(i)^2+q(i)*H(i));
end
Kam(o)=min(Ka);
for j=1:180
if Ka(j)==Kam(o)
    y(j)=j;
else
    y(j)=0;
end
end
Hm(o)=H(max(y));
Ngm(o)=Ngxx(max(y));
Nqm(o)=Nqxx(max(y));
```

## A.3. Calculation of $N_{cm}$

```
if phi==0
    for i=1:180
    roAc(i)=pi()*i/360;
Ncm1(i)= (2.83+2*tan(roAc(i))+cot(roAc(i)))/(k(o)*cos(theta(o))*(in(o)*
    cot(roAc(i))+1));
end
Nc1(o)=min(Ncm1);
for j=1:180
if Ncm1(j)==Nc1(o)
```

```
        t1(j)=j;
    else
        t1(j)=0;
    end
    end
    Ncm(o)=Ncm1(max(t1));

    else
        D=c/(gamma*Hm(o));
    Kpc(o)=((sin(phi))^2+1)/(cos(phi))^2+2*D*tan(phi)+sqrt((2*D*tan(phi)+((
        sin(phi))^2+1)/(cos(phi))^2)^2+(2*D)^2+4*D*tan(phi)-4*(tan(theta(o)))
        ^2/(cos(phi))^2-1);
    Kac(o)=((sin(phi))^2+1)/(cos(phi))^2+2*D*tan(phi)-sqrt((2*D*tan(phi)+((
        sin(phi))^2+1)/(cos(phi))^2)^2+(2*D)^2+4*D*tan(phi)-4*(tan(theta(o)))
        ^2/(cos(phi))^2-1);

    alfaA(o)=atan(2*tan(theta(o))/(1-Kac(o)+sqrt((1-Kac(o))^2+4*tan(theta(o))
        ^2)));
    alfaP(o)=atan(2*tan(theta(o))/(Kpc(o)-1+sqrt((Kpc(o)-1)^2+4*tan(theta(o))
        ^2)));

    alfa1(o)=pi()/4+phi()/2+alfaA(o);
    alfa2(o)=pi()/4+phi()/2-alfaA(o);
    alfa3(o)=pi()/4-phi()/2+alfaP(o);
    alfa4(o)=pi()/4-phi()/2-alfaP(o);

    ro(o)=b(o)*sin(alfa2(o))/sin(alfa1(o)+alfa2(o));

    Ppc(o)=2*c*sqrt(Kpc(o))*(sin(alfa3(o)))^2/cos(phi)*ro(o)*exp(2*(pi()-
        alfa1(o)-alfa3(o))*tan(phi))+c*ro(o)/sin(phi)*(exp(2*(pi()-alfa1(o)-
        alfa3(o))*tan(phi))-1);
    for  i=1:10000
    m(i)=i/10000;
    phim(i)=atan(m(i)*tan(phi));
    cm(i)=m(i)*c;
    Pmc(i)=2*cm(i)*sqrt(Kpc(o))*(sin(alfa3(o)))^2/cos(phi*m(i))*ro(o)*exp(2*(
        pi()-alfa2(o)-alfa3(o))*tan(phi*m(i)))+cm(i)*ro(o)/sin(phi*m(i))*(exp
        (2*(pi()-alfa2(o)-alfa3(o))*tan(phi*m(i)))-1);
```

```
Ca(o)=c*b(o)*sin(alfa2(o))/sin(alfa1(o)+alfa2(o));
Cam(i)=cm(i)*b(o)*sin(alfa1(o))/sin(alfa1(o)+alfa2(o));
qe(i)=(Ppc(o)*cos(alfa1(o)-phi)+Pmc(i)*cos(alfa2(o)-phim(i))+Ca(o)*sin(
    alfa1(o))+Cam(i)*sin(alfa2(o)))/b(o);
Ncm1(i)=qe(i)/c;
Ncm2(i)=1/in(o)*((Ppc(o)*sin(alfa1(o)-phi)-Pmc(i)*sin(alfa2(o)-phim(i)))
    /(c*b(o))-(sin(alfa2(o))*cos(alfa1(o))-m(i)*sin(alfa2(o))*cos(alfa2(o)
    ))/sin(alfa1(o)+alfa2(o)));
x1(i)=Ncm1(i)-Ncm2(i);
end
z(o)=min(abs(x1));
for j=1:10000
if abs(x1(j))== z(o)
    y2(j)=j;
else
    y2(j)=0;
end
end
Ncm(o)=Ncm1(max(y2))/(k(o)*cos(theta(o)));
ks(o)=k(o);
```

## A.4. Calculation of $N_{qm=0}$ and $N_{\gamma m=0}$

```
for i=1:180
    roA(i)=pi()*i/360;
Ho(i)=b*tan(roA(i));
R1o(i)=cos(roA(i)-phi)*cot(roA(i))/cos(roA(i)-phi-delta);
R2o(i)=sin(roA(i)-phi)*cot(roA(i))/cos(roA(i)-phi-delta);
Ppo(i)=0.5*gamma*Ho(i)^2*Kpo+gamma*d*Ho(i)*Kpo;
Ngo(i)=(Kpo-R1o(i)*sin(0)-R2o(i)*cos(0))/((R1o(i)+in*R2o(i))*cos(0))*tan(
    roA(i))/k;
Nqo(i)=Kpo/((R1o(i)+in*R2o(i))*k*cos(0));
qo(i)=0.5*gamma*b*Ngo(i)+gamma*d*Nqo(i);
Kao(i)=Ppo(i)/(0.5*gamma*Ho(i)^2+qo(i)*Ho(i));
end
KAo=min(Kao);
for j=1:180
if Kao(j)==KAo
    v(j)=j;
```

```
else
    v(j)=0;
end
end
Ngo=Ngo(max(v));
Nqo=Nqo(max(v));
Hmo=Ho(max(v));
```

## A.5. Calculation of $N_{cm=0}$

```
if phi==0
    for i=1:180
    roAco(i)=pi()*i/360;
Ncmo1(i)= (2.83+2*tan(roAco(i))+cot(roAco(i)))/(k*cos(theta)*(in*cot(
    roAco(i))+1));
end
Nco1=min(Ncmo1);
for j=1:180
if Ncmo1(j)==Nco1
    t2(j)=j;
else
    t2(j)=0;
end
end
Ncmo=Ncmo1(max(t2))/k;
else
   Ncmo=((tan(pi()/4+phi/2))^2*exp(pi()*tan(phi))-1)*cot(phi)/k;
end
```

## A.6. Iteration of $k$ for Unknown Weight

```
if vehicle_type=='w'
    b(o)=B;
    k(o)=(lf+h*in(o))/l;
else
    e(o)= B/2-tg+in(o)*h;
    b(o)=B-2*e(o);

    if e(o)<=B/6
```

```
        k(o)=(B+6*e(o))/B;
    else
        k(o)=4*B/b(o)/3;
    end
end
```

## A.7. Iteration of $N_{qm}$ and $N_{\gamma m}$ for Unknown Weight

```
for i=1:180
    roA(i)=pi()*i/360;
H(i)=b(o)*tan(roA(i));
R1(i)=cos(roA(i)-phi)*cot(roA(i))/cos(roA(i)-phi-delta);
R2(i)=sin(roA(i)-phi)*cot(roA(i))/cos(roA(i)-phi-delta);
Pp(i)=0.5*gamma*H(i)^2*Kp(o)+gamma*d*H(i)*Kp(o);
Ngxx(i)=(Kp(o)-R1(i)*sin(theta(o))-R2(i)*cos(theta(o)))/((R1(i)+in(o)*R2(
    i))*cos(theta(o)))*tan(roA(i))/k(o);
Nqxx(i)=Kp(o)/((R1(i)+in(o)*R2(i))*k(o)*cos(theta(o)));
q(i)=0.5*gamma*b(o)*Ngxx(i)+gamma*d*Nqxx(i);
Ka(i)=Pp(i)/(0.5*gamma*H(i)^2+q(i)*H(i));
end
Kam(o)=min(Ka);
for j=1:180
if Ka(j)==Kam(o)
    y(j)=j;
else
    y(j)=0;
end
end
Hm(o)=H(max(y));
Ngm(o)=Ngxx(max(y));
Nqm(o)=Nqxx(max(y));
```

## A.8. Iteration of $N_{cm}$ for Unknown Weight

```
if phi==0
    for i=1:180
    roAc(i)=pi()*i/360;
Ncm1(i)= (2.83+2*tan(roAc(i))+cot(roAc(i)))/(k(o)*cos(theta(o))*(in(o)*
    cot(roAc(i))+1));
```

```
end
Nc1(o)=min(Ncm1);
for  j=1:180
if  Ncm1(j)==Nc1(o)
    t1(j)=j;
else
    t1(j)=0;
end
end
Ncm(o)=Ncm1(max(t1));

else
    D=c/(gamma*Hm(o));
Kpc(o)=((sin(phi))^2+1)/(cos(phi))^2+2*D*tan(phi)+sqrt((2*D*tan(phi)+((
    sin(phi))^2+1)/(cos(phi))^2)^2+(2*D)^2+4*D*tan(phi)-4*(tan(theta(o)))
    ^2/(cos(phi))^2-1);
Kac(o)=((sin(phi))^2+1)/(cos(phi))^2+2*D*tan(phi)-sqrt((2*D*tan(phi)+((
    sin(phi))^2+1)/(cos(phi))^2)^2+(2*D)^2+4*D*tan(phi)-4*(tan(theta(o)))
    ^2/(cos(phi))^2-1);

alfaA(o)=atan(2*tan(theta(o))/(1-Kac(o)+sqrt((1-Kac(o))^2+4*tan(theta(o))
    ^2)));
alfaP(o)=atan(2*tan(theta(o))/(Kpc(o)-1+sqrt((Kpc(o)-1)^2+4*tan(theta(o))
    ^2)));

alfa1(o)=pi()/4+phi()/2+alfaA(o);
alfa2(o)=pi()/4+phi()/2-alfaA(o);
alfa3(o)=pi()/4-phi()/2+alfaP(o);
alfa4(o)=pi()/4-phi()/2-alfaP(o);

ro(o)=b(o)*sin(alfa2(o))/sin(alfa1(o)+alfa2(o));

Ppc(o)=2*c*sqrt(Kpc(o))*(sin(alfa3(o)))^2/cos(phi)*ro(o)*exp(2*(pi()-
    alfa1(o)-alfa3(o))*tan(phi))+c*ro(o)/sin(phi)*(exp(2*(pi()-alfa1(o)-
    alfa3(o))*tan(phi))-1);
for  i=1:10000
m(i)=i/10000;
phim(i)=atan(m(i)*tan(phi));
```

```
cm(i)=m(i)*c;
Pmc(i)=2*cm(i)*sqrt(Kpc(o))*(sin(alfa3(o)))^2/cos(phi*m(i))*ro(o)*exp(2*(
    pi()-alfa2(o)-alfa3(o))*tan(phi*m(i)))+cm(i)*ro(o)/sin(phi*m(i))*(exp
    (2*(pi()-alfa2(o)-alfa3(o))*tan(phi*m(i)))-1);
Ca(o)=c*b(o)*sin(alfa2(o))/sin(alfa1(o)+alfa2(o));
Cam(i)=cm(i)*b(o)*sin(alfa1(o))/sin(alfa1(o)+alfa2(o));
qe(i)=(Ppc(o)*cos(alfa1(o)-phi)+Pmc(i)*cos(alfa2(o)-phim(i))+Ca(o)*sin(
    alfa1(o))+Cam(i)*sin(alfa2(o)))/b(o);
Ncm1(i)=qe(i)/c;
Ncm2(i)=1/in(o)*((Ppc(o)*sin(alfa1(o)-phi)-Pmc(i)*sin(alfa2(o)-phim(i)))
    /(c*b(o))-(sin(alfa2(o))*cos(alfa1(o))-m(i)*sin(alfa2(o))*cos(alfa2(o)
    ))/sin(alfa1(o)+alfa2(o)));
x1(i)=Ncm1(i)-Ncm2(i);
end
z(o)=min(abs(x1));
for j=1:10000
if abs(x1(j))== z(o)
    y2(j)=j;
else
    y2(j)=0;
end
end
Ncm(o)=Ncm1(max(y2))/(k(o)*cos(theta(o)));
ks(o)=k(o);
end
```

## A.9. Iteration of $N_{qm=0}$ and $N_{\gamma m=0}$ for Unknown Weight

```
for i=1:180
    roA(i)=pi()*i/360;
Ho(i)=b*tan(roA(i));
R1o(i)=cos(roA(i)-phi)*cot(roA(i))/cos(roA(i)-phi-delta);
R2o(i)=sin(roA(i)-phi)*cot(roA(i))/cos(roA(i)-phi-delta);
Ppo(i)=0.5*gamma*Ho(i)^2*Kpo+gamma*d*Ho(i)*Kpo;
Ngo(i)=(Kpo-R1o(i)*sin(0)-R2o(i)*cos(0))/((R1o(i)+in*R2o(i))*cos(0))*tan(
    roA(i))/k;
Nqo(i)=Kpo/((R1o(i)+in*R2o(i))*k*cos(0));
qo(i)=0.5*gamma*b*Ngo(i)+gamma*d*Nqo(i);
Kao(i)=Ppo(i)/(0.5*gamma*Ho(i)^2+qo(i)*Ho(i));
```

```
end
KAo=min(Kao);
for j=1:180
if Kao(j)==KAo
    v(j)=j;
else
    v(j)=0;
end
end
Ngo=Ngo(max(v));
Nqo=Nqo(max(v));
Hmo=Ho(max(v));
```

## A.10. Iteration of $N_{cm=0}$ for Unknown Acceleration

```
if phi==0
    for i=1:180
    roAco(i)=pi()*i/360;
Ncmo1(i)= (2.83+2*tan(roAco(i))+cot(roAco(i)))/(k*cos(0)*(in*cot(roAco(i)
    )+1));
end
Nco1=min(Ncmo1);
for j=1:180
if Ncmo1(j)==Nco1
    t2(j)=j;
else
    t2(j)=0;
end
end
Ncmo=Ncmo1(max(t2))/k;
else
    Ncmo=(tan(pi()/4+phi/2)^2*exp(pi()*tan(phi))-1)*cot(phi)/k;
end
```

## A.11. Iteration of $k$ for Unknown Acceleration

```
if vehicle_type=='w'
    b(o)=B;
    k(o)=(lf+h*in(o))/l;
```

```
else
    e(o)= B/2-tg+in(o)*h;
    b(o)=B-2*e(o);
    if e(o)<=B/6
        k(o)=(B+6*e(o))/B;
    else
        k(o)=4*B/b(o)/3;
    end
end
```

## A.12. Iteration of $N_{qm}$ and $N_{\gamma m}$ for Unknown Acceleration

```
for i=1:180
    roA(i)=pi()*i/360;
H(i)=b(o)*tan(roA(i));
R1(i)=cos(roA(i)-phi)*cot(roA(i))/cos(roA(i)-phi-delta);
R2(i)=sin(roA(i)-phi)*cot(roA(i))/cos(roA(i)-phi-delta);
Pp(i)=0.5*gamma*H(i)^2*Kp+gamma*d*H(i)*Kp;
Ngxx(i)=(Kp-R1(i)*sin(theta)-R2(i)*cos(theta))/((R1(i)+in(o)*R2(i))*cos(
    theta))*tan(roA(i))/k(o);
Nqxx(i)=Kp/((R1(i)+in(o)*R2(i))*k(o)*cos(theta));
q(i)=0.5*gamma*b(o)*Ngxx(i)+gamma*d*Nqxx(i);
Ka(i)=Pp(i)/(0.5*gamma*H(i)^2+q(i)*H(i));
end
Kam(o)=min(Ka);
for j=1:180
if Ka(j)==Kam(o)
    y(j)=j;
else
    y(j)=0;
end
end
Hm(o)=H(max(y));
Ngm(o)=Ngxx(max(y));
Nqm(o)=Nqxx(max(y));
```

## A.13. Iteration of $N_{cm}$ for Unknown Acceleration

```
if phi==0
```

```
    for i=1:180
    roAc(i)=pi()*i/360;
Ncm1(i)= (2.83+2*tan(roAc(i))+cot(roAc(i)))/(k(o)*cos(theta)*(in(o)*cot(
    roAc(i))+1));
end
Nc1(o)=min(Ncm1);
for j=1:180
if Ncm1(j)==Nc1(o)
    t1(j)=j;
else
    t1(j)=0;
end
end
Ncm(o)=Ncm1(max(t1));

else
    D=c/(gamma*Hm(o));
Kpc=((sin(phi))^2+1)/(cos(phi))^2+2*D*tan(phi)+sqrt((2*D*tan(phi)+((sin(
    phi))^2+1)/(cos(phi))^2)^2+(2*D)^2+4*D*tan(phi)-4*(tan(theta))^2/(cos(
    phi))^2-1);
Kac=((sin(phi))^2+1)/(cos(phi))^2+2*D*tan(phi)-sqrt((2*D*tan(phi)+((sin(
    phi))^2+1)/(cos(phi))^2)^2+(2*D)^2+4*D*tan(phi)-4*(tan(theta))^2/(cos(
    phi))^2-1);

alfaA=atan(2*tan(theta)/(1-Kac+sqrt((1-Kac)^2+4*tan(theta)^2)));
alfaP=atan(2*tan(theta)/(Kpc-1+sqrt((Kpc-1)^2+4*tan(theta)^2)));

alfa1=pi()/4+phi()/2+alfaA;
alfa2=pi()/4+phi()/2-alfaA;
alfa3=pi()/4-phi()/2+alfaP;
alfa4=pi()/4-phi()/2-alfaP;

ro(o)=b(o)*sin(alfa2)/sin(alfa1+alfa2);

Ppc(o)=2*c*sqrt(Kpc)*(sin(alfa3))^2/cos(phi)*ro(o)*exp(2*(pi()-alfa1-
    alfa3)*tan(phi))+c*ro(o)/sin(phi)*(exp(2*(pi()-alfa1-alfa3)*tan(phi))
    -1);
```

```
for  i=1:10000
m(i)=i/10000;
phim(i)=atan(m(i)*tan(phi));
cm(i)=m(i)*c;
Pmc(i)=2*cm(i)*sqrt(Kpc)*(sin(alfa3))^2/cos(phi*m(i))*ro(o)*exp(2*(pi()-
    alfa2-alfa3)*tan(phi*m(i)))+cm(i)*ro(o)/sin(phi*m(i))*(exp(2*(pi()-
    alfa2-alfa3)*tan(phi*m(i)))-1);
Ca(o)=c*b(o)*sin(alfa2)/sin(alfa1+alfa2);
Cam(i)=cm(i)*b(o)*sin(alfa1)/sin(alfa1+alfa2);
qe(i)=(Ppc(o)*cos(alfa1-phi)+Pmc(i)*cos(alfa2-phim(i))+Ca(o)*sin(alfa1)+
    Cam(i)*sin(alfa2))/b(o);
Ncm1(i)=qe(i)/c;
Ncm2(i)=1/in(o)*((Ppc(o)*sin(alfa1-phi)-Pmc(i)*sin(alfa2-phim(i)))/(c*b(o
    ))-(sin(alfa2)*cos(alfa1)-m(i)*sin(alfa2)*cos(alfa2))/sin(alfa1+alfa2)
    );
x1(i)=Ncm1(i)-Ncm2(i);
end
z(o)=min(abs(x1));
for  j=1:10000
if  abs(x1(j))== z(o)
     y2(j)=j;
else
     y2(j)=0;
end
end
Ncm(o)=Ncm1(max(y2))/(k(o)*cos(theta));
ks(o)=k(o);
end
```

# REFERENCES


1. Craig, R.F., *Soil Mechanics*, Spon Press, London, 1997.

2. Prandtl, L., *Uber die Eindringungsfestigkeit (Harte) Plastischer Baustoffe und die Festigkeit von Schneiden.* , Zeitschrift fur Angewandte Mathematik und Mechanik, Vol.1, No.1, pp. 1520, 1921.

3. Terzaghi, K., *Theoretical Soil Mechanics*, John Willey and Sons, New York, 1943.

4. Meyerhof, G.G., *The Bearing Capacity of Footing Under Eccentric and Inclined Loads.*, E q E Proc., 3rd Int. Conf. on Soil Mechanics and Foundations Engineering, I, Zurich, Switzerland, 1953.

5. Meyerhof, G.G., *Some Recent Research on The Bearing capacity of Foundations*, Canadian Geotechnical Journal, Vol.1, No. 1, pp.16-26,1963.

6. Hansen, J.B., *A Revised and Extended Formula For Bearing Capacity.*, Danish Geotechnical Institute Bull. No. 28, p.p. 5-11,1970.

7. Vesic, A.S., *Foundations Engineering Handbood.*, H. F. Winterkorn and H. Fang, eds., Van Nostrand Reinhold, New York.,1975.

8. Richards R., D.G. Elms, M. Budhu, *Dynamic Fluidization of Soils*, Journal of Geotechnical Engineering, Vol. 116, No. 5, May, 1990

9. Jacky, J., *The Coefficient of Earth Pressure at Rest*, Journal for Society of Hungarian Architects and Engineers, pp. 355-358, 1944.

10. Budhu, M. and A. Al-Karni, *Seismic Bearing Capacity of Soils*, Geotechnique, Vol. 43, No. 1, pp. 181-187, Mar, 1993.

11. Richards R., D.G. Elms, M. Budhu, *Seismic Bearing Capacity and Settlements of*

*Foundations*, Journal of Geotechnical Engineering, Vol. 119, No. 4, April, 1993

12. Lambe, T. W., R. V. Whitman, *Soil Mechanics*, John Wiley and Sons Inc., New York, 1969.

13. Tschebotarioff, G., *Soil Mechanics, Foundations, and Earth Structures*, McGraw-Hill, New York, 1951.

14. Richards, R., D. G. Elms, *Seismic Behavior of Tied Back Walls*, Report 87-8, Dept. of Civil Engineering, Univ. of Canterbury, Christchurch, N.Z., 1987.

15. Mononobe, N., H. Matsuo, *On the Determination of Earth Pressures During Earthquakes.*, Proceedings, World Engineering Congress, 9, 176, 1929.

16. Okabe, S., *General Theory of Earth Pressure.*, Journal of the Japanese Society of Civil Engineers, 12,1,1926

17. Fishman, K. L., R. Richards, D. Yao, *Inclination Factors for Seismic Bearing Capacity*, Journal of Geotechnical and Geoenvironmental Engineering, Vol. 129, No. 9, pp. 861-865, Sep, 2003.

18. Rula, A. A. and C. J. Nuttal, *An Analysis of Ground Mobility Models (ANAMOB)*, U.S. Army Corps of Engineers Waterways Experiment Station, Technical Report M-71-4, Vicksburg, MS, 1971.

19. Meyer, M. P., I. R. Ehrlich, D. Sloss, N. R. Murphy Jr, R. D. Wismer, T. Czako, *International Society for Terrain-Vehicle Systems Standards*, Journal of Terramechanics, Vol. 14, No. 3, p.p.107-108,1977.

20. Wong , J. Y., *Theory of Ground Vehicles*, John Wiley and Sons Inc, New York, 2001.

21. Priddy, J. D. and W. E. Willoughby, *Clarification of Vehicle Cone Index with Reference to Mean Maximum Pressure*, Journal of Terramechanics, Vol. 43, No. 2,

p: 85-96, 2006.

22. Bekker, M. G., *Theory of Land Locomotion*, The University of Michigan Press,1962.

23. Onafeko, O., A.R. Reece, *Soil Stresses and Deformation Beneath Rigid Wheels*, Journal of Terramechanics, Vol. 4, No. 1, p.p. 59-80, 1967.

24. Janosi, Z. and B. Hanamoto, *The Analytical Determination of Drawbar Pull as a Function of Slip for Tracked Vehicles in Deformable Soils.*, Proc. First Int. Conf. On Terrain-Vehicle Systems, Torino, Italy,1961.

25. Söhne, W., *Fundamentals of Pressure Distribution and Soil Compaction Under Tractor Tires* , Agricultural Engineering, May,1958.

26. Potyondy, J.G., *Skin Friction Between Various Soils and Construction Materials*, Geotechnique, London, Vol. 2, No. 4, December, 1961.

27. Al-Hussaini M. M. and P.A. Gilbert, *Stressed and Shearing Resistance in Soil Beneath a Rigid Wheel*, Waterways Experiment Station, 1974.

28. Ampera, B., T. Aydogmus, *Skin Friction between Peat and Silt Soils with Construction Materials*, Electronic Journal of Geotechnical Engineering, Vol. 10, Bundle D, 2005.

# REFERENCES NOT CITED

1. Karafiath, L. L., and E.A. Nowatzki, *Soil Mechanics For Off-Road Vehicle Engineering*, Trans Tech Publications, Clausthal, 1978.

2. Shi, X. and R. Richards, *Seismic Bearing Capacity with Variable Shear Transfer*, Earthquake-Induced Movements and Seismic Remediation of Existing Foundations and Abutments, 1995, pp. 17-32, Aug,1995,